Progress in Quantum Electronics 68 (2019) 100227

Contents lists available at ScienceDirect

Progress in Quantum Electronics

journal homepage: www.elsevier.com/locate/pqe

Review

Cr:Colquiriite Lasers: Current status and challenges for further progress

Umit Demirbas [a,b,*]

[a] Laser Technology Laboratory, Department of Electrical and Electronics Engineering, Antalya Bilim University, 07190, Antalya, Turkey
[b] Center for Free-Electron Laser Science, Deutsches Elektronen Synchrotron, Hamburg, 22607, Germany

A B S T R A C T

Cr: Colquiriite laser materials (Cr:LiCAF, Cr:LiSAF, Cr:LiSGaF) own broad absorption bands in the visible region that allow direct-diode pumping by well-developed low-cost red diodes. Moreover, they possess broad emission bands in the near infrared that enable widely tunable laser operation (720–1110 nm), and generation of sub-10-fs light pulses via mode-locking. Furthermore, Cr: Colquiriite crystals can be grown with a very low loss level of 0.2%/cm, which enables the construction of high-Q-cavities, resulting in lasing thresholds below 1 mW, and slope efficiencies above 50%. High-Q-cavities constructed with Cr: Colquiriites could store large amount of intracavity laser powers which is off great interest: (i) for increasing the efficiency of intracavity nonlinear processes such as intracavity frequency-doubling, and (ii) for minimizing laser noise such as timing jitter noise in femtosecond operation. However, thermally and mechanically Cr: Colquiriites have glass like properties. Hence, average power scaling has been challenging in the cw and femtosecond Cr: Colquiriite lasers, as well as in their amplifiers. In this paper, we will review research efforts over the last decades, in developing robust, low-cost, highly-efficient, and tunable cw and femtosecond laser sources based on diode-pumped Cr:Colquiriite gain media. Challenges for future progress will also be discussed.

1. Introduction

1.1. Historic review and general categorization of lasers

The underlying idea of Light Amplification by Stimulated Emission of Radiation (LASER) is stimulated emission, which was proposed by Albert Einstein in 1917, in his famous paper on "Quantum theory of radiation" [1,2]. It took quite a while for physicists to use the idea of stimulated emission and realize it experimentally. In 1947 Willis Lamb and Robert Retherford from Colombia University used stimulated emission to amplify the microwave frequency radiation emitted by hydrogen molecules at a wavelength of 2.74 cm [3]. In 1954, Charles H. Townes, J. P. Gordon, and H. J. Zeiger build the first maser (microwave amplification by stimulated emission of radiation) using the vibrational energy levels of ammonia molecules in a resonant cavity, obtaining only nW level powers at a wavelength of around 1.25 cm [2,4,5]. C. H. Townes and A. L. Schawlow suggested the extension of maser technology to higher (optical) frequencies, and they proposed the idea of Fabry-Perot resonators for feedback [6]. It took a while to find an appropriate gain media and a suitable way for excitation that could generate enough population inversion [7]. Finally, in 1960, T. Maiman build the first laser operating at 694.3 nm using the ^2E, $^4A_2$ transition of ruby (Cr^{+3} in corundum, crystalline form of Al_2O_3) as the gain medium where flahslamps were used as the excitation mechanism [8].

Since then, lasing has been demonstrated in thousands of different gain media, and the Handbook of Laser Wavelengths by M. J. Weber lists more than 15,000 laser lines (most gain media have more than one lasing line) [9–11]. Among all these available lasers, only a few hundreds of them are used most frequently, and maybe around ten dominates most of the laser field (like Ti:Sapphire and Yb:YAG

* Laser Technology Laboratory, Department of Electrical and Electronics Engineering, Antalya Bilim University, 07190, Antalya, Turkey.
E-mail address: umit79@alum.mit.edu.

https://doi.org/10.1016/j.pquantelec.2019.100227

Available online 2 August 2019
0079-6727/

being the main workhorse of today's ultrafast laser technology) [10]. One can categorize these lasers in several ways, using their operational wavelength (UV, visible, IR, etc.), operational mode (continuous-wave, q-switched, gain-switched, mode-locked, etc.), excitation mechanism (electrically pumped, flashlamp pumped, diode-pumped, etc.), their historic role (first generation, second generation, third generation [12]), and their application area. Maybe one of the most convenient ways of categorizing lasers is made by differentiating them according to the type of gain media used. In this respect lasers can be categorized as (a) gas lasers, (b) liquid lasers, and (c) solid-state lasers [18].

Most of the known laser transitions belong to gas lasers [9,10]. The lasing lines of gas lasers are quite narrow in general (Doppler, collisional and rotational line broadening effects are present but they are not very strong), and without a tuning element, an individual laser can lase at several different distinct wavelengths simultaneously [9,13,14]. The transition involved in the stimulated emission process might be between electronic, vibrational or rotational energy levels, enabling gas lasers to cover a quite wide spectral range [9, 15,16]. The wavelengths available from gas lasers start from ~3.9 nm and covers all the vacuum ultraviolet, ultraviolet, visible, infrared, far infrared, and millimeter-microwave regions [9].

Liquid lasers are mostly based on organic dye lasers, which are basically dye molecules (e.g. rhodamine, fluorescein) in an organic solvent such as ethanol, p-dioxane or dimethylsulfoxide [9,17]. Dye lasers were discovered quite early in 1966, by P. P. Sorokin and F. P. Schäfer around the same time [18,19]. They have relatively broad absorption and emission bands due to the coupling of electrons with molecular vibrations [17]. Hence they could provide tunable laser operation over 10's of nanometers, and also facilitate sub-100-fs pulse generation in mode-locked regime (27 fs pulses directly from the oscillator [20] and down to 6 fs pulses with external pulse compression [21]). Using different dye molecules, the laser wavelength range from 330 nm to 1800 nm could be covered [9]. Dye gain media have relatively high gain and their upper-state lifetimes are in the ns range; hence, they don't have the tendency for q-switching instabilities during mode-locked operation [22,23]. In 1970's and 1980's most of the ultrafast laser technology was based on dye lasers [22,23]. Unfortunately, the dye lasers have several disadvantages including low output powers, low pulse energies in Q-switched mode (due to short lifetimes), requirement for expensive pump sources in the green or blue region of the spectrum and rapid degradation during laser operation [22]. Moreover, dye gain media and/or the solvents are sometimes highly toxic and carcinogenic [22]. Hence, today dye lasers are mostly replaced by solid state laser technology, and mostly with Ti:Sapphire [14,24]. Besides the organic dye lasers, liquid lasers also include rare-earth chelate lasers and inorganic aprotic solvents, which also had very little practical usage, due to their corrosive and toxic nature [9].

Solid state lasers are based on solid-state crystalline or amorphous hosts and have laser transitions originating from the doping of paramagnetic ions (with incompletely filled electron shells), organic dye molecules and color centers [9]. The typical doping concentrations of active ions are less than 1% in general, but can reach to 100% (stoichiometric lasers) for some specific cases like LiChrom ($LiSrCrF_6$, 100% Cr doped $LiSrAlF_6$) [9,25]. Semiconductor lasers are also listed under solid-state lasers, since they are also solid-state devices, but actually they use completely different physics in the generation of laser active centers [9]. Today solid-sate lasers has an important part in laser market, due to their several favorable properties including robustness, reliability, safety, user-friendliness, compactness, and low-cost per performance [26]. They can cover the spectral region from 170 nm to 360 μm (see Figs. 1–2 in Ref. [9]), enabling the generation of laser radiation at the optimum wavelength for many different applications.

Solid-state lasers based on paramagnetic ions can be categorized in two sub segments: rare earth element and transition metal-doped solid-state lasers. Rare earth elements/metals are a collection of 17 chemical elements which includes lanthanoids (lanthanides), scandium and yttrium. The lasing lines of rare-earth doped gain media originate mostly from the transitions between the partially filled

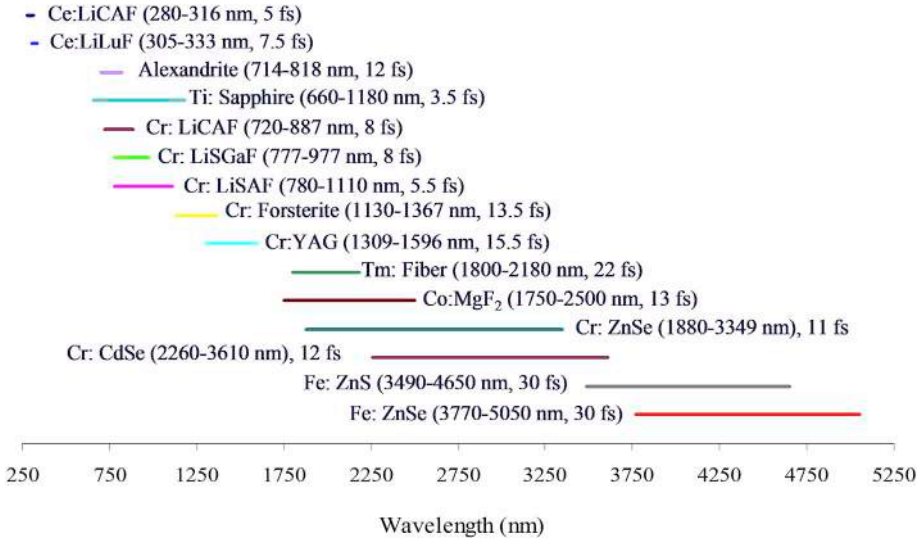

Fig. 1. Summary of tuning ranges for selected broadly tunable solid-state laser gain media. Demonstrated tuning ranges and theoretically estimated minimum pulse durations are indicated. Inspired from Ref. [39].

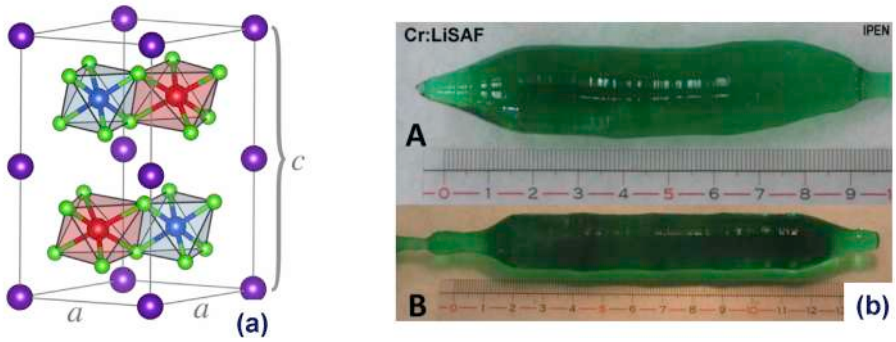

Fig. 2. (a): Unit cell of LiCAF: lithium (red), aluminum (blue), fluorine (green), calcium (purple). Cr ions replace some of the aluminum atoms (Reprinted with permission from Ref. [141]). (b): Cr:LiSAF crystals grown by the Czochralski method (Reprinted with permission from Ref. [119]).

4f shells. These states are split by Coulomb interaction, spin-orbit coupling and crystal-field interaction [27]. Coulomb interaction has the strongest effect on the lines which separates the lines typically by ~10,000 cm^{-1} (~1.24 eV, λ~1000 nm photon), followed by the spin orbit coupling which creates an additional splitting of around ~3,000 cm^{-1} (0.37 eV, λ~3350 nm photon) [27]. Since the 4f shell is shielded by the outer 5s and 5p electrons, the effect of crystal field is relatively weak, which further splits each manifold by only ~200 cm^{-1} (25 meV, λ~50 μm photon) [27,28]. The shielding of crystal field results in relatively narrow but strong emission lines in rare-earth doped gain media (σ_{em} is high), and also the position and width of the emission lines does not differ a lot from host to host [7,9,27]. Hence, most of the rare-earth doped gain media provide very little tunability and the obtainable pulsewidths in mode-locked regime are relatively long. Moreover, dipole transitions between the 4f shells are parity forbidden, and a mixture of wave functions with opposite parity is required for a transition [27]. These opposite parity wave functions are generated by the weak crystalline field, hence these transition probabilities are quite weak also [27]. This results in relatively long upper state lifetimes (τ) in rare-earth doped gain media [27]. Hence in general, rare-earth doped gain media has a very high $\sigma_{em}\tau$ value, resulting in low lasing thresholds at low concentration values (at high concentrations increased nonradiative decay rates might lower the lifetime) [27]. We note here that, in some cases, rare-earth doped gain media can also have lasing transitions between 4f and 5d shells, and in this case laser lines are quite broad and one can possibly obtain broad tunability and ultrashort pulses (examples are Ce^{+3}:$LiCaAlF_6$, Sm^{+2}:SrF_2 and Sm^{+2}:CaF_2) [9,11]. This is because unlike the 4f shell, the 5d shell has no shielding and hence it is exposed to the crystalline environment, which broadens the emission lines [13].

As a side note, one should differentiate rare-earth doped glasses from rare earth doped crystals [29]. Rare-earth doped glasses can take the form of bulk materials, fibers or planar waveguides [9]. In glassy structure the crystalline field surrounding the active ions are not as well defined as crystalline hosts; hence, laser emission lines can be slightly broader [7], enabling relatively broadband tuning and shorter pulses in mode-locked operation. Other advantages of glass hosts include ability to produce large samples for high energy applications, and ease of fabrication, whereas the drawbacks include lower thermal conductivity, lower emission cross section, and thermally induced birefringence problems [7].

Transition metal elements are elements whose atom has an incomplete d sub-shell, or elements which can give rise to cations with an incomplete d sub-shell [30,31]. The name "transition" comes from the place they appear on periodic table: they represent transition between group 2 and group 13 elements [30]. So far, lasing have been reported in the transition metal elements of titanium (Ti), vanadium (V), chromium (Cr), manganese (Mn), iron (Fe), cobalt (Co) and nickel (Ni), and gain has been reported in transition metal elements of copper (Cu), silver (Ag) and rhodium (Rh) [9]. Example gain media include Ti^{+3}:Al_2O_3(sapphire), Co^{+2}:MgF_2, Cr^{+2}:ZnSe, Cr^{+2}:ZnS, Cr^{+3}:Al_2O_3 (ruby), Cr^{+4}:Mg_2SiO_4 (forsterite), Cr^{+4}:YAG and Fe^{+2}:ZnSe.

Cr^{3+}:Colquiriites of the general formula Li Me^{II} $Me^{III}F_6$ (Me^{II} = Ca, Sr, Cd; Me^{III} = Al, Ga, Ti, V, Cr, Fe) (e.g. Cr:LiSAF [32,33], Cr:LiCAF [34–36], Cr:LiSGaF [37], Cr:LiSCAF [38] and $LiSrCrF_6$ (LiChrom) [25]), the topic of this review article also belong to the family of transition metal doped solid state lasers. The most important point here is that the d orbitals determine optical properties of ions, and since the d orbitals are not shielded (as in the case of rare-earth ions), the optical properties are greatly influenced by the host [14]. Moreover, absence of shielding in transition-metal doped gain media enables strong phonon broadening in the absorption and emission lines, which enables ultrabroad tuning ranges and ultrashort pulse generation in mode-locked operation. Dipole transitions between the 3d shells are also parity forbidden, however due to the strong crystal field, opposite parity wave functions are generated more easily, resulting in higher transition rates and shorter lifetimes [27]. Compared to the rare-earth-doped gain media, $\sigma_{em}\tau$ value is an order of magnitude smaller [27].

1.2. Where does Cr:Colquiriite stand among other tunable solid state laser gain media?

In tunable solid-state lasers, by definition the output wavelength can be tuned over a substantial fraction of the central emission wavelength (at least several percent of the laser central wavelength) [14,39]. This enables the generation of coherent optical radiation at the desired wavelength as well as generation and amplification of ultra short pulses. Usually, the fractional tuning range, defined as $\Delta\lambda/\lambda_0$ ($\Delta\lambda$= full width of the tuning range and λ_0 = the central emission wavelength) is used to compare different gain media. A good

reason for this is the pulse width that could be obtained from a gain medium scales inversely with $\Delta\lambda/\lambda_0$ [40]:

$$\tau \propto \lambda_0 \frac{\lambda_0}{\Delta\lambda} \quad (1)$$

Basically, the pulse duration is linearly proportional to the wavelength (λ_0) and the number of optical cycles of the electric field of the pulse (the number of optical cycles scales with $\lambda_0/\Delta\lambda$) [28].

Table 1 shows selected examples of tunable solid-state gain media and their reported fractional tuning range at room temperature. Demonstrated shortest pulsewidths in mode-locked regime are also reported along with the estimated minimum pulsewidths that are supported by the gain bandwidth of the materials. Fig. 1 graphically provides similar information. Note that the spectral region in the 350–700 nm range is rather empty: we don't have any known efficient and broadly tunable solid-state laser gain media that emits in this region. Ce:LiCAF, Ce:LiSAF, Ce:LLF cover the near ultraviolet region (280–330 nm), and Ti:Sapphire, Alexandrite, and Cr:Colquiriites cover the long end of visible and near-infrared spectral regions. Then laser materials such as Cr:Forserite, Cr:YAG, Co:MgF_2, Cr:ZnSe and Fe:ZnSe cover the whole near-to-mid infrared region till around 5000 nm. Each wavelength region is important, since different applications and different tasks could provide optimized performance with specific laser wavelengths.

Note from Eq. (1) that, the required fractional bandwidth to support an ultrashort pulse is smaller at shorter wavelengths, providing advantage to laser gain media with a tuning range in the near ultraviolet and visible. One of the best studied tunable near-ultraviolet solid state gain medium is Ce^{+3}:LiCAF. As mentioned above Ce^{+3}:$LiCaAlF_6$ is an exceptional rare earth doped gain media, where the lasing transitions between 4f and 5d shells can be used to generate broadly tunable laser operation (280–316 nm) [41–43]. Ce:LiCAF has a fluorescence lifetime (τ) of only 25 ns, and has an emission cross section (σ_{em}) of 9.6×10^{-19} cm^2; hence, the product $\tau\sigma_{em}$ is only 2.4×10^{-20} μs cm^2 [42], which is about 50 times smaller compared to Ti:Sapphire (131×10^{-20} μs cm^2). This prevents continuous wave lasing operation in this gain media (due to high lasing thresholds), and so far only gain switched operation have been reported with ps to ns pulse durations, upon pumping with the 4th harmonic of pulsed Nd-lasers [42]. The demonstrated tuning range in gain switched operation extends from 280 nm to 316 nm, with ~W level average output powers from ~ns pulses at ~ kHz repetition rates [41]. Mode-locked operation with Ce:LiCAF has also been reported, where 6 ps pulse durations were demonstrated upon synchronously pumping [44]. Ce:LiCAF gain media has also been used in chirped pulse amplification of ultraviolet femtosecond pulses around 290 nm [45], which is attractive due to its high saturation fluence (115 mJ/cm^2) [43]. We note here that the bandwidth of Ce^{+3}:LiCAF is broad enough to support ~5-fs pulses [44]. Other important Ce^{+3} doped solid state gain media include Ce:*LiLuF4* (LiLuF) with a tunability from 305 nm to 333 nm [46], and Ce:LiSAF with a tunability from 288 nm to 313 nm [47]. Unfortunately, ultrafast pulse generation with these gain media is hindered by their small gain cross section.

Probably the most important known member of broadly tunable solid-state lasers is Ti^{+3}: Sapphire (660–1180 nm). Ti^{+3}:Al_2O_3 gain medium has been discovered by Dr. Peter Moulton in 1982, and with time it has quickly become the workhorse of ultrafast laser technology, by replacing the dye lasers [12,24,83]. Among solid-state lasers, Ti:Sapphire has the broadest fractional tuning range (660–1180 nm), and can directly generate the shortest possible pulses from a laser oscillator (sub-5-fs) [24,48,84]. Ti:Sapphire lasers are commercial standards today, and systems can provide (i) more than 5 W of output power with continuous-wave (cw) tuning from 675 to 1100 nm, and (ii) peak powers of hundreds of kW in mode-locked operation with either ~100 fs tunable pulses (680–1080 nm) or ~10

Table 1
Room-temperature tuning ranges and calculated fractional tuning percentage of several broadly tunable transition metal and rare-earth ion-doped solid state laser gain media. Minimum theoretical pulse durations supported by the gain bandwidth of the material and demonstrated shortest pulse widths are also included.

Gain Medium	Tuning Range (nm)	$\Delta\lambda/\lambda_0$ (%)	Minimum theoretical pulse duration (fs)	Shortest demonstrated pulsewidth (fs)
Ce^{+3}:$LiCaAlF_6$	280-316 [41]	12	5	6×10^3 [44]
Ce^{+3}:$LiSrAlF_6$	288-313 [47]	8	7.5	–
Ce^{+3}:$LiLuF_4$	305-333 [46]	9	7.5	–
Ti^{3+}:Al_2O_3	660-1180 [24]	57	3.5	5 [48]
Cr^{3+}:$BeAl_2O_4$	714-818 [49]	14	12	70 [50]
Cr^{+3}:$LiCaAlF_6$	720-887 [34,51,52]	21	8	9 [53]
Cr^{+3}: $LiSrGaF_6$	777-977 [51,54]	23	8	14 [55]
Cr^{+3}:$LiSrAlF_6$	775-1110 [51,56,57]	36	5.5	10 [58]
Nd:GSAG:YSGG	–	–	–	260 [59]
Nd^{+3}:glass	–	–	53 [60]	60 [61]
Cr^{4+}:Mg_2SiO_4	1130-1367 [62]	19	13.5	14 [63]
Cr^{4+}:$Y_3Al_5O_{12}$	1309-1596 [64]	20	15.5	20 [65]
Yb^{+3}:$Y_3Al_5O_{12}$	1016–1108	9	26	35 [66]
Tm,Ho:BaY_2F_8	2005–2094 [67]	4	100	120×10^3 [67]
Tm:YAG	1870-2160 [68]	15	30	3×10^3 [69]
Tm:YLF	1910–2070 [70]	8	52	515 [72]
	2200-2460 [71]	11	44	
Co^{2+}:MgF_2	1750-2500 [73]	35	13	–
Cr^{2+}:ZnS	1962-3195 [74,75]	48	12 [60]	29 [76]
Cr^{2+}:CdSe	2180-3610 [77–79]	49	12	–
Cr^{2+}:ZnSe	1880-3349 [75,80]	56	11 [60]	47 [81]
Fe^{2+}:ZnSe	3770-5050 [82]	21	30	–

fs pulses around 800 nm. Ti:Sapphire gain media has a quite broad absorption band centered around 490 nm, with a FWHM of ~120 nm (460–580 nm) [85]. Until recently, due to the absence of high power laser diodes in this wavelength range, efficient direct diode pumping of Ti:Sapphire gain media was not possible, which has been the main disadvantage of Ti:Sapphire technology. Direct diode pumping of Ti:Sapphire with single-emitter diodes in the blue and green spectral region has been shown in the last decade, both in cw and cw mode-locked operation [85–98]. Currently, the Ti:Sapphire laser systems on the market are still not based on diode pumping, and mostly rely on 2nd harmonics of Nd-based lasers. On the other hand, further progress in brightness and robustness is expected for the relatively new green/blue pump diodes used in pumping Ti:Sapphire. We believe as the diode technology at these wavelengths get more mature, this will enable further improvements in performance of diode pumped Ti:Sapphire lasers over the coming decades, enabling cost and complexity reduction in Ti:Sapphire laser and amplifier systems.

Cr^{3+}-doped Colquiriite crystals (Cr:LiCAF, Cr:LiSAF and Cr:LiSGaF) and Alexandrite possess emission bands that cover a spectral region similar to Ti:Sapphire. Cr:Colquiriite have broad absorption bands around ~650 nm (compared to 490 nm band of Ti:Sapphire), and hence enables direct diode pumping with the mature red diode technology. Thermo-mechanical and optical properties of Cr:Colquiriites, Alexandrite and Ti:Sapphire will be discussed in great detail in the next sections in a comparative manner.

It is important to note that, Nd and Yb-based systems are also attractive gain media for the development of diode-pumped low-cost cw and ultrafast laser and amplifier systems due to the existence of low-cost InGaAs diodes around 975 nm [99–103]. For example, state-of-the-art Yb-doped systems could provide down to 35 fs pulses [104], with optical-to-optical conversion efficiencies above 50% [105], and average powers above 1 kW [12,106,107]. Their long upper state lifetimes also enable efficient energy storage that makes them suitable especially as an amplifier media [102,108–111]. However, due to their relatively narrow gain bandwidths, the obtainable pulsewidths from Yb-based systems are limited to at best about 50 fs level in oscillators and to about 1 ps in amplifiers [12,111]. Hence, these systems work in a set of parameters that do not substitute Ti:Sapphire and Cr:Colquiriite systems for many applications. On the other hand, optical parametric amplification driven by high peak and average power Yb-systems could combine short pulsewidths with high peak/average power, but these are quite complex and expensive systems [12,112].

At this point, for a review of other broadband solid-state gain media, we refer the reader to several excellent review articles such as [14,113–118].

1.3. Thermo-mechanical parameters of Cr:Colquiriites

The laser host must have good optical, mechanical and thermal properties to withstand the expected operating conditions of practical lasers and amplifiers [14,119]. Desirable thermo-opto-mechanical properties include hardness, chemical inertness, absence of internal strain and refractive index variations, resistance to radiation induced color center, ease of fabrication, large damage threshold, high thermal conductivity values, etc. [7,119]. In this section, we will compare laser related thermo-mechanical parameters of Cr:Colquiriites with the other competitive crystals, namely: Ti:Sapphire, Alexandrite and Yb:YAG. Spectroscopic and optical properties will be discussed in the next section. For this purpose, important thermo-mechanical properties of these gain media are listed in Table 2.

As mentioned earlier, currently Ti:Sapphire is the dominant player and the workhorse of ultrafast lasers, whereas Yb:YAG and Yb-based materials in general dominate the field in terms of high average powers at the expense of longer pulsewidth. Alexandrite has also been included in the discussion, since its operation range partly matches (and partly extends) Cr:Colquiriites, and it possess interesting spectroscopic properties (such as improved laser performance at elevated temperatures), and we believe that it has the potential to be one of the critical players in the field of diode pumped ultrafast systems in the coming decades.

In Cr:Colquiriites the dopant Cr^{+3} ion substitutes Al in Cr:LiSAF ($LiSrAl_{1-x}Cr_xF_6$) and Cr:LiCAF ($LiCaAl_{1-x}Cr_xF_6$), and substitutes Ga in Cr:LiSGaF ($LiSrGa_{1-x}Cr_xF_6$). The dopant density at 1% doping corresponds to 0.875×10^{20} ions/cm^3 in Cr:LiSAF. The typical doping concentration of Cr^{+3} ions in Cr:Colquiriites are in the 0.5–10% range; however, up to 100% doping is possible: (e.g. LiChrom: $LiSrCrF_6$, 100% Cr doped $LiSrAlF_6$) [9,25]. Mass density (ρ) of Colquiriites are similar to Sapphire and Alexandrite, which are slightly lower compared to YAG.

Moh hardness values determines the scratch hardness of minerals, a scale which goes from 1 (for talc) to 10 (for diamond), where each mineral will scratch the one on the scale below it but will not scratch the one above it [125]. The Moh hardness values could be scaled to more empirical hardness tests such as Knob hardness [125]. Note that Cr:Colquiriites has a Moh hardness value of around 3–4, showing their susceptibility to get scratches, whereas sapphire, alexandrite and YAG has values of 8–9 showing their superiority in this respect. For comparison, the Moh hardness of glass and YLF ($LiYF_4$) is around 5. Hence, in handling Cr:Colquiriites soft tools such as usage of plastic tweezers are recommended.

One of the most important parameter for power scaling of laser and amplifier materials is thermal conductivity (κ) of the host material. Thermal conductivity of the uniaxial Cr:LiSAF is only 1.8 W/Km in a-axis, and 3 W/Km in the c axis [33,121]. Unfortunately, these values are an order of magnitude lower than Sapphire (31 W/Km) [127], and about 1/4th of the value for YAG (10 W/Km) [129]. Cr:LiCAF has more isotropic and higher thermal conductivity values (4.58 in a and 5.14 in c axis [129]), making it the best candidate amongst Cr:Colquiriites for power demanding applications. The thermal conductivity values for Cr:LiCAF are similar to YLF (5.3 (//a), 7.2 (//c) [142], a fluoride laser host that is in common usage. Unfortunately, to the best of our knowledge, for Cr:Colquiriites variation of thermal conductivity (and other thermo-mechanical parameters) with temperature and doping is not reported in the literature. For example, in Yb:YAG thermal conductivity improves from around 10 W/Km at room temperature to around 50 W/Km at 80 K for a 2% Yb-doped sample [133]. Such improvements in thermal parameters at low temperatures enabled power scaling of Yb:YAG amplifiers at cryogenic temperatures [143,144], which is still an open research question for Cr:Colquiriites. It is educational to compare these values with thermal conductivity of glass (0.6 W/Km [7]), copper (400 W/Km) and diamond (2200 W/Km [145]).

Thermal expansion coefficient (α) is a material property that is indicative of the extent to which a material expands upon heating. As

Table 2
Comparison of the laser related thermo-mechanical parameters of the Ti:Sapphire, Cr:LiSAF, Cr:LiSGaF, Cr:LiCAF, Alexandrite and Yb:YAG gain media.

Gain Medium	Ti^{3+}:Al_2O_3 (Ti:Sapphire)	Cr^{+3}:$LiSrAlF_6$ (Cr:LiSAF)	Cr^{+3}: $LiSrGaF_6$ (Cr:LiSGaF)	Cr^{+3}:$LiCaAlF_6$ (Cr:LiCAF)	Cr^{+3}:$BeAl_2O_4$ (Alexandrite)	Yb^{+3}:$Y_3Al_5O_{12}$ (Yb:YAG)
Dopant site	$(Ti_xAl_{1-x})_2O_3$	$LiSrAl_{1-x}Cr_xF_6$	$LiSrGa_{1-x}Cr_xF_6$	$LiCaAl_{1-x}Cr_xF_6$	$Be(Al_{1-x}Cr_x)_2O_4$	$(Yb_xY_{1-x})_3Al_5O_{12}$
Dopant density at 1% doping [$x10^{20}$ ions/cm^3]	4.7 [120]	0.875	0.835	0.775	3.51 [7]	1.38 [120]
Mass density [g/cm^3], ρ	3.98	3.45 [33]	3.89 [121]	2.99 [122]	3.69 [123]	4.56 [7]
Melting point [°C]	2040	766 [37]	716 [37]	810 [37]	1870	1970
Specific heat capacity [J/g°C], C_p	0.761	0.842 [33]	0.76 [124]	0.935 [122]	1.05 [122]	0.59 [7]
Moh hardness	9	~3–4 [125]	~4	~4	8.5	8.5
Knoop hardness [kg/mm^2]	1800(//c), 2200(//a)	197 [7]	–	–	1600-2300 [126]	1320 [7]
Thermal conductivity [W/K.m], κ	30.3 (//a) 32.5 (//c) [127]	1, 1.8 (//a), 1.68, 3 (//c) [33,121,128]	1.3 (//a), 2.6 (//c) [121], 3.6 [13]	4.58 (//a) 5.14 (//c) [129]	23 (//a-b-c) [126, 130]	10 [129]
Thermal expansion coefficient [$x10^{-6}$/K], α	4.8 & 5.3 [129]	22.2, 25, 26 (//a) −9.8, −10, −8.1 (//c) [128,131,132]	12, 23 (//a) 0, −5.4 (//c) [128,131,132]	22, 21 (//a) 3.6, 3.1 (//c) [37, 122,132]	6 (//a) 6 (//b) 7 (//c) [123]	6.7 [129,133]
Thermal diffusivity [$x10^{-3}$ cm^2/s], D	92.5	6(//a), 10 (//c) [121]	4.4 (//a), 8.8 (//c)	16.4 (//a), 18.4 (//c)	60	37
Young modulus [$x10^9$ Pa], E	335	109 (avg) [33,128], 85 (//c) [128], 120 (//a) [128]	–	96 [122]	469 [123]	280 [122], 310 [7]
Poisson's Ratio, ν	0.29	0.3 [33]	–	0.25 [122]	–	0.3 [7]
Tensile (fracture) strength [$x10^6$ Pa], σ_f	400	38.5 ± 8 [7,128]	–	–	457-948 (//a), 520 (//b) [134]	200 [7]
Fracture toughness [$x10^6$ Pa $m^{1/2}$], K_{1c}	2.2 [129]	0.33, 0.4 [33,128,135]	–	0.31 [129] 0.18–0.37 [135]	2.6 [122]	1.4 [129]
Thermal figure of merit [W/$m^{1/2}$], $R_T^{'}$	22 [129]	0.42(//a), 0.80 (//c) [129]	0.55	0.53 [122,129]	14 [122]	5.1 [129]
Thermal shock resistance parameter [W/cm], R_T (for 2a = 50 μm flaw)	44	0.84(//a), 1.60 (//c) [129]	1.1 [136]	1.06	28	10.4 [136]
Maximum acceptable thermal power density (for t = 2 mm slab size) [kW/cm^3], $P_{ter,\ max}$	13.2	0.25	0.33	0.32	8.4	3.1
Maximum temperature difference before cracking, rod geometry [°C], $\Delta T_{max,rod}$	520	60(//a), 180 (//c)	60(//a), 290 (//c)	65(//a), 440 (//c)	275	270
Maximum temperature difference before cracking, thin disk geometry [°C], $\Delta T_{max,disk}$	740	85(//a), 265 (//c)	90(//a), 415 (//c)	87(//a), 590 (//c)	395	380
Damage threshold [J/cm^2]	7.8 @ 0.5 ps 80 @ 50 ps [137] 210 @ 8 ns [138]	1.5 @ 20 ps [139] 8-24 @ 50 ps [128]	20-26 @ 50 ps [128]	20-25 @ 50 ps [128]	270 @ 12 ns [130]	110 @ 4.5 ns [140]

we will discuss in more detail later, smaller values of thermal expansion coefficient is generally desired to minimize bulging/deformation contribution to thermally induced lensing [131]. An interesting property of Cr:LiSAF is its relatively large thermal expansion coefficients with opposite signs for a and c axis (expanding in an axis: 25×10^{-6}/K, contracting in c axis: -10×10^{-6}/K [131,132]). There is some variance in the reported values of thermal expansion in literature, but reported values for Cr:LiCAF is more homogenous and all positive in different axis [37,122,132]. Thermal expansion values for sapphire, Alexandrite and YAG are in the 5–7 $x10^{-6}$/K range [123,129]. For comparison, thermal expansion coefficient for glass is around 10×10^{-6}/K [7], and it is around 1×10^{-6}/K for diamond [146].

Thermal diffusivity (D) is the ratio of thermal conductivity (κ) to the product of specific heat capacity (C_p) and density of the material (ρ) and it is a measure of the rate of heat transfer for a material and determines how quickly a material reacts to a change in temperature (could also be named as thermal inertia). Specific heat capacity and mass density values of Cr:Colquiriites are similar to sapphire and alexandrite. On the other hand, due to their low thermal conductivity values, Cr:Colquiriites also possess an order of magnitude lower thermal diffusivity values compared to Sapphire, Alexandrite and YAG, and again the LiCAF host provides the highest value among Cr:Colquiriites.

Young modulus (E) is a measure of the stiffness of a material, and represents the ability of a material to withstand changes in length when under lengthwise tension or compression. Young's modulus of Cr:Colquiriites are around 100 GPa [7,33,122], about 1/3rd the

value of YAG (300 GPa) and sapphire (335 GPa) [122]. Among the laser materials considered in Table 2, Alexandrite has the highest value of Young modulus: 469 GPa [123]. For comparison young modulus for glass and diamond are >50 GPa and >1000 GPa, respectively [7].

Tensile (fracture) strength (σ_f) is the measure of maximum stress that a material can withstand while being stretched or pulled before breaking. The theoretically estimated tensile strength of materials is in the order of one tenth of the Young modulus (E/10) [147]. However, materials are more brittle in general due to their sensitivity to small flaws, and the real-life tensile strengths are orders of magnitude lower [147]. Unfortunately, the tensile strength of Cr:Colquiriite is measured to be only around 40 MPa, even smaller than typical glass (50 MPa) [7]. Note that, Ti:Sapphire (400 MPa), YAG (200 MPa) and Alexandrite (500–900 MPa) [134] all has much higher tensile strengths.

Fracture toughness (K_{1c}), is the ability of a material to resist fracture, and this parameter is related with the tensile strength (σ_f) of the material, but the relation depends on the fracture mechanism, and displays a wide variation across materials [147,148]. To relate this quantities, Marion introduces the following formula [147]:

$$K_{1c} = \sigma_f \sqrt{a} \tag{2}$$

where a is the one half the length of the pre-existing flaw that causes fracture. Note that the fracture toughness of the material (K_{1c}) is an intrinsic property of the material. On the other hand, tensile/fracture strength (σ_f) depends on extrinsic quality of the material, and earlier work has shown that it can be improved an order of magnitude by minimization of flaws via deep chemical polishing [147,149]. Note that, fracture toughness values for Cr:Colquiriites are in the 0.2–0.4 M Pa $m^{1/2}$ range, that is typical for fluoride laser hosts (e.g. YLF:0.27 M Pa $m^{1/2}$ [122]). These values are about 1/5th of the value in sapphire and alexandrite, indicating that Colquiriites would require 2–3 times smaller surface flaw size to reach similar σ_f values. However, looking at the measured values of σ_f in Table 2, we estimate a flaw size of 30 μm for Ti:Sapphire and 100 μm for Cr:LiSAF, resulting in a σ_f value for Cr:LiSAF that is 10 times lower than Ti:Sapphire. This shows that, due to their weak thermomechanical strength, it is also harder to obtain nice polishing finish with Cr:LiSAF samples, and they might require additional care to reach higher tensile fracture values.

Thermal shock parameter (R_T) is defined as:

$$R_T = \frac{K_{1c}\kappa(1-\nu)}{\alpha E\sqrt{a}} \tag{3}$$

where all the parameters are same as what is described above [33]. For materials selection process, a measure of the intrinsic strength is desired (similar to tensile and fracture toughness that is discussed) [147]. Removing the extrinsic parameter a, which depends on the quality of surface polish, an overall intrinsic thermo-mechanical figure of merit (also named as thermal-stress-resistance figure of merit) R_T' is usually defined as [33,147]:

$$R_T^{'} = R_T\sqrt{a} = \frac{K_{1c}\kappa(1-\nu)}{\alpha E} \tag{4}$$

Relevant values of thermal shock parameter and thermo-mechanical figure of merit for Cr:Colquiriite and others have been listed in Table 2. As it is also pointed out by Koechner, comparing the intrinsic thermal-stress-resistance figure of merit (R_T') parameters, it is clear that Cr:Colquiriites which has values around 0.5 W/$m^{1/2}$ are rather soft and mechanically weak materials with properties more related to glass [7,122,129]. Thermal-stress-resistance figure of merit for Ti:Sapphire is more than an order of magnitude better (22 W/$m^{1/2}$ [129]), enabling superior power scaling potential and reduced crystal damage due to thermally induced stress. YAG has a value of around 5 W/$m^{1/2}$ [129], but due to the lower quantum defect, thermal loading in Yb:YAG based lasers/amplifiers are usually much lower, enabling power scaling to kW average power levels [150]. Alexandrite also has quite large intrinsic thermo-mechanical figure of merit (14 W/$m^{1/2}$ [122]), providing the strength required in handling sometimes harsh requirements from the laser host. This parameter clearly shows the main intrinsic challenge in power scaling of Cr:Colquiriite systems.

There are other ways to look at this issue. For example, it can be shown that, for a slab amplifier cooled through two faces, the maximum thermal power density ($P_{ter,max}$) that may be applied without laser material fracture is given by:

$$P_{ter,\max} = \frac{12R_T}{t^2} \tag{5}$$

where R_T is the thermal shock parameter, t is the thickness of the slab [33]. For a 2 mm thick slab, the calculated values for the maximum heat load is presented in Table 2.). For Cr:LiSAF, $P_{ter,max}$ is estimated to be 0.25 kW/cm^3, and assuming a fractional thermal load of 50% (a safe number), and keeping the thermal load to 1/3rd of the maximum acceptable value, we end up with a safe pumping power density of around 150 W/cm^3. This analysis also clearly indicates advantages of Sapphire, YAG and Alexandrite over Cr:Colquiriites in handling higher (at least an order of magnitude) incident pump powers.

As another approach, the thermal stress and strain in rod and disc geometry of laser gain media could be calculated assuming plane-stress and plane-strain approximations, and then one can estimate the maximum temperature differences that the laser gain media can handle without fracture in rod and thin-disk geometry using [151]:

$$\Delta T_{\max,rod} \approx \frac{4(1-\nu)\sigma_f}{\sqrt{2}\alpha E} \tag{6}$$

$$\Delta T_{\max,disk} \approx \frac{4\sigma_f}{\sqrt{2}\alpha E} \quad (7)$$

Calculated parameters of $\Delta T_{max,rod}$ and $\Delta T_{max,disk}$ for Cr:Colquiriites, Yb:YAG, Ti:Sapphire and Alexandrite are presented in Table 2 (assuming a flaw size of $2a = 50\ \mu m$). Note that these numbers should be taken as rough estimates for comparison purposes only. The calculations show that in rod geometry, fracture could be observed in Cr:LiSAF at temperature difference values even around 50 C°, whereas Ti:Sapphire, Alexandrite and Yb:YAG could handle temperature differences above 200 C°. The simple estimate we have made here also clearly shows tendency of Cr:Colquiriite for thermally induced fracture, requiring great deal of attention in power scaling studies compared to Ti:Sapphire, Alexandrite and Yb:YAG. It is also interesting to see that, for the c axis, Cr:Colquiriite are expected to handle much higher temperature gradients, which might be used in optimizing the laser performance [152]. We also note here the potential advantage of thin-disk like laser structures in handling high power compared to regular slab geometry [152], which might be one of the promising paths for further power scaling of Cr:Colquiriite laser and amplifier systems.

Laser induced damage (F_{th}) of Cr:Colquiriites have been reported by Richardson et al. using 50 ps long pulses at 1064 nm [128]. Their results indicate a damage threshold of around 20 J/cm^2. Damage threshold of materials usually reported for 10 ns pulsewidths, and using the well-known heat diffusion dominated scaling of damage threshold with pulsewidth ($F_{th} \propto \sqrt{\tau}$) [153], the scaled value for 10 ns pulses is around 280 J/cm^2, which is similar to the vales measured for YAG, sapphire and Alexandrite [130,138,140]. Hence, on this respect Cr:Colquiriites seems to have similar peak power handling capability.

1.4. Spectroscopic parameters of Cr:Colquiriites

In the previous section we have presented a summary of thermo-mechanical properties of Cr:Colquiriite lasers, and discussed the challenges in terms of mechanical handling and power scaling. In this section, we will look at laser related optical and spectroscopic parameters of Cr:Colquiriites in comparison with Ti:Sapphire, Alexandrite and Yb:YAG laser gain media. Table 3 provides a detailed summary of relevant parameters.

Cr:Colquiriites are positive uniaxial materials with a refractive index of around 1.4. The nonlinear refractive index of Cr:Colquiriites are also relatively low. For example, Cr:LiCAF has an n_2 of $0.4 \times 10^{-16}\ cm^2/W$ [13,128], which is 1/8th the value for Ti:Sapphire ($3.2 \times 10^{-16}\ cm^2/W$). In mode-locking using the Kerr-effect the low n_2 value might be a disadvantage. On the other hand, for amplifiers, a low n_2 value could help to lower the overall B-integral of the system, minimize undesired degradation of beam quality and could serve positively to the design of high peak power amplifiers. Among Cr:Colquiriites, Cr:LiSAF has the highest n_2 value, providing easiness in Kerr-lens mode-locking studies.

One of the important parameters effecting the overall thermal lensing observed in laser crystals is the temperature dependence of refractive index (dn/dT parameter). One interesting property of Cr:Colquiriites is that they have negative thermal refractive coefficients for both axis, which is actually typical for the fluoride crystals [131,133]. We note here that, the thermal lensing due to the negative thermal refractive coefficients of Cr:Colquiriites tend to balance other contributions of thermal lens (bulging and stress induced), resulting in a relatively small and positive thermal lensing [131]. Unlike Cr:Colquiriites thermo-optic coefficients are positive and slightly larger in magnitude for YAG, sapphire and Alexandrite materials, and their overall thermal lens ends up being relatively larger [131]. As a result, in a first order discussion, we can say that Cr:Colquiriites are superior to YAG, sapphire and Alexandrite in terms of thermal lensing.

For the generation of ultrashort pulses, careful optimization of total cavity second and third order dispersion is required. Initially, there was some discrepancy between measured and calculated dispersion values for Cr:Colquiriites from reported Sellmeier equations; however, the issue has been resolved by careful measurement of dispersion parameters by several groups, and typical values are listed in Table 3 [53,154–158]. The group velocity dispersion (GVD, which is also named as second order dispersion) is in the order of 20–25 fs^2/mm for Cr:Colquiriites in the 800 nm region (around half to 1/3rd of what Sapphire, YAG and Alexandrite has), enabling easier dispersion control of the laser cavities when soliton pulse shaping is desired.

In order to discuss the relevant absorption and emission profiles, as an example, Tanabe-Sugano diagram and configurational coordinate diagram of energy levels for Cr^{+3} ions in the octahedral field [13,183,184], as well as a simplified energy level diagram for Cr:LiSAF without the configuration coordinate shift is shown in Fig. 3. In these systems, independent of the crystal field strength, the ground state is always the $^4A_2$ level [183]. In the Tanabe-Sugano diagram, "Dq/B″ parameter in the horizontal axis represents the normalized crystal field strength, and in the vertical axis the normalized energy difference between the lowest lying $^4A_2$ level and the excited states (E/B) are plotted [183]. Note from Fig. 3 (a) that, the energy difference between the $^4A_2$ level and ^2E level is relatively insensitive to the crystal field strength, since this interaction is due to spin-orbit coupling which is intrinsic to Cr^{+3} activators [14]. The transitions between the ground level and ^2E level is parity and spin forbidden, resulting in a metastable state with relatively long lifetime, and narrowband emission [13,14]. On the other hand, the energy difference between the laser active $^4T_2$ level and $^4A_2$ ground level is created by the crystal field (zero in free space for a free Cr^{+3} ion), and their separation follows an almost linear increase with the crystal field [14]. The phonon broadened transition between the $^4T_2$ level and the ground state is spin allowed, resulting in shorter lifetimes. Note that at around $Dq/B = 2.3$, $^4T_2$ and ^2E level crosses each other and become degenerate, creating a border crystal field strength value.

The solid vertical line in the Tanabe-Sugano diagram (Fig. 3 (a)) represents the low crystal field gain media (where $Dq/B < 2.3$), such as Cr:Colquiriites (e.g. $Dq/B = 2.15$ for Cr:LiCAF [178]), where the energy difference between the $^4T_2$ level and ground state is smaller than the energy of the ^2E level ($\Delta E<0$) [183]. As a result, the ^2E level lies within the phonon broadened $^4T_2$ level. The transition between

Table 3
Comparison of the spectroscopic and laser parameters of the Ti:Sapphire, Cr:LiSAF, Cr:LiSGaF, Cr:LiCAF, Alexandrite and Yb:YAG gain media.

Gain Medium	Ti^{3+}:Al_2O_3 (Ti:Sapphire)	Cr^{+3}:$LiSrAlF_6$ (Cr:LiSAF)	Cr^{+3}: $LiSrGaF_6$ (Cr:LiSGaF)	Cr^{+3}:$LiCaAlF_6$ (Cr:LiCAF)	Cr^{+3}:$BeAl_2O_4$ (Alexandrite)	Yb^{+3}:$Y_3Al_5O_{12}$ (Yb:YAG)
Birefringence	Negative uniaxial	Positive uniaxial	Positive uniaxial	Positive uniaxial	Biaxial	Isotropic
Refractive index, n	1.7655 (//a) 1.7573 (//c) [159]	1.3873 (//a) 1.3940 (//c) [158]	1.3893 (//a) 1.391 (//c) [158]	1.380 (//a) 1.3808 (//c) [158]	1.7367 (//a), 1.7421 (//b) 1.7346 (//c) [7]	1.82 [102]
Nonlinear refractive index [$x10^{-16}$ cm^2/W], n_2	3.2 [13]	0.8 [13] 0.52–2.15 [128]	1.2 [13]	0.4 [13] 0.36–0.66 [128]	2 [123], 3.54 [160]	6.9 [102]
Temperature dependence of refractive index [$x10^{-6}$/K], dn/dT	13 [120]	−2.5, −4.5 (//a) −4, −9.1 (//c) [121,131,132]	−7, −2.7 (//a) −1.8 (//c) [121,132]	−4.2, −7.3 (//a) −4.6, −4.9 (//c) [129,132]	5.5, 9.4 (//a) 7, 8.3 (//b) 14.9 (//c) [122,161]	9.9 [120]
Group velocity dispersion (fs^2/mm), GVD	56.6 [162]	22.7 [154,156]	~25 [157]	24 [53]	60.7 [163]	66.6 [142]
Third order dispersion (fs^3/mm), TOD	41.4 [162]	22.5 [154,156]	154 [158]	22 [53]	39.5 [163]	66.7 [142]
Pump wavelength (nm)	480 [24]	650	630	630	550 (//a), 595 (//b), 570(//c) [164]	940 [120]
Absorption bandwidth (nm)	125	100	85	90	90 (//a), 80 (//b), 70 (//c) [164]	12.5 [120]
Peak absorption cross section [$x10^{-20}$ cm^2], σ_{ab}	6.4 (//c), 2.6 (//a) [24]	4.5 (//c), 2.5 (//a) [136]	3 (//c), 1.5 (//a) [136]	1.3 (//c), 0.9 (//a) [136]	3.9 (//a), 19(//b), 9(//c) [165]	0.83 [120]
Maximum gain wavelength [nm]	790 [13]	855	840	780	750	1030
Quantum Defect (%), q_d	40	24	25	19	20	9
Gain bandwidth, FWHM (nm)	260	170	100	85	55	15
Tuning range [nm]	660-1180 [84]	770-1110 [56,57]	777-977 [51, 54]	720-887 [34,52]	714-818 (300 K) up to 858 nm (800 K) [166–169]	1016–1108
Minimum theoretical pulse duration [fs]	3.5	5.5	8	8.2	11.9	26
Demonstrated shortest pulse duration [fs]	~5 [48]	10 [58]	14 [55]	9 [53]	70 [50]	35 [66]
Peak emission cross section [$x10^{-20}$ cm^2], σ_{em}	41 (//c), 15 (//a) [24]	4.8 (//c), 1.6 (//a) [60]	3.3 (//c), 1.4 (//a) [37]	1.3 (//c), 0.9 (//a) [60]	0.7 @ 22 °C, 3 @ 290 °C (//b) [130]	2.1 [7]
Room-temperature fluorescence lifetime [μs], τ_f	3.2 [60]	67 [60]	88 [37]	175 [60]	262 [130]	940 [120]
$T_{1/2}$, τ_f ($T_{1/2}$) = 0.5τ_R [°C]	~100 [24]	69 [170]	88 [131]	190-255 [131, 170]	530 °C [166,171]	–
Radiative lifetime [μs], τ_R	3.9 [24]	67 [32]	88	200 [34]	1540 @ 0 K, 262 @ 300 K [130]	–
High temperature limit of the nonradiative lifetime [fs], τ_{NR0}	4×10^5 [24]	24 [170]	6.9 [172]	1.3 [170]	~750	–
Nonradiative decay activation energy [cm^{-1}], ΔE	2350 [24]	5125 [170]	5155 [172]	8532 [170]	~12000	–
$\sigma_{em}\tau_f$ [$x10^{-26}$ cm^2s]	131 [60]	322 [60]	290 [60]	228 [60]	183 @ 22 °C, 210 @ 290 °C [130]	1975
Auger upconversion rate [10^{-16} cm^3/s], γ	–	4 + 0.85*doping [33] 2.7 + 0.28*doping [173]	6.5 [136] 0.2 + 0.2*doping [157]	1.65 [136] 2.8 [174]	–	–
Intrinsic slope efficiency [%],η_0	64 [175]	53 [32], 54 [51]	52% [37], 60 [51]	67 [34], 69 [51]	65 [176]	>85% [177]
Relative strength of excited-state absorption at the laser wavelength	0 [24]	0.33 [136], 0.30 [178]	0.33 [37]	0.18 [136], 0.23 [178]	0.1 [179]	0 [180]
Passive losses [%/cm]	2 [85]	0.15 [52]	~0.15	0.15 [52]	0.06 [176]	–
Crystal figure of merit (FOM)	150 [85]	3300 [181]	~2000	2150 [52]	3000 [182]	–
Gain saturation fluence [J/cm^2], J_{sat}	0.6 (//c)	4.8 (//c)	7.5 (//c)	19.1 (//c)	38 @ 22 °C, 9 @ 290 °C (//c)	8.8 [102], 9.2
Gain saturation intensity [kW/cm^2]	189 (//c)	73 (//c)	86 (//c)	109 (//c)	145 @ 22 °C, 125@290 °C (//c)	9.7
Pump saturation intensity [kW/cm^2]	1210 (//c)	77.5 (//c)	94 (//c)	57 (//c)	5.3 (//b), 11.2 (//c)	24.5

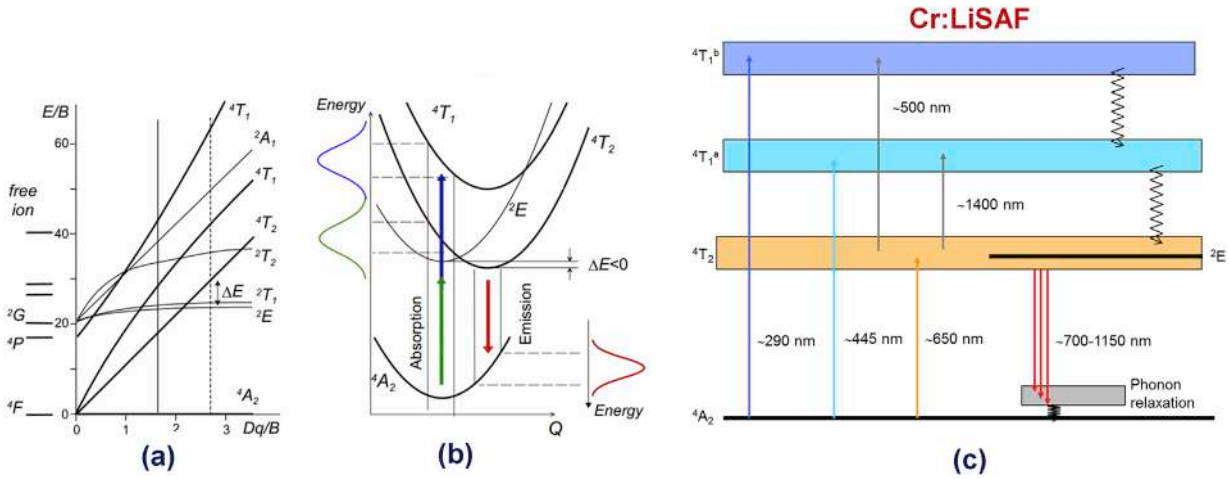

Fig. 3. (a) Simplified Tanabe-Sugano diagram and (b) configurational coordinate diagram of energy levels for Cr^{+3} ions in the octahedral field (Reprinted with permission from Ref. [13]). (c): A simplified energy level diagram for Cr:LiSAF.

^2E and $^4T_2$ states is very fast (in picosecond time scale). The lowest energy level of $^4T_2$ state ($^4T_2^a$) lies below the ^2E state; hence, at equilibrium the $^4T_2$ state is heavily populated, and the ^2E state does not play a significant role in lasing except acting like a reservoir (due to parity and spin forbidden nature of transitions from this level). In other Cr^{+3}-doped gain media, in a high strength crystal field ($Dq/B > 2.3$), like ruby ($Dq/B = 2.8$) and alexandrite, the ^2E energy state can be below the $^4T_2$ state (see the dashed line in the Tanabe-Sugano diagram in Fig. 3 (a)), which then considerably changes the laser properties [7,27,183]. Fig. 4 shows simplified energy level diagrams for ruby (a) and Alexandrite (b), where the main difference between Cr:LiSAF is the position of the ^2E energy level with respect to the $^4T_2$ level. Moreover, due to the large Dq/B value, energy differences between levels are larger, resulting in blue shifted absorption and emission profiles.

For example, as also mentioned in the introduction section, ruby (Cr^{+3}: Al_2O_3) is the first gain medium where lasing is demonstrated [8]. However unlike Cr:Colquiriites, ruby is not a phonon broadened laser system (Fig. 4 (a)). This is because, in ruby the ^2E energy level lies well below the $^4T_2$ level (~4.35 μm or ~2220 cm^{-1}). The excited state of the Cr^{+3} ion is a superposition of the $^4T_2$ and ^2E state, but at room temperature in thermal equilibrium, using Boltzmann distribution one can easily show that the population of the $^4T_2$ level is ignorable [27]. The $^4T_1$ and $^4T_2$ states have very short lifetimes (1 ps), and decay back to the metastable ^2E level, which has a lifetime of about 3 ms [7,27]. Hence, at room temperature, one can assume that only the ^2E state is occupied in ruby upon optical excitation. Lasing transition occurs between the ^2E and $^4A_2$ states and transitions between these states are not phonon broadened. So ruby lasing line around ~690 nm is quite sharp, enabling only ps pulse generation in mode-locked regime [185].

Before we proceed with Cr:Colquiriites, for the sake of completeness, we would like to review the situation in Alexandrite as well. As also discussed earlier, Alexandrite (Cr^{+3}: $BeAl_2O_4$) was the first broadly tunable ion solid state laser that can be operated at room temperature, which was discovered while trying to find an alternative to ruby [7,27,130,164,166,186,187]. Fig. 4 (b) shows a simplified energy level structure for alexandrite gain medium, which actually looks quite similar to ruby, where the ^2E state lies below the vibronically broadened $^4T_2$ level. However, the energy difference between the ^2E and $^4T_2$ levels is lower in alexandrite (~12.5 μm or ~800 cm^{-1}), which is only a few kT at room temperature (~48 μm). Hence, in thermal equilibrium, upon excitation, a reasonable level

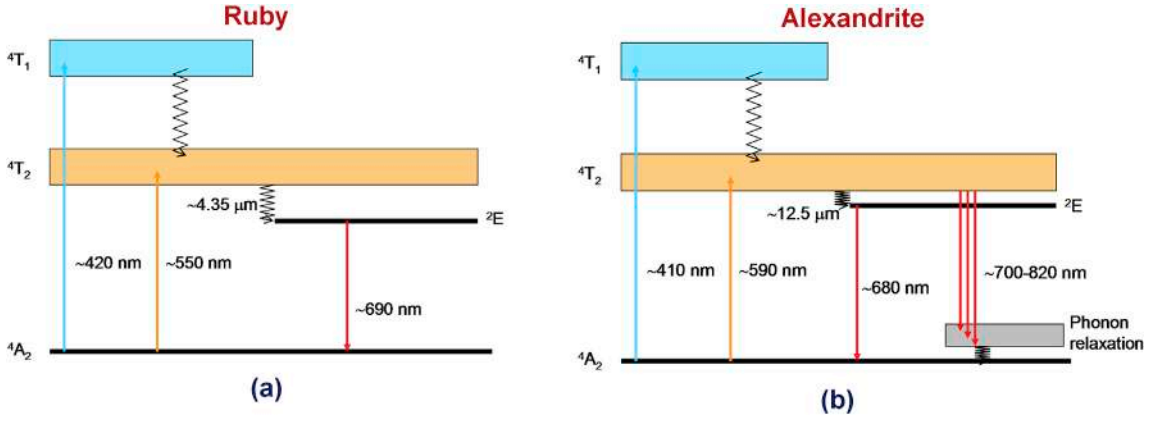

Fig. 4. Simplified energy level diagram for ruby (a) and for Alexandrite for E//c polarization (b).

of the states in the $^4T_2$ level is populated. Due to Franck-Condon principle, transitions from the $^4T_2$ level to $^4A_2$ is preferable over transition from the ^2E level to $^4A_2$ level; hence, alexandrite can produce broadly tunable laser radiation in the 700–820 nm wavelength range [7,27]. To increase the performance of alexandrite lasers, the crystal is usually held at elevated temperatures (~100 °C), which increases the effective emission cross section values for the $^4T_2$ level to $^4A_2$ transition [7,27,188]. In the last few years, Alexandrite gain media has seen a returned interest, and diode pumping as well as femtosecond operation have been investigated by several groups [50,168,169,182,189–194]. We believe that, with its superior mechanical properties, and interesting laser related spectroscopic properties, Alexandrite might become a strong competitor to Ti:Sapphire and Cr:Colquiriite laser and amplifier systems in the coming years.

As mentioned above, strong electron-phonon coupling in Cr^{+3}:Colquiriite gain media creates three strong and broad absorption bands (Fig. 5) that are centered around ~275 nm, ~445 nm ($^4A_2$ level to $^4T_1$ transition) and ~640 nm ($^4A_2$ level to $^4T_2$ transition) [32,36]. Existence of these broad absorption bands and a relatively long upper state lifetime, which allows reasonable energy storage, enable flashlamp pumping of Cr:Colquiriites. Even though flashlamp pumping is still used for pumping Cr:Colquiriites for some applications, direct diode pumping of Cr:Colquiriite by low cost AlGaAs and/or AlGaInP diodes around 650 nm enables a more advantageous approach. Note that, the absorption profile of Cr:Colquiriites are relatively broad, which enables wavelength flexibility in selection of the diode sources. Moreover, unlike for systems like Yb:YAG, the laser diodes do not require precise control of laser wavelength (and hence laser diode temperature). Also wavelength coupling of diodes at several different wavelengths could be applied to increase the diode brightness. Furthermore, the absorption cross section of Cr:Colquiriites are relatively high for both polarizations, enabling polarization coupling of diodes as well. Due to all these advantages, direct diode pumping of Cr:Colquiriite allows the construction of compact, efficient and low-cost laser systems. As another example, for Alexandrite, the absorption peak lies at 595 nm for E//b polarization, at 570 nm for E//c polarization, and at 550 nm for E//b polarization, respectively. Hence, with the currently available red diode technology, that could provide efficient emission in the 640–680 nm region, only the E//b polarization could be used effectively for diode pumping, and hence polarization coupling of pump diodes is not possible. Even for E//b polarization, the shortest wavelengths available from the state-of-the-art high power red diodes (640 nm) is relatively far away from the absorption peak (595 nm). This is probably one of the reasons for slower progress in diode pumped Alexandrite systems compared to Cr:Colquiriites. Also, for Ti:Sapphire the absorption band is centered around 480 nm and as mentioned earlier, diodes in this spectral region (blue and green) just became available in the last decade, resulting in even slower progress. What is clear is future progress in diode technology will play a significant role in what we could achieve with diode pumping of these systems.

Broad emission bands of Cr:Colquiriite centered around 800–850 nm region (Fig. 5), enables broadband tuning of laser wavelength as well as generation/amplification of ultrashort pulses. Birefringent nature of Cr:Colquiriites create an uneven strength of emission for the E//a and E//c polarizations, and this can be used as an advantage by exploiting the polarization with higher cross section in lasers/amplifiers (which is E//c in Colquiriites). Note that the cross section values in Cr:LiSAF and Cr:LiSGaF is around 2 times higher than Cr:LiCAF (Table 3). On the other hand, compared to Ti:Sapphire, emission cross section of Cr:Colquiriites are ~8–32 times lower. As will be discussed in detail later, a lower emission cross section increases the tendency of the laser towards q-switched mode-locking instabilities. Especially for Cr:LiCAF, which has the lowest emission cross section value among Cr:Colquiriites, the stable working range of cw mode-locked lasing is quite narrow for sub-50-fs pulses, and this issue will be discussed in more detail later (Fig. 32).

On the other hand, room temperature upper state fluorescence lifetimes of Cr:Colquiriites (τ_f) are ~20–55 times longer than Ti:Sapphire (67 μs in Cr:LiSAF compared to 3.2 μs in Ti:Sapphire). Hence, actually for Cr:Colquiriites the product of room temperature upper state lifetime and emission cross section ($\sigma_{em}\tau_f$) is ~2–2.5 times higher. Another major advantage of Cr:Colquiriites is the ability to grow high quality crystals with minimal passive losses below 0.15% per cm [52,135,181]. If we compare the figure of merit (FOM) of the crystals, which is defined as the ratio of absorption coefficient at the lasing wavelength to that at the pump wavelength, Cr:Colquiriite crystals has about one order of magnitude higher FOM than those for Ti:Sapphire (Table 2). Moreover, similar crystal quality could be obtained even from highly doped crystals. Lastly, Cr:Colquiriites do not suffer from concentration quenching of fluorescence lifetime, and the room-temperature fluorescence lifetime values reported in Table 3 for Cr:Colquiriites is doping independent. This enables efficient laser operation even in 100%-doped Cr:LiSAF (LiChrom: $LiSrCrF_6$) at least at low pumping intensities (we will discuss later that Auger upconversion process limits the usability of highly-doped crystals for strongly pumped systems) [25].

The laser threshold pump power (P_{th}) for continuous-wave operation could be estimated using [34,195]:

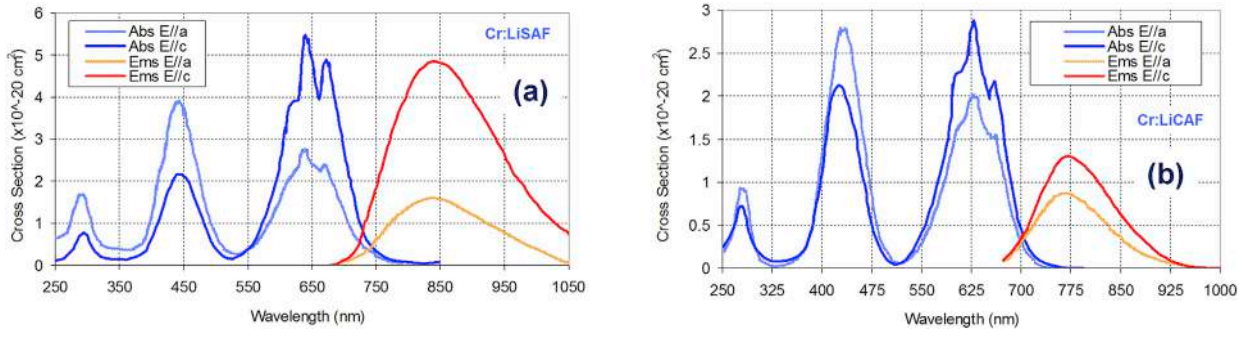

Fig. 5. Measured room-temperature absorption and emission spectrum of (a) Cr:LiSAF and (b) Cr:LiCAF gain media for E//a and E//c axis (Reproduced with permission from Refs. [32,36]).

$$P_{th} = \frac{\pi\left(w_p^2 + w_c^2\right)}{4(\sigma_{em} - \sigma_{ESA})\tau_f} \frac{h\nu_p}{\eta_p}(2A_g + T + L) \tag{8}$$

where h is Planck's constant, ν_p is the pump photon frequency, η_P is pumping efficiency, w_p (w_c) is the pump (cavity) beam waists, σ_{em} (σ_{ESA}) is the emission (excited state absorption) cross section, τ_f is the fluorescence lifetime of the upper laser level, A_g is the ground state absorption of the Cr^{3+} ions, L is the total round trip loss and T is the transmission of the output coupler. A larger $\sigma_{em}\tau_f$ product, along with low crystal passive losses results in record low lasing thresholds (sub mW) in Cr:Colquiriites, as it will be presented in the next sections.

In general a higher $\sigma_{em}\tau_f$ product also means a higher small signal gain, but in Cr:Colquiriites this is only true at low pumping densities. This is because small signal gain is proportional to the product of emission cross section and population inversion, and even though Cr:Colquiriites has a quite long upper state lifetime, it is not trivial to achieve high population inversion levels, since the fluorescence lifetime in Cr:Colquiriites is quite sensitive to temperature and inversion.

To elaborate this issue in detail, we need to look at the important mechanisms that play a role in population dynamics of Cr:Colquiriite lasers/amplifiers. In Cr:Colquiriites, there are four main mechanisms that contribute to thermal loading: (a) quantum defect, (b) thermal quenching of the upper laser level, (c) excited-state absorption, and (d) upconversion (Fig. 6). The first of these effects is the quantum defect, which is due to the energy difference between the pump (λ_p) and laser (λ_l) photons. As discussed above this phonon based effect also enables the desired absorption/emission broadening process, and facilitates the 4-level laser structure. However, as a side back, difference in energy is transferred to the crystal via nonradiative transitions (phonon emission) causing an inevitable heat source, and in that respect a pump wavelength as close to the laser wavelength as possible is desired. If we define the quantum defect q_d as ($1-\lambda_p/\lambda_l$), the quantum defect in Yb:YAG is around 9% (Table 3), and in Ti:Sapphire it is around 40%, which is the main advantage of Yb:YAG systems for power scaling. Cr:Colquiriites has quantum defect values in the 20–25% range, and among them Cr:LiCAF have the lowest value (19%).

The second mechanism, thermal quenching is a phenomenon where excited ions at the upper laser level, which ideally contributes to amplification/lasing process via stimulated emission, decays back to the ground state via nonradiative processes. As a result, the mechanism reduces achievable gain, reduces upper state lifetime via this nonradiative channel, and creates an undesired heat load. As noted by Stalder et al. in Cr:Colquiriites, this nonradiative processes is due to the tunneling of excited ions from excited vibrational states of the $^4T_2$ level to highly excited vibrational levels of the electronic $^4A_2$ ground state [170,196,197]. Mott equation is generally used to describe the strength of temperature-dependent nonradiative relaxation processes [198,199], where the temperature dependence of the fluorescence lifetime τ_f (T) is described using:

$$\frac{1}{\tau_f(T)} = \frac{1}{\tau_R} + \frac{1}{\tau_{NR}(T)} = \frac{1}{\tau_R} + \frac{1}{\tau_{NR0}} \mathrm{Exp}\left(-\frac{\Delta E}{kT}\right) \tag{9}$$

Here, τ_R^{-1} is the radiative decay rate, τ_{NR} $(T)^{-1}$ is the temperature-dependent nonradiative decay rate, τ_{NR0}^{-1} is the high temperature limit of the nonradiative decay rate, ΔE is the activation energy, k is the Boltzmann's constant and T is the absolute temperature in degrees Kelvin.

Fig. 7 shows the calculated variation of fluoresce lifetime with temperature in Cr:Colquiriites, Ti:Sapphire and Alexandrite (parameters that are used in the calculation is listed in Table 3) [131,170]. The table also lists the critical temperature, $T_{1/2}$ [170], which is the temperature at which the fluorescence lifetime drops to half of the radiative lifetime value (above this temperature thermal quenching starts to cause significant nonradiative decay of the excited-state ions from the upper laser level $|l\rangle$ to the ground state $|g\rangle$). Note that, among Cr:Colquirrites, Cr:LiSAF has the lowest critical temperature 69 °C for thermal quenching [170], indicating the difficulty of power scaling with this material. Actually, this property (sharp variation of lifetime with temperature) makes Cr:LiSAF a good temperature sensor also (Fig. 8 [200]). Within Cr:Colquiriites, Cr:LiCAF has the highest critical temperature for thermal quenching

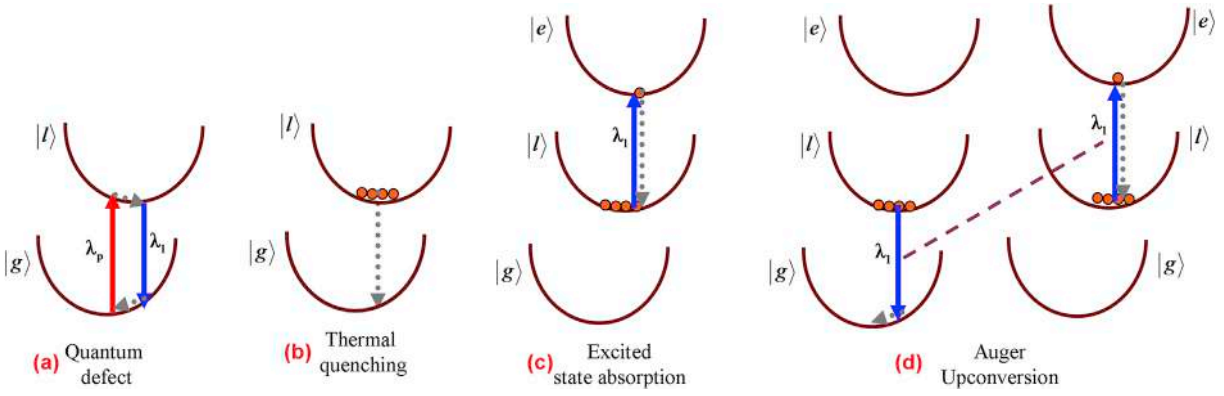

Fig. 6. (a) Quantum defect, (b) thermal quenching, (c) excited-state absorption (at the laser wavelength) and (d) Auger upconversion process cause thermal loading in Cr:Colquiriites.

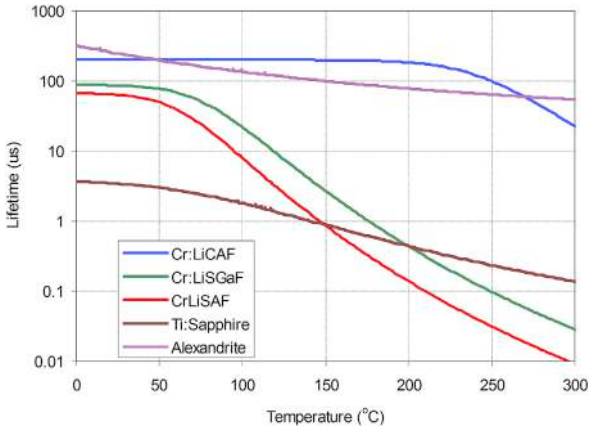

Fig. 7. Calculated effect of temperature on fluorescence lifetimes of Cr:LiCAF, Cr:LiSAF, Cr:LiSGaF, Ti:Sapphire and Alexandrite gain media.

(190–255 °C [131,170]), again making it the material of choice when power scaling is desired. Note that in Alexandrite $T_{1/2}$ is as high as 530 °C [166,171], and the observed shortening of fluorescence lifetime at lower temperatures is due to the strong coupling of the ^2E and $^4T_2$ levels: effective radiative lifetime also decreases, the quantum efficiency is known to be close to unity (0.95 ± 0.05) for temperatures below 425 °C [171,201]. This provides Alexandrite great advantages in power scaling studies. Before we pass to the third effect, we would like to underline the nonlinear nature of the lifetime thermal quenching process. Due to the cascading nature of this mechanism; the rate of heat generation via thermal quenching is itself temperature-dependent. Once thermal quenching becomes significant, and temperatures close to $T_{1/2}$ is reached, additional heating increases its rate even further in an exponential manner (fractional thermal load increases). This finally leads to a rapid decay of all the excited ions to the ground state, sometimes even leading to permanent damage to the crystal due to the low fracture toughness of Cr:Colquiriite gain media (as also observed several times by this author).

The third mechanism that creates thermal loading in Cr:Colquiriites is excited state absorption (ESA), where an ion in the upper laser level $|l\rangle$ absorbs a laser or a pump photon and gets promoted to a higher lying excited level $|e\rangle$ [32,34,37,178,202–205]. The ion then relaxes back to the upper laser level $|l\rangle$ via nonradiative decay, and hence heats up the crystal (Fig. 6 (c)). Hence, similar to thermal quenching, the process uses up an ion at the lasing level, which should ideally contribute to the lasing process and creates undesired heat load. For Cr^{3+}:Colquiriites, ESA at pump wavelengths is due to the transition between $^4T_2$ and $^4T_1^b$ (Fig. 3), covers the region from around 475–555 nm in Cr:LiCAF, and do not really pose a problem, especially while pumping with diodes around 650 nm [178]. Beaud et al. studied ESA at the lasing wavelength in Cr:LiCAF and Cr:LiSAF in detail as a function of wavelength (which is due to the transition between $^4T_2$ and $^4T_1^a$ levels) [178]. For Cr:LiSAF, ESA cross section is estimated to increase from about 1×10^{-20} cm^2 at 780 nm to around 2×10^{-20} cm^2 at 920 nm, and the peak is estimated to be at longer wavelengths [178]. Note that this corresponds to a relative ESA cross section (σ_{ESA}/σ_{em}) of around 30% at 850 nm. For Cr:LiCAF an ESA cross section of around 3×10^{-21} cm^2 is estimated around 800 nm, corresponding to a relative ESA cross section of 23% [178].

According to Caird analysis, the slope efficiency η of the laser can be expressed as:

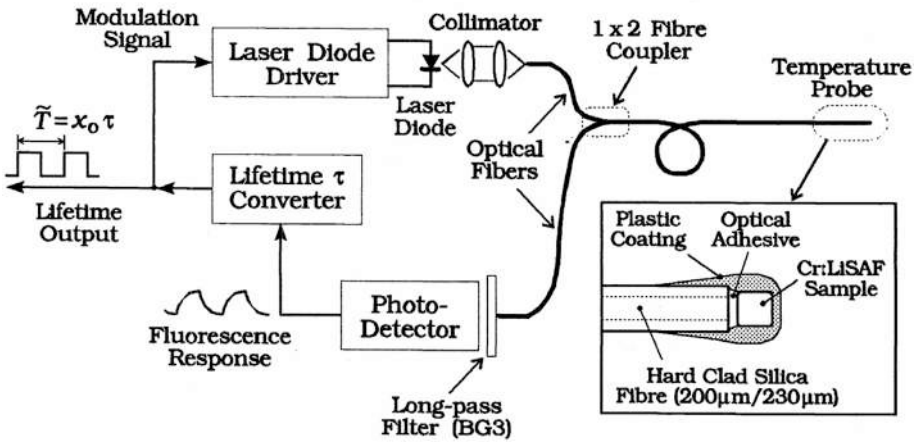

Fig. 8. A temperature sensor proposal based on temperature dependence of lifetime in Cr:LiSAF (Reprinted with permission from Ref. [200]).

$$\eta = \left[\left(\frac{h\nu_l}{h\nu_p}\right)\eta_p\left(\frac{\sigma_e - \sigma_{ESA}}{\sigma_e}\right)\right]\ \frac{T}{T+L} = \eta_0\frac{T}{T+L} \tag{10}$$

where ν_l is the laser photon frequency, η_0 is the maximum (intrinsic) slope efficiency that can be obtained at high output coupling and the other terms are same as Eq. (8). If we look at Eq. (8), we see that ESA increases the laser threshold, and from Eq. (10), we see that it also reduces the laser slope efficiency. Moreover, we can look at the effect of ESA on the small signal gain (g_0) of an amplifier, which can be calculated using [206,207]:

$$g_o = \frac{J_{sto}}{J_{sat}} \sim (\sigma_{em})\left(1 - \frac{\sigma_{ESA}}{\sigma_{em}}\right) \tag{11}$$

where J_{sat} is the saturation fluence of the gain medium ($J_{Sat} = h\nu/\sigma_{em}$), J_{Sto} is the stored energy density ($J_{Sto} = (E_{abs}/A_{eff})(\lambda_P/\lambda_L)$), E_{abs} is the stored pump energy, A_{eff} is the effective pump beam area. As it is also clear from Eq. (11), excited state absorption also decreases small signal gain in amplifiers. Note that unlike Cr:Colquiriites, Ti:Sapphire and Yb:YAG does not suffer from ESA, and relative strength of ESA is only around 10% in Alexandrite at room temperature (in Alexandrite ESA is also significant at pump wavelengths) [24,179,180,208,209]. Hence, ESA (especially at the lasing wavelength) is another significant mechanism that reduces the performance of Cr:Colquiriite lasers/amplifiers.

Another very important mechanism that creates thermal loading in Cr^{3+}:Colquiriites and limits the obtainable gain at high power levels is the Auger energy transfer upconversion (ETU) process [136,174,210,211]. In ETU, excited neighbor ions at the upper laser level $|l\rangle$ interact with each other and exchange energy, where the energy generated from decay of one of the ions is used to excite another neighboring ion to the upper lying excited level $|e\rangle$ (Fig. 6 (d)). Once excited to level $|e\rangle$, the ion non-radiatively decays back to the laser level $|l\rangle$ and heats up the crystal. ETU is due to the interaction of the ions in the upper laser level and it scales with the square of the upper state population density (N), meaning the process gets faster as inversion increases. Because of the ETU process, the fluorescence lifetime of the upper lying laser level depends on inversion density, and this dependence can be estimated using:

$$\frac{1}{\tau_f(N)} = \frac{1}{\tau_R} + \gamma N \tag{12}$$

where N is the population inversion density of the laser level $|l\rangle$ and γ is the Auger energy transfer upconversion rate. An important point here is, since ETU involves interaction of neighboring ions, the ETU rate (γ) is higher at crystals with higher doping. Table 3 lists the reported ETU rates for Cr:Colquiriites as a function of doping. Assuming a ETU rate of 2×10^{-16} cm^3/s for Cr:LiCAF and 5×10^{-16} cm^3/s for Cr:LiSAF (1% doping), we can calculate the expected variation of lifetime with inversion using Eq. (12), and the result is shown in Fig. 9 [33,136,174]. Since Auger upconversion process rate does not depend on temperature, it can be effective even at low temperatures depending on the inversion level. Due to ETU, the upper state lifetime of Cr:LiCAF decreases to half of its value at a population inversion density of 3.5×10^{19} ions/cm^3 (corresponds to a population inversion of around 45% for the 1% Cr-doped crystal). For Cr:LiSAF/Cr:LiSGaF Auger upconversion rate is even higher, and the critical inversion density is only around 2.8×10^{19} ions/cm^3, corresponding to a population inversion of around 32%. As mentioned these number are dopant concentration dependent, and for a 100% Cr-doped LiSAF, the ETU rate increases to 22×10^{-16} cm^3/s [211], and the critical inversion density decreases to 0.7×10^{19} ions/cm^3. It is clear from Eqs. (8), (11) and (12) that, Auger upconversion significantly limits the population inversion densities, lowers the small signal gain and increases the lasing threshold; hence, it is a very important factor to consider for an efficient laser and amplifier design. Basically, higher dopings should not be used in Cr:Colquiriites unless there is a strong motivation for it, and for all cases inversion should be kept below the critical inversion levels.

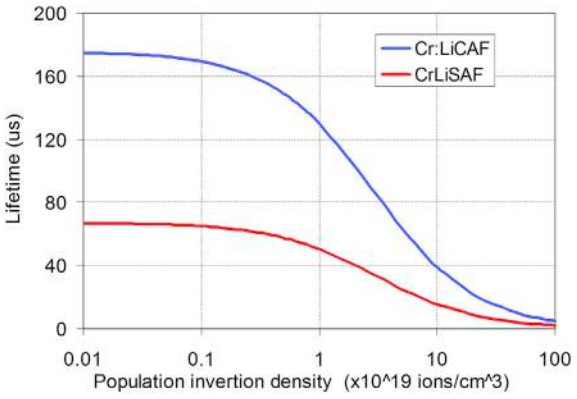

Fig. 9. Calculated effect of Auger upconversion process on fluorescence lifetimes of 1% Cr-doped Cr:LiCAF and Cr:LiSAF gain media.

1.5. Relevant laser technologies

In this section, we will briefly review two kinds of technologies that was routinely used in our studies with Cr:Colquiriites: (i) off-surface optical axis birefringent filters that is used in tuning of cw and femtosecond laser spectra, and (ii) Saturable Bragg Reflectors that is used in mode-locking experiments.

1.5.1. Birefringent filters

As discussed above, Cr:Colquiriite gain media possesses wide gain bandwidths that could provide ultra broadly tunable laser output with the usage of adequate intracavity tuning elements. Among all the options, birefringent filters (BRFs) provide a low-cost and easy to use solution for tuning. BRFs can be inserted at Brewster's angle inside the laser cavity and they do not require anti-reflective coatings. Moreover, tuning of the laser wavelength is facilitated simply by rotation of the birefringent plate about an axis normal to the surface, which increases the stability of the laser cavity.

In standard usage, the BRF optic axis lies on the surface of the filter, and such BRFs are named as on-surface optic axis birefringent filters or regular birefringent filters. On the other hand, for ultra-broad gain media, such as Cr:LiSAF, regular on-surface optic axis BRFs could not provide smooth tuning of laser wavelength in the whole emission range of the laser material. In a nutshell, due to their slow tuning rates regular BRFs could not accommodate a large enough free spectral range with acceptable modulation depth variation while tuning. As an alternative, BRFs with optic axis pointing out of its surface: (i) provides a much broader set of filter parameters, (ii) enables a smoother variation of modulation depth as the wavelength is tuned, (iii) generate larger free-spectral range values, (iv) facilitates faster tuning rates, and (iv) possess a larger range of useable filter rotation angles. These kind of filters are named as off-surface optic axis birefringent filters or diving optic axis birefringent filters, and we refer the reader to the following references for a detailed review of birefringent filter plate physics [81,212–216].

In our studies, a 3-mm-thick crystal quartz birefringent filter with an optical axis 45° to the surface of the plate was available, and it used for the tuning of the continuous-wave as well as femtosecond pulses. The same BRF also enabled two-color operation of Cr:LiSAF lasers. An analysis of this filter shows that filter orders between 2 and 38 could be reached with this plate [215], enabling adjustment of the filter spectral range (FSR) between 400 nm (800/2) and 21 nm (800/38). Especially, at the central wavelength of 800 nm, an FSR of 400 nm and 267 nm could be achieved at filter rotation angles of 7.5° and 16.8°, respectively. As an example, Fig. 10 shows the calculated transmission of the BRF containing linear laser cavity around the 3rd filter order (around 16.8°) for one round trip calculated using Jones matrices. As expected, around this order, the filter has an FSR of around 300 nm, a tuning rate of 40 nm/degree, and a full width half maximum of around 20 nm that could potentially enable tuning with sub-50-fs long pulses. Note that, the same filter order could also be used for tuning of the cw laser cavity. Finally, larger filter orders with smaller FSR values could be used to generate two-color operation [214,216,217] with Cr:Colquiriite lasers, as it will be presented later.

1.5.2. Saturable Bragg Reflectors (SBRs)

One widely used method to initiate femtosecond pulses in Cr:Colquiriites is by using semiconductor saturable Bragg reflectors (SBRs) [218], which are also known as semiconductor saturable absorber mirrors (SESAMs) [219–221]. SBRs provide self-starting, robust mode-locked operation with long-term stability. The laser systems with SBR mode-locking are quite immune to environmental fluctuations, have reduced cavity alignment sensitivities and provide higher optical-to-optical conversion efficiencies. On the other hand, in standard SBRs used for Cr:Colquiriites, absorbers are integrated onto AlAs/AlGaAs Bragg mirrors, and for SBRs designed for central wavelengths around 800 nm, the low-index contrast (Δn~0.5–0.6) between the layers limits the reflectivity bandwidth to around

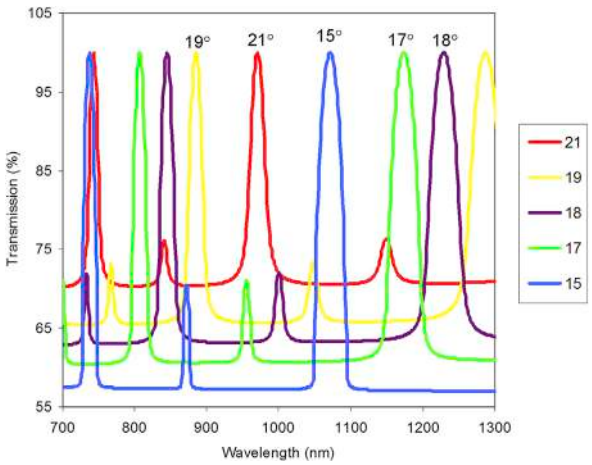

Fig. 10. Calculated transmission characteristics of the Cr:LiSAF laser cavity, as a function of wavelength for different birefringent plate rotation angles (rotation angles around the 3rd filter order is chosen). The calculation has been carried out for a 3-mm-thick crystal quartz BRF with an optical axis tilted 45° with respect to the surface of the plate.

50–60 nm [222]. As a result to cover the full tuning range of the laser, one might need to use several SBRs designed around slightly different central wavelengths. As an example, Fig. 11 shows small signal reflectivity of SBRs designed for Cr:Colquiriites at central reflectivity wavelengths of 800 nm, 825 nm, 860 nm, 880 nm and 925 nm. Note that each device only supports a limited reflectivity bandwidth, requiring the usage of different SBRs to achieve tuning in the whole gain bandwidth of Cr:Colquiriites.

As an example Fig. 12 shows the detailed structure of an SBR designed at a central wavelength of 860 nm. The SBR contains 25 pairs of $Al_{0.95}Ga_{0.05}As/Al_{0.10}Ga_{0.90}As$ as the Bragg stack, and a 7–nm-thick strained $In_{0.10}Ga_{0.90}As$ quantum well fabricated between $Al_{0.10}Ga_{0.90}As$ barriers as the absorber section (Fig. 13 (a)). Also considering the strain effects the band edge of the $In_{0.10}Ga_{0.90}As$ quantum well absorber is around 903 nm. Note that the position of the quantum well inside the standing wave electric field pattern was chosen to obtain a constant linear absorption over the reflectivity bandwidth of the absorber. Moreover, the quantum well thickness was chosen to remove any discontinuities in the density of states in the tuning range of the SBR (at this thickness, there is only one level in the conduction band of the quantum well absorber, so density of states is expected to be smooth). An additional SiO_2–TiO_2 pair could be used as a high-reflection (HR) coating on the surface of the SBR (Fig. 13 (b)). The calculated modulation depth of the SBR is 0.75% and 0.25% for regular and HR-coated versions, respectively. This specific SBR could potentially enable femtosecond tuning of Cr:LiSAF lasers in the 830–870 nm range.

1.6. CW and Quasi-CW lasing performance of Cr:Colquiriites

In this section, we will review continuous-wave and quasi continuous-wave (long pulse: ~>50 μs) lasing results obtained with Cr:Colquiriite gain media. As discussed earlier, broad (100 nm) and smooth absorption bands of Cr:Colquiriite around 650 nm enable direct diode pumping with low-cost red diode lasers. Several different diode types have been used to pump Cr:Colquiriite lasers to date, including single transverse-mode laser diodes (ridge waveguide lasers) [222–230], broad-stripe single-emitter multimode diodes [231–235], tapered diodes [236–239] and laser diode arrays [240,241]. State of the art single transverse-mode (single-mode:SMD) laser diodes provide about 170 mW of output power with an $M^2 < 1.1$ around 650 nm. One can calculate the brightness (B_r) of diodes using:

$$B_r = \frac{P}{\lambda^2 M_{eff}^2} \tag{13}$$

where P is the diode output power, λ is the diode emission wavelength and M^2_{eff} is the effective M^2 factor of the beam, which considers also asymmetric beam profiles ($M^2_{eff} = M^2_x\, M^2_y$) [242]. The corresponds brightness (B_r) of the state-of-the-art SMD diode is then about 330 mW/μm^2. In comparison, single-emitter multi transverse mode diodes (MMDs) with 150 μm stripe width are commercially available and provide up to 1.5 W output power. However, beam profiles of MMDs are asymmetric and of low quality (M^2_{slow}~10, M^2_{fast}<1.1), resulting in a similar brightness value of 320 mW/μm^2. Tapered diode lasers (TDLs) provide the beam quality of ridge waveguide lasers and the output power of broad-stripe single emitters [236,237]. TDLs consist of a straight ridge waveguide section and a tapered section, and any higher-order modes generated in the tapered section are filtered out by the ridge waveguide, resulting in an almost diffraction-limited beam profile [236]. Tapered diodes in the red spectral region could provide 1.2 W of output power at 675 nm together with M^2 values of 1.1 in the fast axis and 2.6 in the slow axis, corresponding to a brightness of about 1000 mW/μm^2. On the other hand tapered diodes are very sensitive to feedback, and great care should be taken while pumping the laser system on opposite sides. Finally, state-of-the-art multimode diode arrays might present very high power levels (40 W from an array), but at the expense of

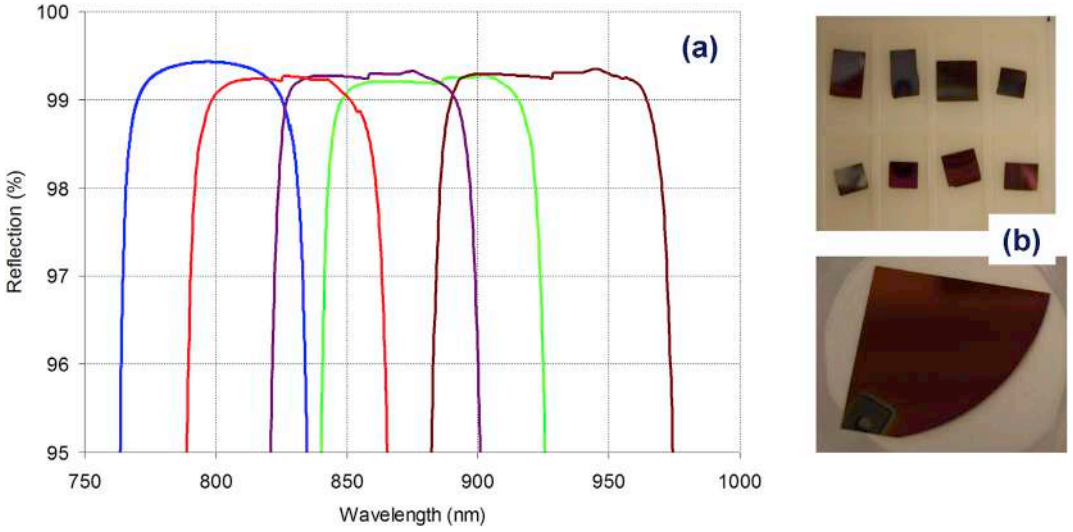

Fig. 11. (a) Calculated small signal reflection of AlGaAs/InGaAs based SBRs with a center wavelength of 800 nm, 825 nm, 860 nm, 880 nm and 925 nm. (b) Pictures of similar SBRs grown by molecular beam epitaxy at the Integrated Photonic Devices and Materials Group of MIT.

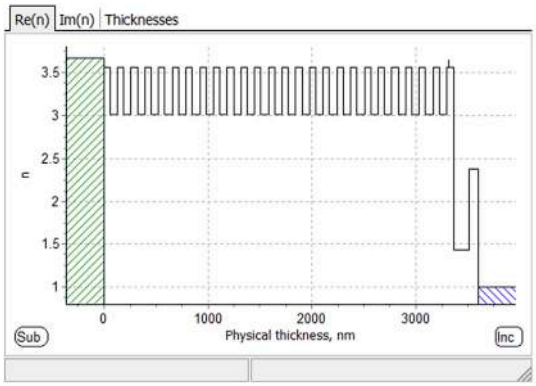

Layer	Material	Physical thickness (nm)	Refractive index	Purpose
0	GaAs	-	-	Substrate
1	$Al_{0.95}Ga_{0.05}As$	71.35	3.01	Bragg layer
2	$Al_{0.10}Ga_{0.90}As$	60.37	3.56	Bragg layer
...	...	...	...	Bragg layers
49	$Al_{0.95}Ga_{0.05}As$	71.35	3.01	Bragg layer
50	$Al_{0.10}Ga_{0.90}As$	60.37	3.56	Bragg layer
51	$Al_{0.95}Ga_{0.05}As$	71.35	3.01	Bragg layer
52	$Al_{0.10}Ga_{0.90}As$	15	3.56	Barrier
53	$In_{0.10}Ga_{0.90}As$	7	3.64	Absorber
54	$Al_{0.10}Ga_{0.90}As$	45	3.56	Barrier/cap

Fig. 12. (Left) Refractive index and physical thickness of each layer in a 860 nm SBR design. (Right) Detailed structure of the design with thickness and material information. The Bragg stack consists of 25 pairs of $Al_{0.10}Ga_{0.90}As/Al_{0.95}Ga_{0.05}As$ designed for a central wavelength of 860 nm. The 7-nm thick strained $In_{0.10}Ga_{0.90}As$ quantum well is sandwiched between $Al_{0.10}Ga_{0.90}As$ barriers. SiO_2–TiO_2 pair was used as a high-reflection (HR) coating on the surface.

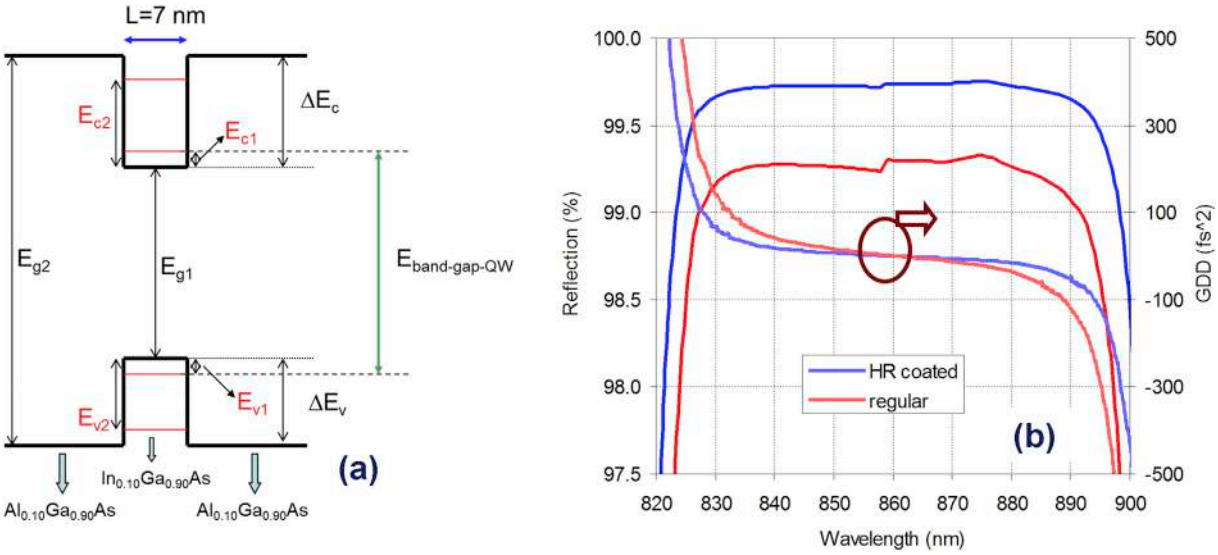

Fig. 13. (a) Structure of the 7-nm thick strained $In_{0.10}Ga_{0.90}As$ quantum well sandwiched between $Al_{0.10}Ga_{0.90}As$ barriers. (b) Calculated small signal reflection and group delay dispersion profiles of the 860 nm SBR. Regular indicates the as grown SBR, and HR-coated indicates the SBR that contains an additional single pair of SiO_2–TiO_2 HR coating on top.

reduced beam quality in the slow axis (M^2 of 250) [240], and hence posses even smaller brightness values (80 mW/μm^2). In the following sections, we will review continuous wave lasing performance obtained with Cr:Colquiriites using all of these different diode options.

As a side note, in this review we will be mostly focusing on diode pumping of Cr:Colquiriites due to many apparent advantages that it brings. On the other hand, we would like to mention that, in earlier work, Cr:Colquiriites have been pumped with many other different pump sources like flashlamps [203,243–246], Krypton lasers [55,155,247,248], Argon lasers [249–252], Alexandrite lasers [253], Ti:Sapphire lasers [53], second-harmonic (SH) of Nd:YLF (659 nm) [254,255], SH of Nd:YAG (532 nm) [256]. Many of these sources have lost their advantages with the development of high power and high brightens low-cost red laser diodes in the recent decades. On the other hand, we believe flash lamp pumping is still an interesting pumping route due to relatively long upper state lifetimes of Cr:Colquiriites. Moreover, flash lamps sources are relatively low cost and could provide very high peak powers, which might be attractive especially for high-energy, low-rep rate amplifiers. Hence, as the last part of this section, quasi-cw (long-pulse) operation results obtained under flashlamp pumping of Cr:Colquiriites will also be reviewed.

1.6.1. Cw performance with single-mode diode pumping

As we have discussed earlier (Eq. (8)), the pumping laser power required to attain steady-state lasing (P_{th}) is inversely proportional to the product of emission cross section (σ_{em}) and fluorescence lifetime (τ_f). Moreover, using theoretical considerations one can show that

this product ($\sigma_{em}\tau_f$) is inversely proportional to the linewidth of the transition [14]. As a result of this, earlier laser work has focused on laser media with narrow bandwidth to achieve cw lasing even under pumping with low brightness sources like flashlamps [14], and for broadband gain media like Cr:Colquiriites continuous wave lasing could not be achieved under flashlamp pumping [13] (to our knowledge only with the exception of Alexandrite [187,257]). As mentioned earlier, Alexandrite is the *first tunable laser* crystal operated at room temperature [164,166], and its broadband emission is discovered somehow by chance while searching for an alternative to the narrowband ruby laser [14]. Interestingly, Alexandrite is also the first broadly tunable solid-state laser that was directly diode pumped [258]. In this early work Scheps et al. achieved cw lasing with output power less than 1 mW, using only two 5 mW single mode diodes around 680.4 nm as the pump source [258] (direct pumping into the narrow linewidth storage level ^{2}E [182]). Just one year later, in 1991, two 10 mW SMD diodes around 670 nm has been used to attain cw lasing with sub-mw output powers in Cr:LiSAF [223]. Again a year later, SMD pumping was first applied to cw mode-locked operation of Cr:LiSAF by Valentine et al. [225]. These early studies proved the concept of low-cost and efficient diode-pumped tunable cw and femtosecond lasers that are based on Cr:Colquiriites [224,226–228]. It has been shown that nearly diffraction limited output beam profile of SMDs makes it possible to construct efficient and low-cost solid-state laser systems, and additional advantages including compactness, reduced cooling requirements, portability, improved electrical efficiency and low laser noise bas been achieved.

In recent years, progress in diode technology has enabled the production of higher brightness single-mode diodes in the red spectral window (630–680 nm) and others. Output powers from SMDs increased from around 5 mW level [258] to above 180 mW over the last 20–25 years [169,181]. More importantly, the cost per watt of output power has also been steadily decreasing. With the progress of SMD lasers, efficient cw lasing has been demonstrated in many solid state gain media to date, including Nd:YAG [259], Nd:Glass [260], Cr:LiCAF [261], Cr:LiSAF [223], Yb:YAG [262], Tm:YAG [263], and Alexandrite [258]. In this section, we present cw operation results of Cr:LiCAF and Cr:LiSAF lasers pumped by one state-of-the-art SMD.

A schematic of a typical SMD pumped continuous-wave Cr:Colquiriite laser cavity is shown in Fig. 14. An x-folded, astigmatically compensated laser cavity was employed in our cw laser experiments. The resonator had two curved mirrors (M1 and M2, usually R = 50–75 mm), a flat end mirror (M3), and a flat output coupler (OC). Pump light was coupled through M1, a dichroic mirror which transmits pump light and reflects intracavity laser light. The total cavity length, and arm length was adjusted to reach beam waists of ~15–20 μm inside the laser crystals. A quartz birefringent filter (BRF, as details discussed above) was inserted at Brewster's angle inside the laser resonator for laser wavelength tuning. All the high reflective mirrors had superior reflectivity properties (R>99.99%) to enable construction of a high-Q-cavity. We note here that regular mirrors designed for Ti:Sapphire (with typical reflectivities of ~99.9%) is not sufficient for efficient operation of Cr:Colquiriite lasers due to their sensitivity to losses.

A 660-nm, linearly polarized AlGaInP multi quantum well SMD with a diffraction-limited beam profile was used as the pump source (HL6545MG, Hitachi). Up to 130 mW of out power was provided by the pump diode at a drive current of 180 mA (at 2.5 V driving voltage), corresponding to an electrical-to-optical conversion efficiency of 30% (450 mW electrical consumption). Eight AA type batteries could be used along with a low-cost driver board (LD1255, Thorlabs, ~$100) to power the diodes for 8–10 h. The highly reliable pump diode is used commercially in DVD-writers as well, providing long-term reliable operation. If desired, the diode could be overdriven to obtain 150–160 mW of output power at the expense of reduced diode lifetime. A built-in cylindrical microlens was used to obtain a circular beam profile from the SMD, which eitherwise had an asymmetric output beam profile with an aspect ratio of approximately 2 ($\theta_{\perp}\approx17°$, $\theta//\approx10°$). The diode is commercially available at a cost of only $150 with the build-in cylindrical microlens (VPSL-0660-130-X-5-G, Blue Sky Research). A commercial collimating tube package that uses a 4.5 mm focal length aspheric lens with an NA of 0.55 (LT230P–B, Thorlabs) was used to mount the diode without any active cooling. We note hear that there are other SMDs with even higher output powers such as HL6385DG (642 nm, 170 mW) and HL63133DG (637 nm, 170 mW); however, these diodes require active cooling. In our study we have chosen to use HL6545MG (660 nm, 130 mW) due to its superior thermal specifications. Cr:Colquiriite crystals do not also require active cooling at these pump power levels, which greatly reduces the complexity of the system, saves on cooling costs, and enables the construction of a portable system. The overall estimated material cost of the system is below $5k, the entire laser system has a footprint of only 20 cm × 30 cm, making the system ideal for applications that require portability. A lens of a focal length of 60 mm focused the collimated pump beam into the Cr:LiSAF crystal to a spot size matching the cavity mode, where the 4.5 mm focal length collimating lens within its housing is translated to adjust the focused spot size. A 5% Cr-doped, 4-mm-long, 1-mm thick, Brewster-cut Cr:LiCAF, and a 1.5% Cr-doped, 7-mm-long 2-mm thick, Brewster-cut Cr:LiSAF crystals were employed as active mediums. The Cr:LiCAF crystals used in this study were grown at Leibniz Institute for Crystal Growth in Germany [135], whereas the Cr:LiSAF crystals were obtained from VLOC. Cr:LiCAF and Cr:LiSAF crystals absorbed 95% and 99.5% of the incident TM polarized

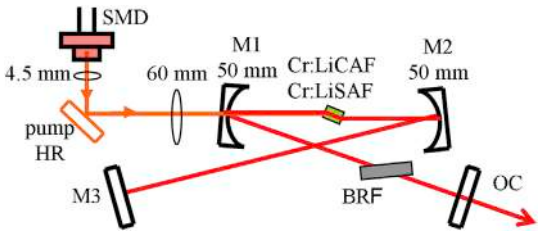

Fig. 14. Schematic of the cw Cr:LiCAF/Cr:LiSAF laser setup. The x-cavity is end-pumped by one 130 mW single-spatial-mode diode (SMD) at 660 nm. BRF: birefringent filter.

pump light at 660 nm, respectively.

Measured cw laser efficiencies of SMD pumped Cr:LiSAF (a) and Cr:LiCAF (b) at representative levels of output coupling are shown in Fig. 15. Using Cr:LiSAF gain media, an output power as high as 58 mW was obtained at an absorbed pump power of 125 mW using the 1% OC. The corresponding lasing threshold and the slope efficiency were 11.2 mW and 52%, respectively. In the case of Cr:LiCAF, the best power performance was obtained with the 0.9% transmitting output coupler where up to 63 mW of output power was obtained at an absorbed pump power of 135 mW (slightly overdriven pump diode). The corresponding lasing threshold and the slope efficiency were 15.3 mW and 53%, respectively. The transverse mode profile of the output beam was symmetric and circular with M^2 below 1.1 in all cases. The measured slope efficiency of the lasers comes close to the reported intrinsic slope efficiency values from the literature, highlighting efficient mode-matching between the pump and cavity modes in our setup. The free running laser output wavelength was around 790 nm for Cr:LiCAF and 860 nm for Cr:LiSAF and shifted only slightly for the different output couplers used.

Similar output power levels above 40 mW were obtained with output couplings in the 0.5–1.5% range, and above these output coupling the obtainable power levels has decreased sharply (Fig. 16). We note here that some portion of this power decrease at high output coupling is due to the Auger upconversion process. Using a high reflector as the output coupler, we have measured record low lasing thresholds of 2 mW with Cr:LiSAF and 3 mW with Cr:LiCAF. Earlier lasing threshold as low as 0.65 mW has been reported with Cr:LiSAF [264], which is to our knowledge one of the lowest lasing thresholds that could be attained from solid-state lasers. These ultralow lasing thresholds enables the usage of pump power efficiently compared to Ti:Sapphire where higher passive losses and sometimes even pump induced parasitic losses results in lasing thresholds above 200 mW [86,265].

Findlay-Clay analysis [34,195] has been employed (Eq. (8)) to estimate the passive losses. Total cavity losses per round trip is estimated to be (0.3 ± 0.1) % for Cr:LiSAF and (0.15 ± 0.05) % for Cr:LiCAF, respectively. This corresponds to a maximum loss level of 0.2% per cm for the Cr:LiSAF and 0.14% per cm for Cr:LiCAF crystal. When we look at the figure of merit (FOM) of the crystals (defined as the ratio of absorption coefficient at the pump wavelength (660 nm) to the absorption coefficient at the lasing wavelength (800 nm or 850 nm)), the Cr:LiCAF and Cr:LiSAF crystals that were used in this study has an estimated FOM of about 2150 ($\cong$ 3/0.0014), and 3300 ($\cong$ 5/0.0015), respectively. Similarly, large FOM (3000) Alexandrite crystals has been reported [182]. On the other hand, Ti:Sapphire has a loss level of around 2% per cm and a FOM of about 150 for typical crystals [85], and a FOM of 500 is only possible for specially ordered hand-selected crystals. The FOM advantage enables the construction of high-Q-cavities with Cr:Colquiriites, where one can store energy efficiently. As an example, in this 150 mW diode pumped system described above, the stored intracavity power levels reach 25 W level at low output coupling (150–200 fold power enhancement). The stored intracavity power can then be used to perform efficient nonlinear conversion even for the cw cavities, as we will describe in more detail below. Moreover, the high-Q-cavities with low passive losses have advantages in building ultra-low-noise oscillators [266].

Figs. 17 and 18 summarizes cw tuning studies performed with the one SMD pumped Cr:LiCAF and Cr:LiSAF lasers respectively. Laser wavelength tuning has been performed simply by rotation of the quartz birefringent filter. Cr:LiCAF laser could be tuned smoothly from 750 nm to 871 nm using a 0.5% output coupler. Decreasing the output coupling to 0.1% enabled extension of the cw tuning range to 746–879 nm, where as an all HR cavity provided tuning in the 746–887 nm range. Cw tuning of Cr:LiCAF laser below 746 nm was not possible due to the self-absorption losses from the laser crystal (emission and absorption band overlap in these region, as in quasi-3-level lasers such as Yb:YAG). Payne et al. realized tuning between 720 and 840 nm in quasi cw operation of Cr:LiCAF (1 ms pulses at 52 Hz, 5.2% duty-cycle, about 2 W incident pump power) [34]. On the long wavelength side, the emission spectrum of Cr:LiCAF laser extends into the infrared to around 925 nm; however, due to the presence of ESA, the effective gain of the system becomes negative for wavelengths above about 895 nm for π-polarized light [34,203], preventing laser emission. In the case of Cr:LiSAF, using a 1% output coupler, the Cr:LiSAF laser could be tuned from 780 to 1050 nm (Fig. 18). Self-absorption losses limited tuning of Cr:LiSAF laser below 780 nm [56,230,267,268]. Lowering the output coupling to 0.4%, the long wave tuning limit has been extended to around 1090 nm. Further reduction of the output coupling to 0.015%, enabled tuning up to 1110 nm.

In the tuning results above, we have used low orders (2nd and 3rd) of the birefringent filter with large FSR values, which allowed

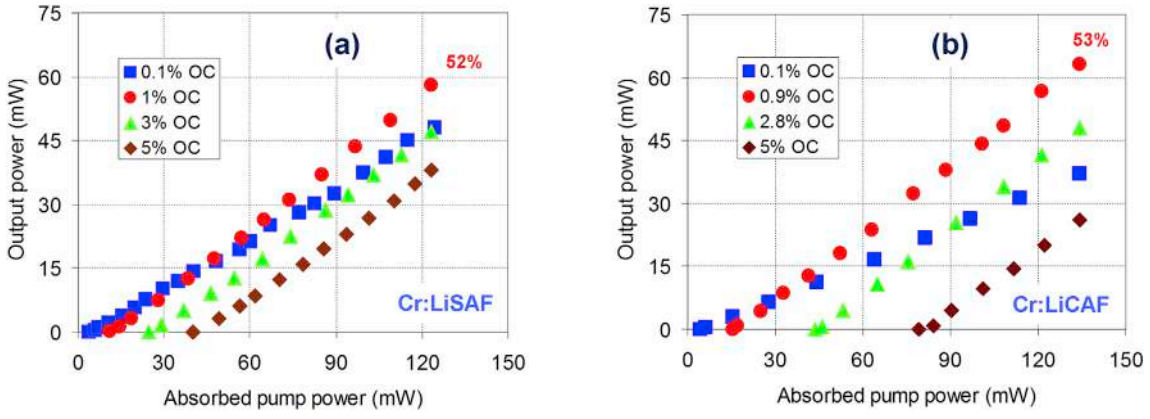

Fig. 15. Continuous-wave power efficiency curves for one single-mode-diode pumped (a) Cr:LiSAF [181], and (b) Cr:LiCAF [52] lasers taken at different output coupling (OC) values. Reproduced with permission from Refs. [52,181].

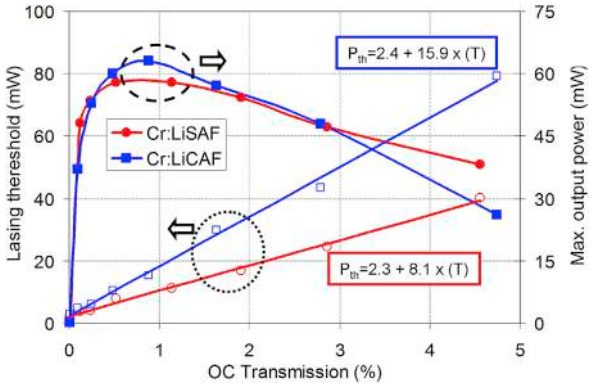

Fig. 16. Right axis: Variation of cw output power of SMD pumped Cr:LiSAF and Cr:LiCAF lasers with output coupling at 125 mW (Cr:LiSAF) and 135 mW (Cr:LiCAF) of absorbed pump power [52,181]. Left axis: Measured variation of the pump power required to attain lasing (P_{th}) as a function of OC transmission T for SMD pumped Cr:LiSAF and Cr:LiCAF lasers. Reproduced with permission from Refs. [52,181].

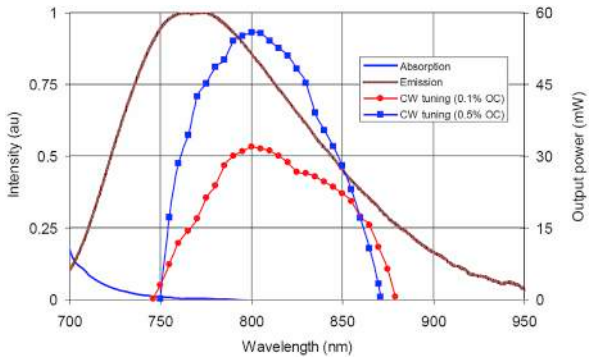

Fig. 17. Continuous-wave tuning curves of Cr:LiCAF laser taken with 0.5% (750–871 nm) and 0.1% (746–879 nm) OCs [52]. Normalized absorption and emission cross section curves are also shown for the c axis. Reproduced with permission from Ref. [52].

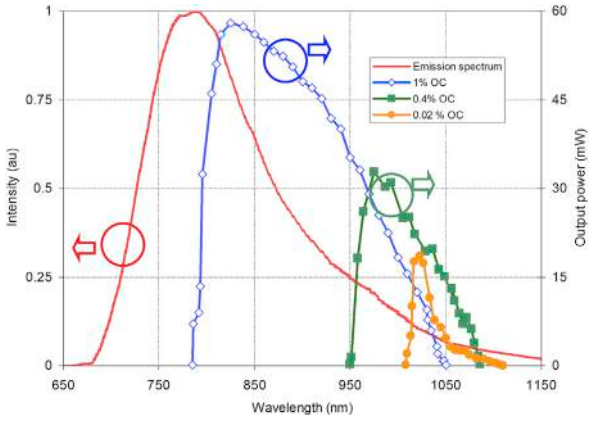

Fig. 18. Continuous-wave tuning curves for Cr:LiSAF (780–1110 nm) taken with different output couplers [181]. Normalized emission cross section curve is also shown for the c axis. Reproduced with permission from Ref. [181].

smooth tuning of Cr:Colquiriite lasers with single wavelength lasing. We also note here that, it was possible to obtain two-color cw operation in the Cr:LiSAF laser using higher orders of the same BRF filter. Multi-color operation of lasers is interesting for many applications such as terahertz generation [269–271], optical communication [272,273], remote sensing [274], and digital holographic microscopy [275]. Using different large orders of the BRF with varying free-spectral range values, it was possible to obtain two-color cw operation in the Cr:LiSAF laser at 10 different wavelength pairs (Fig. 19) [214]. For example, at a central wavelength of 860 nm, a filter orders of 10, 20 and 30, will result in an FSR values of around 86 nm (860/10), 43 nm (860/20) and 29 nm (860/30). As can be observed

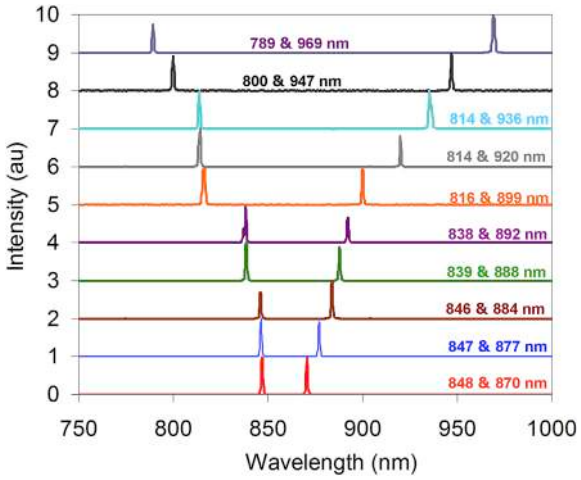

Fig. 19. Sample optical spectra obtained in dual-wavelength operation of the cw Cr:LiSAF laser (reproduced with permission from Ref. [214]).

from Fig. 19, two-color operation with wavelength separations close to these values could all be obtained from the Cr:LiSAF laser, indicating the flexibility of this method in implementing multicolor lasers.

We have seen that the output power levels obtained from Cr:Colquiriite lasers pumped with one single-mode diode might already be enough for some applications like amplifier seeding, spectroscopy, imaging, etc … We believe this one SMD pumped system has advantages in terms of simplicity and cost reduction. If power scaling to higher average powers is desired, one approach is to pump the Cr:Colquiriite lasers with more single mode diodes. As an example Fig. 20 shows a Cr:Colquiriite laser pumped by 6 SMD diodes. The system is pumped by 3 diodes from each side. To couple 3 diodes together, first an SMD at 640 nm is wavelength coupled with another SMD at 660 nm using a dichroic filter. Then these are polarization multiplexed with another 640 nm diode using a polarizing beam splitter (PBS) cube. Up to 1 W of pump power is then available to pump the crystal from these 6 diodes, and continuous-wave output powers above 400 mW could be obtained. Note that for this case, cooling of the crystal as well as the diodes are required. In the following section, we will discuss another approach for power scaling of Cr:Colquiriites: usage of higher power multimode diodes.

1.6.2. Cw and quasi-cw performance with single-emitter multi-mode diode pumping

As mentioned above another method for power scaling of Cr:Colquiriite lasers is usage of higher power multimode diodes as pump sources. Single-emitter broad-stripe diodes (also known as broad area laser diodes or broad emitter laser diodes) emit the pump light from a broader area, and could provide higher pump powers from a multimode-beam. Fig. 21 shows a simplified schematic of the multimode diode-pumped Cr:LiCAF/Cr:LiSAF laser cavity that is used in continuous wave laser experiments. Four state-of-the-art 665 nm linearly-polarized 1.8-W single-emitter multi-mode diodes (MMD-1 to MMD-4) from n-Light Photonics were used as the pump source. Each MMD has a transverse area of 1 μm × 150 μm and contains built-in cylindrical microlenses to collimate the beam along the fast axis (perpendicular to the plane of the junction). The transverse pump characteristics were multimode along the slow axis with an M^2 value of approximately 10, and diffraction-limited along the fast axis with an M^2 below 1.1.

Similar to SMD pumping, the output of the MMD lasers was first collimated with an aspheric lens with a numerical aperture of 0.54 and focal length of f = 4.5 mm. Using a polarizing beam splitter cube (PBS) two of the diodes (MMD1-MMD3) were combined with

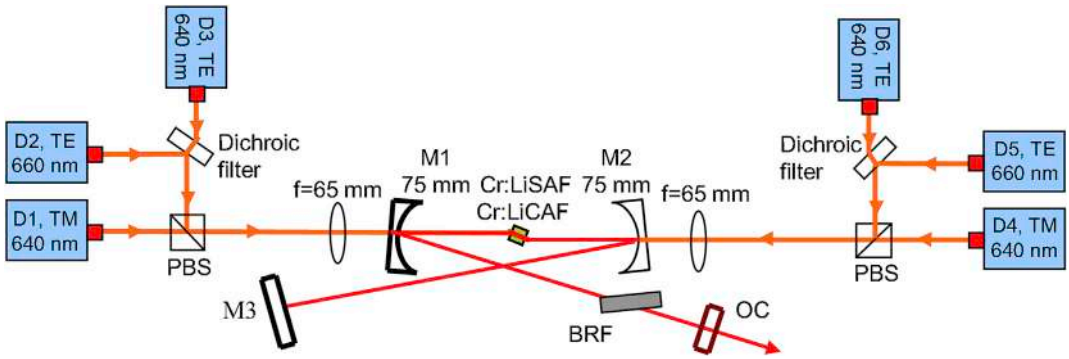

Fig. 20. Schematic of the Cr:LiSAF/Cr:LiCAF laser pumped by six single-mode diodes. PBS, polarizing beam splitter cube; BRF, birefringent tuning filter; D1–D6, diodes 1–6. As much as 400 mW of cw output power is obtained with about 900 mW of absorbed pump power, where the lasing threshold and slope efficiency were 25 mW and 46%, respectively.

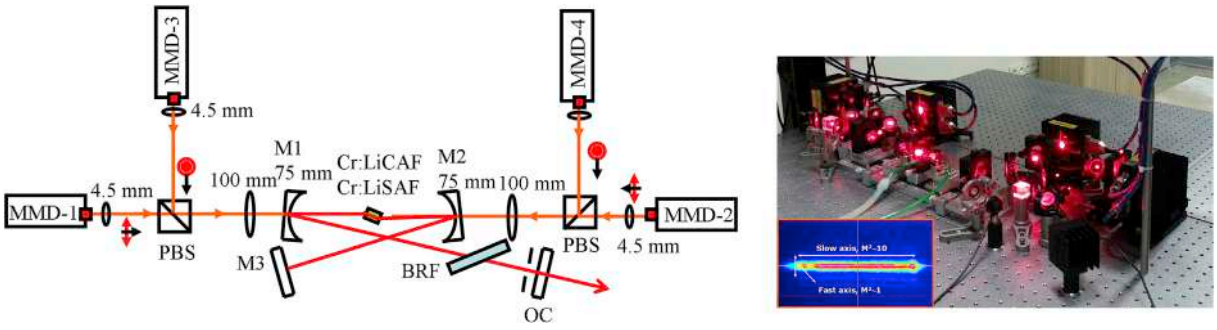

Fig. 21. (left): Experimental setup of cw Cr:LiCAF/Cr:LiSAF lasers pumped by four single-emitter multi-mode diodes (MMDs). (Right): A picture of the setup. Inlet figure shows the beam profile of the multimode diodes.

polarization multiplexing to pump the crystal from one side. The output of MMD-2 and MMD-4 were combined in a similar manner for pumping the crystal from the other direction. After passing through the PBS cubes, the pump beams were focused inside the laser crystal to a spot size of about 25 μm × 100 μm using 100 mm focal length achromatic doublets. The cavity used in cw experiments is similar to what has been described earlier for SMD diode pumping. Larger radius of curvature (75 or 100 mm) pump mirrors and shorter cavity arm lengths are usually employed in MMD pumping, to match to the larger pump spot. Moreover, a vertical slit was also inserted near the output coupler to enable control of the laser output transverse mode.

Fig. 22 shows the measured variation of the laser output power using crystals with different length and doping for the multi-mode diode pumped Cr:LiSAF and Cr:LiCAF laser at 0.75% and 1% output coupling, respectively. In the Cr:LiSAF laser, we have obtained the highest cw laser powers using the 20 mm long 0.8% Cr-doped sample. With this crystal the laser had a lasing threshold of 500 mW and provided up to 2.4 W of cw output power at an absorbed pump power level of 5.45 W. The corresponding slope efficiency with respect to absorbed pump power were 50%, just a few percent below the intrinsic efficiency for system (54% [32]), indicating good mode-matching between the pump and the laser modes. With the other crystals, obtained output powers were lower due to increased role of thermal effects, owing to increased doping and/or decreased crystal length. The optical-to-optical conversion efficiency of the system with respect to the incident pump power was above 33%. Similar results have been obtained with the Cr:LiCAF gain media, where again among the two dopings we have at hand (5 and 10%), and the lower % Cr-doped crystal provided the highest output power. The laser provided up to 2550 mW of output power with 5.48 W of absorbed pump and had a slope efficiency of 49%.

We note here that in the above measurements, the chiller temperature that was cooling the copper holder holding the laser crystals via circulating water was set to 15 °C. Unfortunately, during several of the power scaling experiments we have observed cracking inside the Cr:LiCAF and Cr:LiSAF crystals due to thermal effects. To elaborate this issue, as an example Fig. 23 shows the calculated temperature distribution inside the 0.75% Cr-doped, 1.5 mm thick 20 mm long Cr:LiSAF crystal, while pumped by 2 × 2.5 W of pump power. In this calculation the crystal is assumed to be in thermal contact from top and bottom sides to the thermally cooled copper at 15 °C. A heat transfer coefficient of 5 kW/m^{2}K was presumed between the copper holder and the crystal. Moreover, the fractional thermal load is assumed to be around 35%. Note that the estimated temperatures inside the crystal already exceeds 40 °C, resulting in a temperature difference above 25 °C. As we discussed earlier, in rod geometry, a temperature difference of around 50 °C is enough to

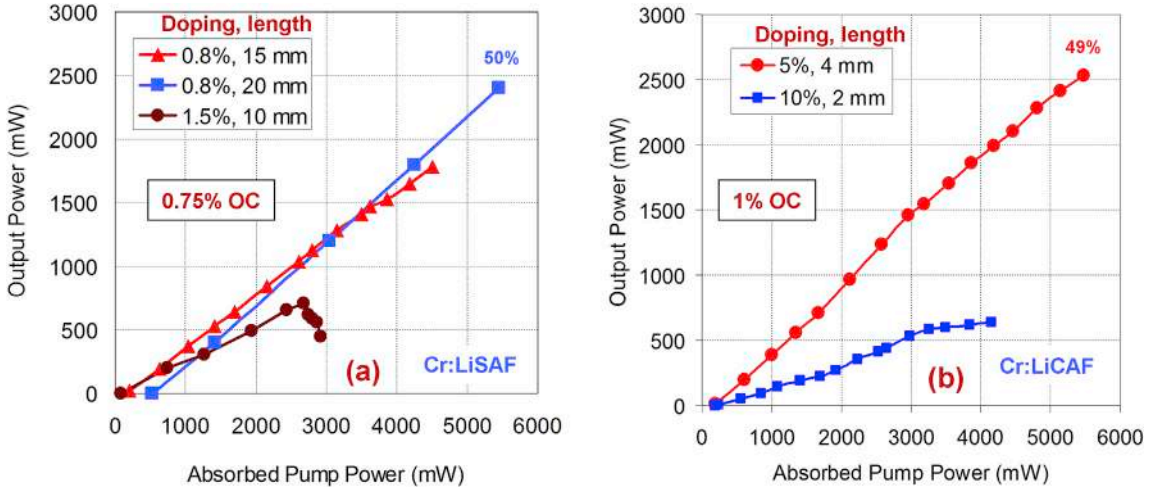

Fig. 22. Measured cw output powers with the multimode diode pumped (a) Cr:LiSAF [57] and (b) Cr:LiCAF [234,276] lasers taken with crystals with different doping at an output coupling ratio of 0.75% and 1%, respectively. Reproduced with permission from Refs. [234,276].

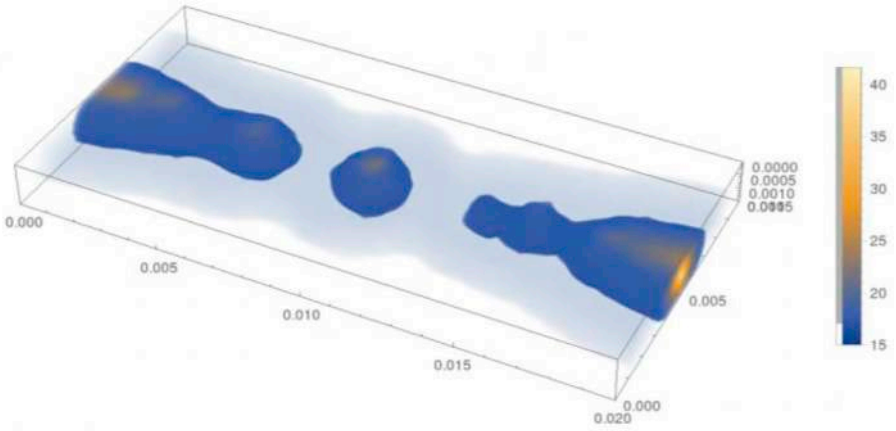

Fig. 23. Calculated temperature distribution inside a 0.75%-doped 1.5 mm thick 20 mm long Cr:LiSAF crystal pumped by 5 W of pump power (pumped by 2.5 W from each side).

generate thermally induced stress values close to the tensile/fracture strength of Cr:Colquiriite materials, explaining the damage we have observed in Cr:Colquiriite samples. We believe that, for Cr:Colquiriites, obtaining cw output powers above 2–3 W is a very challenging engineering problem due to the inherent material limitations (at least in the rod geometry described here). In future studies, we recommend usage of even longer Cr:LiSAF/Cr:LiCAF crystals (30–40 mm), with Cr-doping levels below 0.5%, for further power scaling with minimal risk of crystal damage. We believe this could be employed with Cr:Colquiriites due to the low passive losses and high FOM of the crystals. On the other hand, the increased path length inside the Cr:LiSAF/Cr:LiCAF crystals will create challenges in proper design of femtosecond lasers and amplifiers. Other approaches for power scaling such as thin disk geometry and cryogenic cooling might provide better options in reaching power levels above >10 W level [152]. As another point, due to its better thermal parameters, Cr:LiCAF might provide a more suitable host for power scaling. In our studies, the lowest Cr-doping of the Cr:LiCAF samples we had at hand was 5% (compared to 0.75% in Cr:LiSAF), which prevented us to show the benefits of Cr:LiCAF in terms of power handling. We believe a long (40 mm), and lowly Cr-doped (0.5%) Cr:LiCAF crystal could reach output powers above 5 W level even in simple rod geometry.

To elaborate on the cw laser performance results further, Fig. 24 (a) shows measured laser efficiency under different output coupling for the 0.8% Cr-doped, 15-mm long Cr:LiSAF crystal. Up to 1785 mW output power, and 42% slope was obtained with a 0.75% output coupler. Note that at higher output coupling ratios, the measured laser slope efficiencies were even lower (e.g. 31% with the 2% OC). This phenomenon is unexpected since according to Eq. (10), the laser slope efficiency should increase with increasing output coupling (T), and should approach to η_0 (the intrinsic slope efficiency) at output coupling ratios much higher than the total cavity loss (L). This unexpected phenomena is actually well-known in Cr:Colquiriite lasers, and is due to the presence of Auger upconversion process [170,277,278]. As discussed earlier, the lifetime of the upper laser level depends on inversion as well as temperature. At higher output

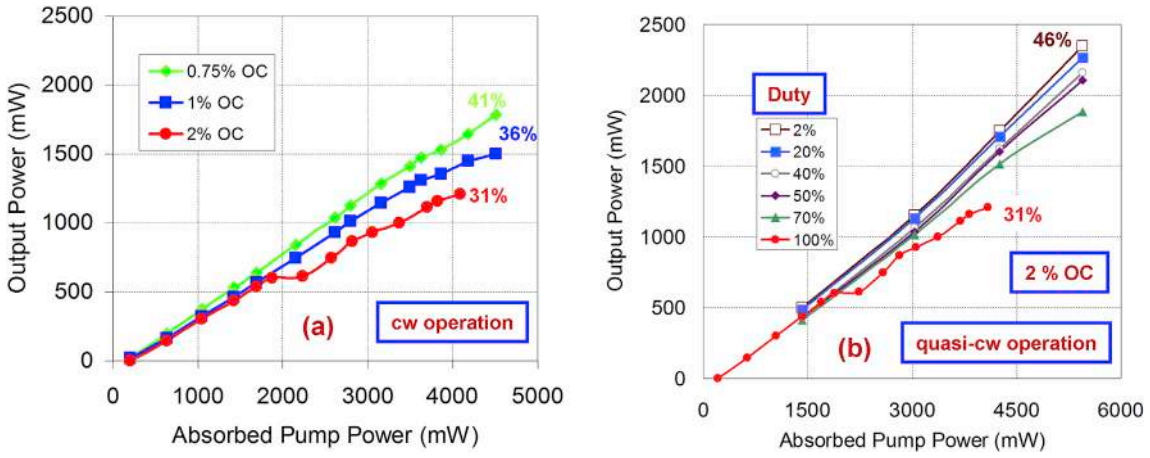

Fig. 24. (a): Measured cw laser performance of the MMD pumped Cr:LiSAF laser at different output coupling using the 15 mm long, 0.8% Cr-doped crystal [57,280]. (b): Measured variation of the quasi-cw laser performance of the Cr:LiSAF laser using the same crystal, as a function of duty cycle of the pump pulses [280]. A pump pulse width of 2 ms and an output coupling of 2% have been used along with the 15 mm long Cr:LiSAF crystal. Slope efficiencies measured at 2% and 100% duty cycle are indicated in the graph. Reproduced with permission from Refs. [57,280].

coupling, intracavity laser power levels are lower and as a result steady sate inversion values are higher [277,279]. Basically, in steady-state, saturated gain should be as high as losses (L + T), which is higher at high output coupling(T). This phenomenon intensifies the Auger upconversion rate (which scales with the square of population inversion level) and as a result shortens the fluorescence lifetime. From Eq. (8), we know that a reduced fluorescence lifetime increases the laser threshold pump power (P_{th}). Hence, the output powers at high output coupling is lower not because of the reduced slope efficiency, but due to the increase in laser threshold pump power.

Fig. 24 (b) shows the measured laser efficiency of the MMD pumped Cr:LiSAF laser with the 2% output coupler in the quasi-cw mode (long pulse operation), again using the 15 mm-long 0.8% Cr-doped crystal, at duty cycle values ranging from 2% to 100% (100% corresponds to the pure cw operation, as in Fig. 24 (a)). The pump pulsewidth was 2 ms in all the measurements. Fig. 24 shows that, in quasi cw operation, due to the reduced thermal load on the crystal, the obtainable output powers from the Cr:LiSAF crystal increased from 1.2 W to 2.35 W, when the duty cycle was reduced from 100% to 2%. We have also investigated quasi-cw performance with the 20 mm-long 0.8% Cr-doped crystal. For this crystal, when the duty cycle decreased from 100% to 10%, due to the reduction of thermal effects, the slope efficiency of the laser increased from 50% to 52%. Moreover, at 10% duty cycle, quasi-cw laser output powers of 3.1 W at an absorbed pump power of around 6.4 W (during the cw burst) has been demonstrated.

We have seen that, while pumping Cr:Colquiriites with single-emitter multimode diodes, laser slope efficiencies similar to SMD pumping could be obtained. Moreover, output powers could be scaled from about 400 mW to 2.5 W level. On the other hand, due to the asymmetric and multimode nature of the laser pump diodes, the Cr:Colquiriite laser transverse mode obtained was also asymmetric and multimode in the MMD pumped system. In the fast (vertical) axes, laser output beam quality (M^2 factor) was 1.1 or better in all cases. On the other hand, in the fast (horizontal) axes the beam quality was steadily deteriorating with increased pump power level, and M^2 values varied between 2 (at low pump powers) and 10 at the highest output power levels. On the other hand, a slit near the OC (tangential plane) could be employed to control the transverse mode structure of the laser output in the slow axis at the expense of decreased levels of output power. When the slit width is adjusted properly, it was possible to achieve a symmetric diffraction limited TEM_{00} laser beam with 1–1.5 W of laser output.

1.6.3. Cw performance with tapered diodes

State-of-the-art tapered diode lasers (TDLs) in the red spectral region could produce 1.2 W of output power with M^2 values of 1.1 in the fast axis and 2.6 in the slow axis, achieving a brightness of about 1000 mW/μm^2. This is almost about 3 times improvement in brightness compared to the state of the art single mode laser diodes and broad-stripe single-emitter diodes. We have also tested the cw laser performance of Cr:Colquiriite lasers pumped TDLs. The laser cavity was similar to what was employed earlier with SMD and MMD pumped systems. As an important difference, TDLs are very sensitive to feedback, and hence only two cross-polarized diodes (one from each side) were used for pumping, and pump protection optics based on polarization decoupling was inserted into the pump beam paths to prevent any feedback into the diodes from each other.

Fig. 25 shows the measured cw laser efficiencies with Cr:LiSAF and Cr:LiCAF at several different output coupling. A 4-mm-long, 7% Cr-doped Cr:LiCAF and a 7-mm-long, 1.5% Cr-doped Cr:LiSAF crystals were used in the studies. Using Cr:LiSAF gain media, output powers as high as 850 mW has been achieved with a 0.5% transmitting output coupler, at an absorbed pump power level of 1740 mW. The laser slope efficiency was 49% with respect to the absorbed pump power, a value very close to what was achieved with SMD pumping (53%). With Cr:LiCAF gain media, an output of 650 mW was obtained at an absorbed pump power of 1780 mW with a 1% output coupler. The corresponding slope efficiency was 42%, which is relatively small compared to what was achieved (53%) while pumping by SMDs. We suspect that the lower efficiency obtained in the TDL pumped study is due the lower FOM and higher passive losses of the Cr:LiCAF crystal compared to what was used in the SMD studies. We note here that, due to the advantage of higher

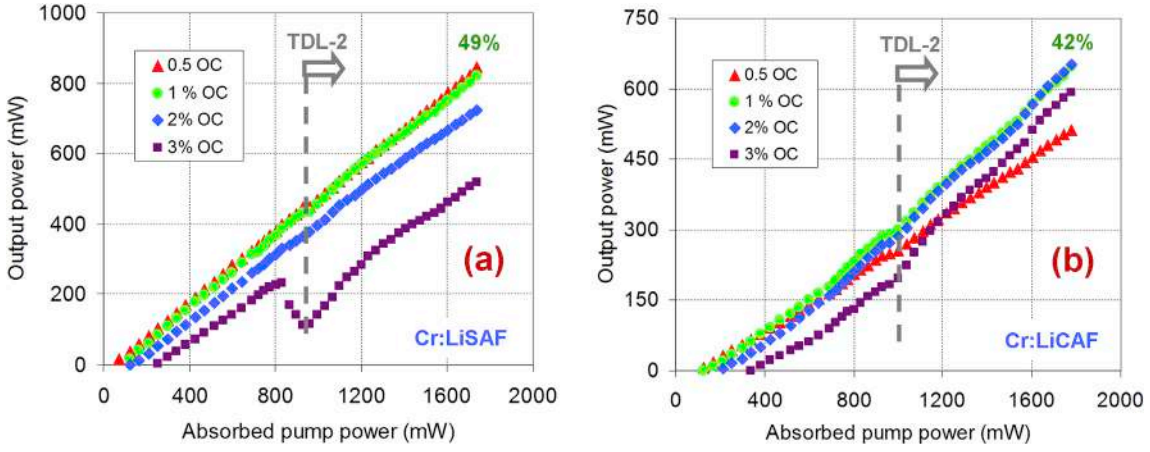

Fig. 25. Continuous-wave output power versus absorbed pump power for the (a) Cr:LiSAF and (b) Cr:LiCAF lasers pumped by two tapered diode lasers (TDLs), measured at various levels of output coupling between 0.5% and 3% [239]. "TDL-2″ in the figure refers to the point where the second tapered diode laser is turned on. Reproduced with permission from Ref. [239].

brightness of TDLs, the transverse mode profile of the output beam was symmetric and circular with M^2 below 1.1 in all the cases. Similar tapered diodes could also used for efficient pumping of Alexandrite [182] and Tm:YAG laser systems.

1.6.4. Cw performance with multimode diode arrays

In this section we would like to review some of the cw laser work that is performed with Cr:Colquiriites while using multimode diode arrays as the pump source. Diode arrays consists of tens to hundreds of single-emitter broad-stripe diodes stacked together, providing much higher pump powers at the expense of further reduction in beam quality. In one of the studies Kopf et al. used a 15 W of output power from a 0.9 cm wide diode array with an M^2 of 1200 and 5 in the slow and fast axis, respectively (Fig. 26) [240]. The brightness of the source was only about 5–10 mW/μm^2, about two orders of magnitude smaller than today's state of the art tapered diode lasers. To fully benefit from such an asymmetric pump beam profile, and also to distribute the thermal load in the Cr:LiSAF crystal, Kopf et al. used a wisely designed laser resonator with cylindrical mirrors to employ a cavity with a laser mode size of 80 μm × 1000 μm (that matches relatively well to the pump mode) [240]. Moreover, a very thin (1 mm) and lowly Cr-doped (0.8%) sample is used to enable efficient cooling of the crystal. The laser provided up to 1.42 W of output power with a slope efficiency of 18% [240]. The laser output had an M^2 of 1 and 2.8 in the fast and slow axis, respectively [240]. The concept used in the study is power scalable, and might enable further power scaling to multiwatt regime [240,281,282]. On the other hand, the slope efficiency obtained is relatively low, probably due to the low brightness of the pump module. We note here that today's state-of-the-art diode arrays have brightness values approaching 80 mW/μm^2 (40 W pump power, with an M^2 of 220), and should ideally provide higher slope efficiencies compared to this initial work.

As an alternative approach Dergachev et al. investigated transverse pumping of a thin (1 mm) Cr:LiSAF slab by multimode diode arrays as shown in Fig. 27 (a) [241,283]. The 27 mm long and 3 mm wide Cr:LiSAF slab is pumped from both sides using two offset multimode diode bars [241]. The fast axis of the diode arrays are collimated by cylindrical lenses, and multipassing the laser mode through the gain material 5 times enabled sufficient extraction of the energy in the pumped volume. In cw laser experiments, using a 0.75% output coupler, cw output powers as high as 3 W has been obtained at a total pump power of 30 W [241]. To our knowledge, this is the highest cw laser output power obtained from Cr:Colquiriite lasers to date (at true 100% duty cycle). Note that the laser threshold pump power was quite high (15 W) and the slope efficiency is just around 10% [241]. Unfortunately, there is no information about the Cr-doping of the Cr:LiSAF crystal used and the output beam quality of the laser for this study [241]. On the other hand, as discussed by Dergachev et al. compared to longitudinally pumped rod lasers, transverse pumped slab laser geometry has advantages in terms of minimization of thermal effects due to the usage of larger pumped volumes [241], and a 10 fold reduction in thermal loading is expected at the similar gain values, and this estimate might be even better in Cr:Colquiriites which suffers from Auger upconversion [241]. We believe that future work with Cr:Colquiriite lasers/amplifiers in carefully/wisely designed thin-disk, zig-zag or multipass slab geometries could enable power scaling of these systems to above 10 W level in cw operation. In comparison, cw powers as high as 26 W, and a slope efficiency of 49% has already been achieved from a diode-end pumped cylindrical Alexandrite laser in rod geometry [191], showing the benefits of Alexandrite's thermo-opto-mechanical properties discussed earlier.

1.6.5. Quasi-cw performance under flashlamp pumping

In this subsection, we would like to review some representative results obtained from flashlamp pumped Cr:Colquiriite lasers in quasi-cw (long-pulse) operation. The first flashlamp pumping of Cr:LiCAF has been demonstrated by Payne et al. where flashlamp pulses of 325 μs and 280 J were used to pump a 1.8% Cr-doped 6.35 mm diameter, 80 mm length Cr:LiCAF rod [36]. At an output coupling of 38%, a slope efficiency of only 1.55% and pulse energies up to around 2 J has been demonstrated at 1 Hz (around 2-W average output power) [36]. The loss for the Cr:LiCAF crystal was estimated to be around 27%, corresponding to 3.8%/cm, which was the main reason for the low conversion efficiency obtained in this initial work [36]. As mentioned above, current Cr:LiCAF crystals could have passive losses in the order of 0.2%/cm. Compared to Cr:LiCAF, lower loss Cr:LiSAF boules were available even at early 90s, and first flashlamp

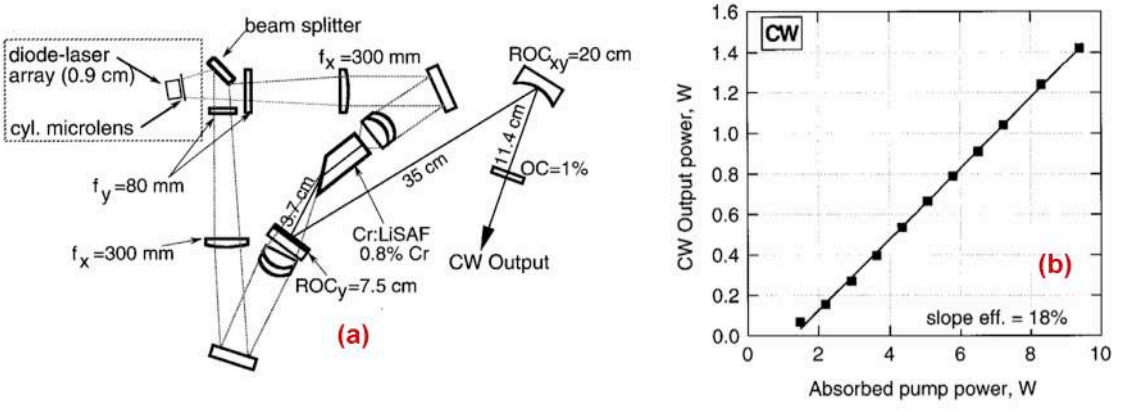

Fig. 26. (a) Multimode diode array pumped Cr:LiSAF laser with cylindrical cavity mirrors that is used by Kopf et al. in power scaling studies [240]. (b) Measured laser slope efficiency of the system with a 1% output coupler. Reprinted with permission from Ref. [240].

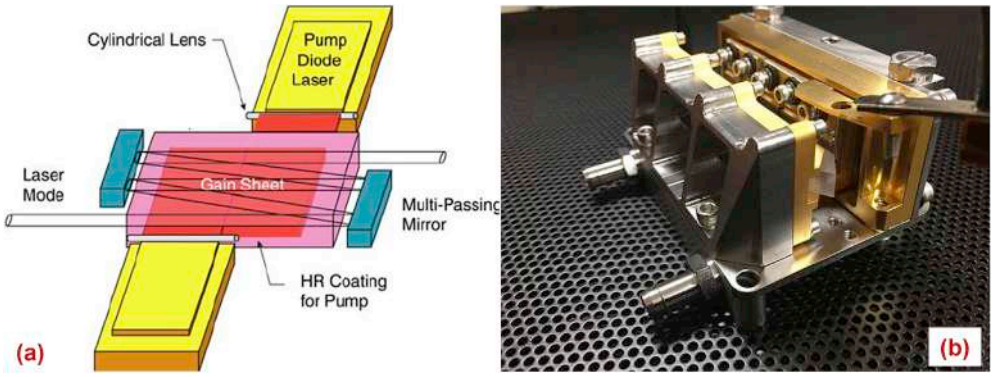

Fig. 27. (a) Schematic of the cw Cr:LiSAF laser as employed by Moulton et al. in multipass slab laser geometry (reprinted with permission from Ref. [283]). (b) Picture of the diode pumped high gain multi-pass chisel slab amplifier: an upgraded and more compact version compared to the initial geometry (Courtesy of Q-peak [284]).

pumping of Cr:LiSAF produced slope efficiencies up to 5%, and pulse energies up to around 2.8 J at 1 Hz (2.8 W average output power) [56].

Recently, Samad et al. scaled the output powers obtained from long-pulse Cr:LiSAF lasers to 30 W level (Fig. 28 (a)) [245]. Using a Brewster-Brewster cut 1.5% Cr-doped, 6.35 mm diameter and 102 mm length Cr:LiSAF gain element, 0.7 J pulses at 30 Hz (20 W output) [285] and 2 J pulses at 15 Hz were demonstrated (30 W output) [245]. Further power scaling of flashlamp pumped Cr:Colquiriites to around 44 W level has been achieved in multipass zig-zag geometry (Fig. 28 (b)) [246,286]. In their work Klimek and Mand, used two 5.5% Cr-doped Cr:LiSAF samples with a thickness of 1.5 mm, that is pumped by high energy flashlamps from both sides [246]. Using a 48% transmitting output coupler, pulse energies up to 8.8 J has been obtained at a repetition rate of 5 Hz, corresponding to 44 W of average output power [246]. To our knowledge, this result still represent the highest output powers obtained from flashlamp pumped Cr:LiSAF lasers (also from any quasi-cw Cr:Colquiriite laser). For comparison, average output powers up to 100 W was demonstrated in flashlamp pumped Alexandrite systems (400 mJ pulses at 250 Hz), where further power scaling was limited due to thermal distortions, and degradation of output beam quality [287].

1.7. Mode-locked operation of Cr:Colquiriite Lasers

Several different methods have been used to mode-lock Cr:Colquiriite lasers including Kerr-lens mode-locking (KLM) [57,58,238,289,290], acusto optic mode-locking (AOML) [254], dye-cell mode-locking [249,251], saturable Bragg Reflector mode-locking, carbon nanotube mode-locking [291] and graphene saturable absorber mode-locking [292,293]. It is interesting to note that, most of the mode-locking work in the literature has been focused on Cr:LiSAF mostly due to easiness to access to lower-loss crystals and its broader tuning range. Moreover, Cr:LiSAF has an emission cross section that is 3–4 times larger than of Cr:LiCAF, which minimizes Q-switched mode-locking tendency of the laser gain medium. This greatly reduces the difficulty in obtaining stable cw mode-locked laser operation in the laboratory, making Cr:LiSAF a much easier gain medium to work with in mode-locking experiments. Note that most of the studies have used KLM and SBR mode-locking in Cr:Colquiriites. In general KLM studies provided the shortest pulses and highest peak powers from Cr:Colquiriites [53,58,294,295] whereas SBR mode-locking enabled generation of the highest average output powers and higher optical-to-optical conversion efficiencies [240,276]. Other recently developed mode-locking mechanisms such as carbon nanotubes and

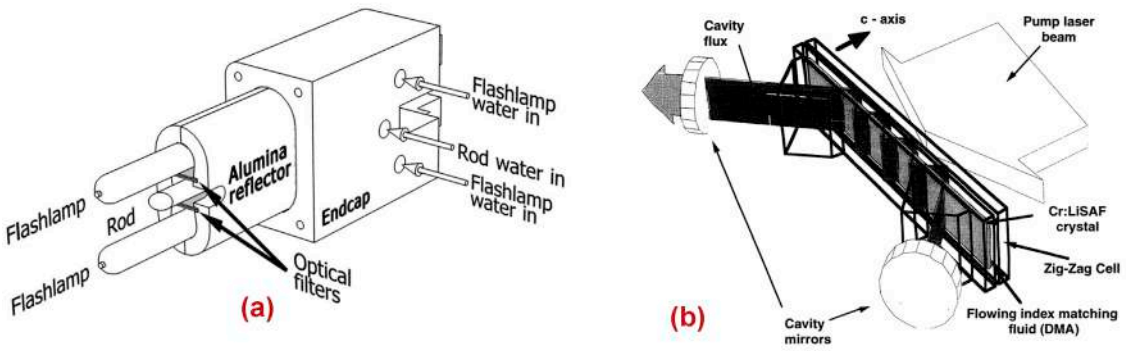

Fig. 28. (a) Flashlamp pumped Cr:LiSAF laser rod [285]. (b) A flashlamp pumped Cr:LiSAF laser in thin-slab multipass zig-zag geometry [288]. Reprinted with permission from Refs. [285,288].

graphene currently provides moderate average power levels due to the relatively high passive losses of these structures [291–293], and future progress in these new technologies are required for competitiveness with already developed methods. In the following sections we will provide a detailed review of results obtained with SBR and KLM mode-locking techniques.

1.7.1. SBR mode-locked Cr:Colquiriite Lasers

1.7.1.1. Cavity schematic. As mentioned earlier, SBRs provide self-starting, robust mode-locked operation with long-term stability, and hence they are widely employed in mode-locking of Cr:Colquiriite lasers. Fig. 29 shows schematic of typical cavities used in SBR mode-locked Cr:Colquiriites. For high repetition rate cavities (>500 MHz), the SBR could be inserted directly at the place of the high reflector mirror (Fig. 29 (a)). For lower rep rates, usually another curved mirror with a radius of curvature in the 50–250 mm range is used to create a second focus, where the SBR is placed (Fig. 29 (b)). Sometimes additional mirrors (such as M4-M5 in Fig. 29 (c)) are also employed for dispersion compensation. In case ultrashort (sub-50-fs) pulses are desired double-chirped mirrors (DCMs) and/or prism pairs are used for dispersion control. Around 800 nm, DCM mirrors typically provide relatively flat group delay dispersion (GDD) curves with average GDD values of -50 fs^2 to -100 fs^2 in a relatively broad wavelength range (100–300 nm), and with low level of GDD oscillations (± 10 to $\pm 25\%$). For high average power operation, where large total GDD vales are required, many bounces on DCM mirrors are needed and this might not be very practical. As an alternative, Gires-Tournois interferometer mirrors could also be employed where GGD values of -500 ± 50 fs^2 could be achieved in a single bounce, at the expense of reduced bandwidth (50 nm) and lower reflectivity (99.9%).

1.7.1.2. Stable cw mode-locked working range of SBR mode-locking. In SBR mode-locked lasers, once the dispersion is set correctly, the cavity is well aligned and the focusing on the SBR is optimized, the laser is self-starting and immune to environmental fluctuations and well-engineered systems could work for months to years without requiring any adjustment, enabling turn-key operation for users. To demonstrate this turn-key operation capability, in one of our experiments, we modulated the pump diode current with an external modulation signal (a square wave current input). With the modulation signal, the pump diodes turned on and off repeatedly, and the response of the laser was measured by monitoring the lasers output with a fiber-coupled 2-GHz silicon detector and a 1-GHz oscilloscope. Fig. 30 (a)-(d) shows the response of the laser for a typical SBR mode-locked Cr:Colquiriite laser system (Cr:LiCAF crystal, 1% output coupler, 600 mW absorbed pump power, an SBR with a modulation depth of around 1%). Fig. 30 (a) shows that, each time the pump diode is turned on, after an initial recovery time, stable cw mode-locking was acquired. Fig. 30 (b) illustrates the process in more detail. When the pump is first turned on, the laser requires around 30–50 μs to start lasing. During this time, pumping fills in the upper laser level, and collects enough inversion/gain for the stimulated emission process to initiate lasing. As expected, then the laser starts with a relaxation oscillation, with a relaxation frequency in the order of 10s of kHz (~125 kHz for the specific example in Fig. 30 (c)). Then relatively stable cw operation was observed with quite low output power levels (~20–40 mW). Here, the powers are low due to the high level of losses (~1%) of the SBR at low incident fluencies. Then in time scales roughly ranging from 0.5 ms to 5 ms, the SBR initiates pulsing, and the losses of the SBR gets saturated, and the average laser powers jump to above 100 mW. At first the initiated mode-locking is usually unstable and it requires a few more milliseconds for the laser to reach stable mode-locking regime (unstable mode-locking is shown in Fig. 30 (b)). After all this initialization process, in around 5–20 ms, stable cw mode-locking with an average power of around 150 mW was obtained (Fig. 30 (d)). The observed gradual decrease (5–10%) of average mode locked power with time as seen in Fig. 30

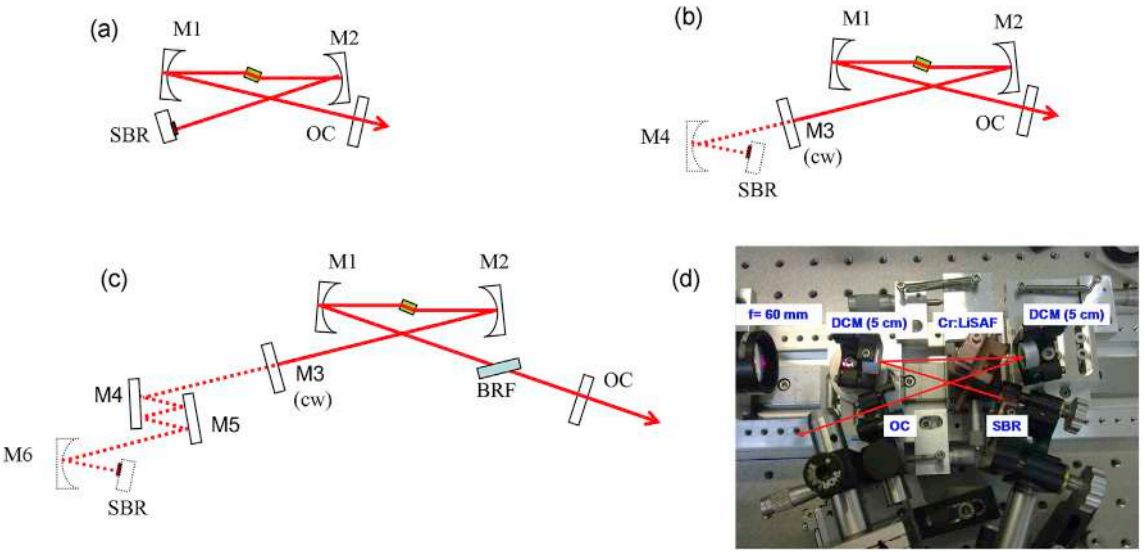

Fig. 29. (a–c) Schematics of the saturable Bragg reflector (SBR) mode-locked Cr:Colquiriite lasers that was used in mode-locking experiments. (d) Picture of an SBR mode-locked Cr:LiSAF laser cavity.

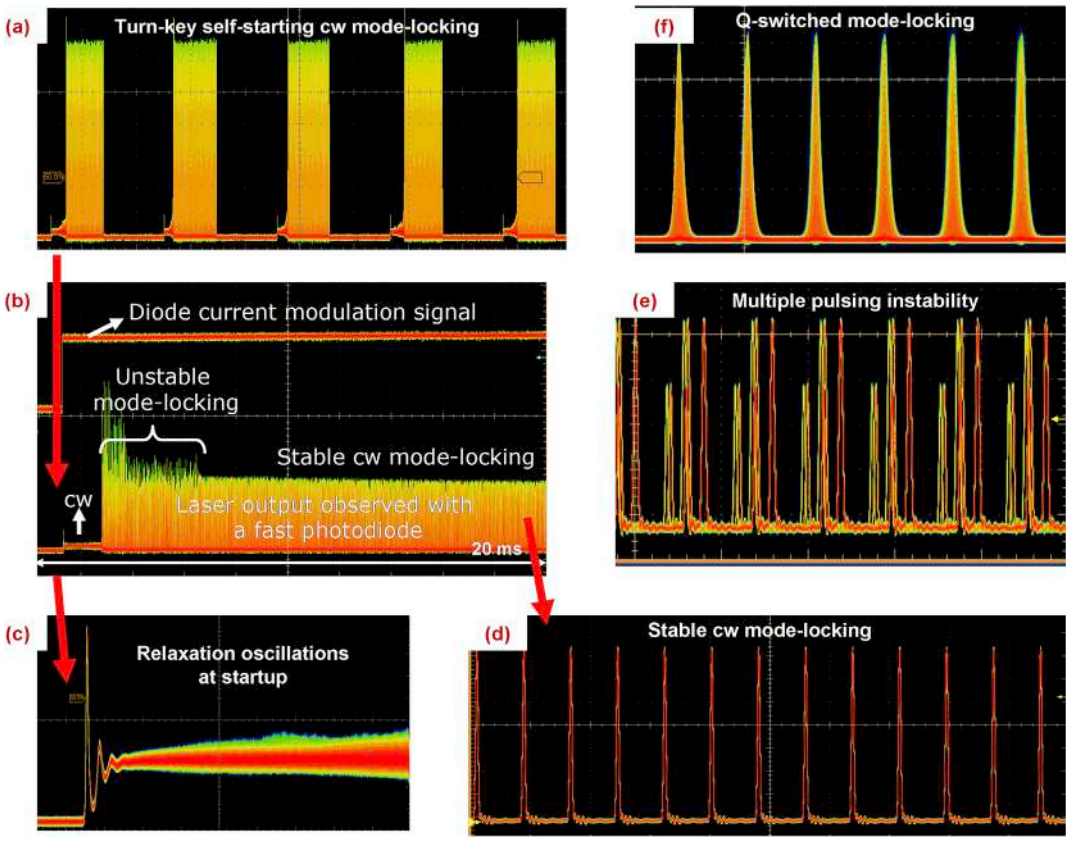

Fig. 30. (a) Oscilloscope train showing stable turn-key cw mode-locked operation in Cr:Colquiriite lasers. Diode current is modulated to demonstrate self-starting operation. (b) Measured starting dynamics in more detail. (c) Initial relaxation oscillation. (d) Stable cw-mode-locked pulse train. (e) Multiple pulsing instability observed in the pulse train when the fluence on the SBR is too high. (f) Q-switched mode-locking observed when the fluence on the SBR is too low.

(b) is mostly due to the initial heating of the pump diodes and the laser crystal. It requires 100s of milliseconds for the diodes and the laser crystal to reach their thermal equilibrium and then the laser output power is stable.

We note here that, if the intracavity laser fluence on the SBR is not adjusted correctly, Q-switching (Q-switched mode-locking, Fig. 30 (f)), or multiple pulsing instabilities (Fig. 30 (e)) could be observed in SBR mode-locked lasers. These instabilities of SBR mode-locked lasers are very well known in literature [220,296,297]. Using laser rate equations, one can show that in order to obtain stable cw mode-locking (without Q-switching), the intracavity pulse energy should be above a critical value ($E_{P,c}$) [296,297]:

$$E_{P,c} = \sqrt{E_{\mathrm{sat},L} E_{\mathrm{sat},A} \Delta R} \tag{14}$$

where $E_{sat,A}$ is the absorber (SBR) saturation energy, ΔR is the modulation depth of the SBR, and $E_{sat,L}$ is the saturation energy of the gain medium. Saturation energy of the gain medium ($E_{sat,L}$) could be calculated from Ref. [296]:

$$E_{\mathrm{sat},L} = \frac{h\nu_l}{(m\sigma_{\mathrm{em}})} A_{\mathrm{eff},L} \tag{15}$$

where m is the number of passes through the laser crystal in one round trip, $A_{eff,L}$ is the effective laser mode area inside the gain medium (and σ_{em} is the emission cross section of the gain medium at the wavelength of interest). Absorber saturation energy ($E_{sat,A}$) is defined as the product of effective laser mode area on the SBR ($A_{eff,A}$) and absorption saturation fluence ($F_{sat,A}$) [296]:

$$E_{\mathrm{sat},A} = F_{\mathrm{sat},A} A_{\mathrm{eff},A} \tag{16}$$

With these, Eq. (14) could be rewritten as:

$$E_{P,c} = \sqrt{\frac{h\nu_l}{(m\sigma_{\mathrm{em}})} A_{\mathrm{eff},L} F_{\mathrm{sat},A} A_{\mathrm{eff},A} \Delta R} \tag{17}$$

Here, we note that, the critical pulse energy defined by Eq. (17) considers a laser mode-locked by SBR mechanism only. In dispersion controlled lasers, SBR initiates and sustains stable mode locking; however, the pulses are shaped mainly by soliton mechanism enabling fs pulse generation [296]. The effect of soliton pulse shaping is to lower the critical pulse energy required for stable cw mode-locking to values below what is estimated using Eq. (17) [296].

In general, it is desirable to have a laser with low $E_{P,c}$ in order to obtain stable cw mode locking even at low pump powers (especially for systems pumped with SMDs). One challenge with Cr:Colquiriites, especially with Cr:LiCAF gain medium is its lower emission cross section. Investigating Eq. (17), we see that the emission cross section is the only intrinsic parameter, and all the other parameters (m, $A_{eff,L}$, $A_{eff,A}$, ΔR, $F_{sat,A}$) could be engineered by design of the SBR structure and the laser cavity geometry. Note that, keeping all the other external parameters in Eq. (17) the same, due to its much higher emission cross section, a Ti:Sapphire laser has ~6 times lower $E_{P,c}$ than a Cr:LiCAF laser. Also, once initiated, the pulse energies in Q-switched mode-locked lasers are much higher than stable cw mode-locked operation, which might cause permanent damage to the SBR surface due to large fluence values. Hence, in Cr:LiCAF, obtaining stable mode-locked operation, without Q-switching instabilities requires careful laser design and wise selection of operating parameters. Finally, it is important to note that Q-switched mode-locked operation of Cr:LiCAF might be advantageous in some applications such as micromachining, surgery, and nonlinear microscopy [296], and such an operation regime will be described in detail later in this section.

Looking at Eq. (17), one might suggest arbitrarily decreasing the effective spot size on the SBR or inside the gain medium, to decrease the required critical pulse energy levels. However, in general there is an optimum spot size for the gain medium, and decreasing it in an arbitrary way might lower the laser slope efficiencies or might generate too much self-phase modulation or local heating, which would be hard to balance/compensate. Also, one cannot decrease the spot size on the SBR too much. This is because at tighter focusing and at high intracavity intensity levels, two-photon absorption (TPA) process will start on the SBR, which can generate pulse to pulse instability in the mode-locked pulse train (pulse energy and pulse duration might fluctuate). As an example, Fig. 31 shows this type of instability in the cw mode-locked laser due to the tight focusing on the SBR. Note that even a small increase in pump power (5–10%) above a certain level is enough for TPA induced laser instabilities. Increasing the focusing on the SBR further might even cause multiple pulsing instabilities as shown earlier in Fig. 30 (e), or might damage the structure due to local heating and/or high fluence. We note here that TPA effect starting threshold is a function of peak power. Hence, for pulses with same energy, shorter pulses will be more susceptible to TPA effects.

In short, there is a limited working range for an SBR mode-locked laser, where it produces stable cw mode-locking (Fig. 32). Increasing the spot size on the SBR or decreasing the intracavity pulse energy levels too much, might cause q-switched mode-locking instability. On the other hand, focusing too tight on the SBR or increasing the intracavity pulse energies too much might cause two photon absorption induced multiple pulsing instabilities and even burning of the SBR structure. Note that for gain media with higher emission cross section, working range of the SBR is broader, since the critical pulse energy for stable cw mode-locking is an inverse function of emission cross section. Also note that, the working range is also wider for longer pulses, because the TPA effects starting threshold will be higher. Due to these facts, it is quite challenging to generate short (sub-50-fs) pulses with high pulse energy from SBR mode-locked gain media with low emission cross section such as Cr:LiCAF. For comparison, at room temperature the peak emission cross section of Alexandrite is only around 0.7×10^{-20} cm^2 [130], which is around 2 times smaller than the value of Cr:LiCAF. This small emission cross section value creates difficulties in obtaining stable cw mode-locked operation in Alexandrite, slowing down progress towards development of high average power short-pulse (sub-50-fs) oscillator systems. As a result, mode-locking of Alexandrite with sub-ps pulses could only been demonstrated recently [50,192,193,298].

1.7.1.3. SBR mode-locking performance with single-mode diode pumping. As representative examples, Figs. 33 and 34 shows SBR mode-locking data obtained with Cr:LiSAF and Cr:LiCAF lasers pumped by one 130–150 mW single-mode diode. As mentioned earlier, at this pump power levels neither the diode, nor the laser crystal requires active cooling, greatly simplifying the laser structure. The gain media was a 7-mm-long, 1.5% Cr-doped Cr:LiSAF and 4-mm doped 5%-doped Cr:LiCAF in these sample results. A 0.5% transmitting output coupler was used in both cases. DCMs were used for dispersion compensation, and SBRs with central reflectivity around 850 nm and 800 nm and modulation depths of around 0.5% were used for mode-locking of Cr:LiSAF and Cr:LiCAF lasers, respectively.

When mode-locked, one SMD pumped Cr:LiSAF laser produced as much as 38 mW of average mode-locked output power at the full pump power. The pulses were 103-fs long, and had an optical spectrum centered around 872 nm (Fig. 33). The repetition rate of the pulses were 235 MHz, and this corresponds to an output pulse energy of 162 pJ and to an output peak power of 1.38 kW. One thing to

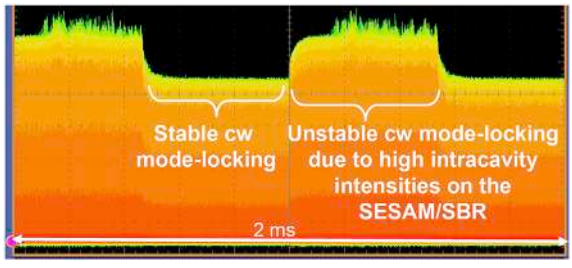

Fig. 31. Transition of the laser from stable cw mode-locked operation to unstable cw mode-locked operation due to increased pump power (too much intracavity laser fluence on the SBR). This instability is caused by two photon absorption effects on the SBR.

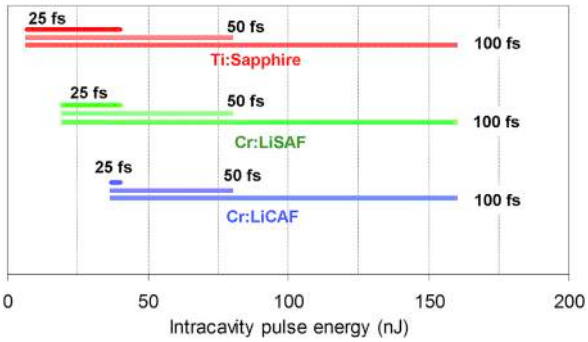

Fig. 32. Calculated stable cw mode-locking working ranges for SBR mode-locked Ti:Sapphire, Cr:LiSAF and Cr:LiSAF laser materials for pulse lengths of 25 fs, 50 fs and 100 fs. The following parameters are used in the calculations: laser wavelength 800 nm, SBR modulation depth 0.6%, SBR saturation fluence 300 μJ/cm^2, SBR two-photon absorption effect starts above ~20 mJ/cm^2 for 100-fs long pulses, effective beam sizes inside the gain media and on the SBR: $A_{eff,L} \cong \pi(16)$ (20) μm^2, $A_{eff,A} \cong \pi(16)^2$ μm^2.

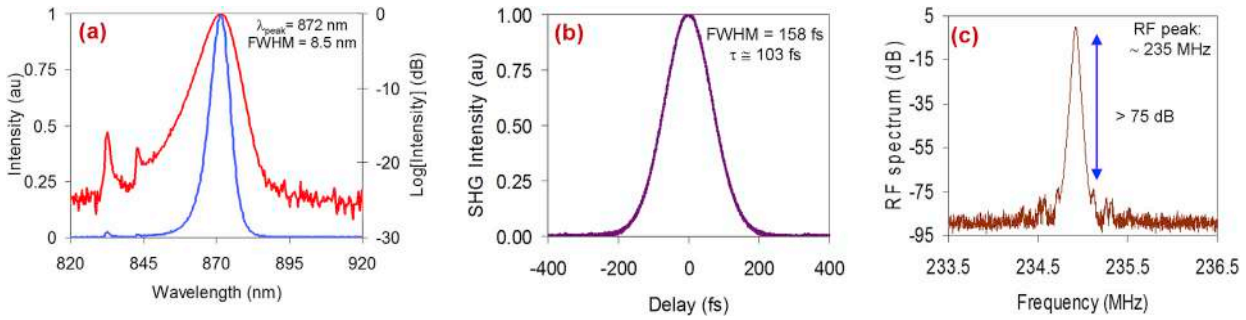

Fig. 33. Sample cw mode-locked operation results obtained by one SMD pumped Cr:LiSAF laser using a 0.5% output coupler. The laser produced 103 fs, 162 pJ pulses centered around 872 nm at a repetition rate of 235 MHz [181]. (a) Optical spectrum, (b) background-free intensity autocorrelation trace, and (c) microwave spectrum. Reproduced with permission from Ref. [181].

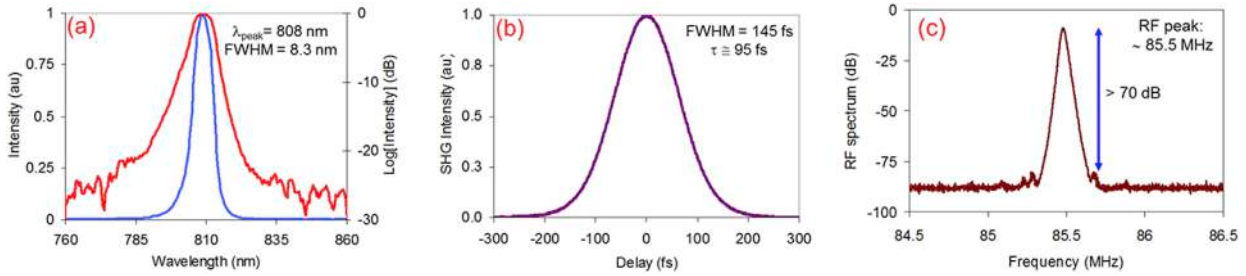

Fig. 34. Sample cw mode-locked operation results obtained by one SMD pumped Cr:LiCAF laser using a 0.5% output coupler. The laser produced 95 fs, 385 pJ pulses centered around 808 nm at a repetition rate of 85.5 MHz [52]. (a) Optical spectrum, (b) background-free intensity autocorrelation trace, and (c) microwave spectrum. Reproduced with permission from Ref. [52].

mention here is that, due to the usage of high-Q-cavities, the intracavity average and peak powers were as high as 7.6 W and 275 kW, respectively (32.5 nJ intracavity pulse energy). It is interesting to see such high peak power levels from an oscillator just pumped by 130 mW of pump power. Moreover, the optical-to-optical conversion efficiency was ~29% (38 mW/130 mW) and the electrical-to-optical conversion efficiency was ~8.4% (38 mW/450 mW). To our knowledge, these values are one of the highest electrical-to-optical conversion efficiencies that could be obtained from femtosecond laser systems [105,224,227,299]. Finally, with the one SMD pumped SBR mode-locked Cr:LiSAF laser (Table 4), repetition rates up to 757MHz could also be obtained (130 fs pulses with 33 mW average power).

On the other hand, as discussed above, Cr:LiCAF systems have high tendency for q-switched mode-locking due to their lower emission cross section, and this is especially true for systems that are pumped with limited pump powers (such as the one described here). Hence, in case of Cr:LiCAF, with the available pump power of 150 mW from one SMD, stable cw mode-locking could only be achieved for repetition rates below 100 MHz. Hence, an 85.5 MHz cavity is developed and at the full pump power of 145 mW, the

Table 4
Summary of SBR mode-locking results obtained with Cr:LiSAF gain medium using single-transverse-mode (SMD) laser diodes as pump sources.

Pump source	Pulse width (fs)	Average power (mW)	Pulse energy (pJ)	Peak power (W)	Rep rate (MHz)	Year	Ref.
2 × 50 mW	90	9	60	588	150	98	[226]
	57	6.5	43	670	150		
2 × 55 mW	136	20	43	276	470	02	[227]
4 × 55 mW	122	35	75	1.2×10^3	~210		
2 × 55 mW	151	20	50	292	~400	02	[228]
	113	15	38	293			
4 × 55 mW	146	3	3	18	1002	02	[227,300]
4 × 55 mW	200	45	140	680	330	02	[301]
3 × 50 mW	39	6.5	756	17×10^3	8.6	03	[302]
4 × 150 mW	46	150	1800	33.8×10^3	85	09	[230]
6 × 150 mW	55	110	110	1.8×10^3	1000	10	[303]
4 × 200 mW	26	85	1000	38.5×10^3	85	11	[222]
1 × 130 mW	103	38	162	1.4×10^3	235	12	[181]
	95	32	87	770	366		
	110	29	58	462	503		
	70	20	39	510	509		
	130	33	44	295	757		
6 × 150 mW	100	250	2500	22×10^3	100	17	[81,304]
	100	185	2160	19×10^3	85.5		

Cr:LiCAF laser produced 95-fs long pulses with 33 mW of average mode-locked output power around a central wavelength of 808 nm (Fig. 34). The corresponding pulse energy and pulse peak power was 386 pJ and 3.58 kW, respectively.

To our knowledge, Tables 4 and 5 presents a literature review of all the SBR mode-locking results obtained with SMD pumped Cr:LiSAF and Cr:LiCAF lasers, respectively. One interesting observation is the gradual increase of the available pump powers from red SMD diodes over the years, starting with 30 mW in late 90s to the current 200 mW level. Note also that, by pumping Cr:Colquiriite laser systems with 4 and sometimes up to 6 SMD diodes, average output powers obtained from SBR mode-locked lasers could be scaled to 150–250 mW level at the expense of increased complexity [81,230,304].

As discussed in the previous section on SBRs, regular AlGaAs based SBRs centered around 800 nm has a reflectivity bandwidth of around 50 nm. Hence, the pulsewidths obtained from SBR mode-locked Cr:Colquiriite lasers are limited by the bandwidth of the SBR structure. To our knowledge, the shortest pulses obtained from SBR mode-locked Cr:LiSAF and Cr:LiCAF lasers are 26 fs and 39 fs, respectively [222]. Optical spectra of these pulses as well as the reflectivity bandwidth of the SBRs used for mode-locking is shown in Fig. 35. For the 26-fs long pulses obtained from Cr:LiSAF, a fused silica prism pair with 28 cm separation was used to fine tune the intracavity dispersion. After optimizing the prism insertion, the laser produced 26-fs with 85 mW of average power at an absorbed pump power of 700 mW. The laser repetition rate was 85 MHz, corresponding to a pulse energy of 1 nJ,a and peak power of 38.5 kW. In the case of Cr:LiCAF, the total cavity dispersion is optimized by adjusting the number of bounces on DCM mirrors and set to around −100 fs^2. The Cr:LiCAF laser produced 39-fs pulses with 125 mW of average output power at an absorbed pump power of 700 mW. The laser repetition rate was 77 MHz, corresponding to a pulse energy of 1.62 nJ and peak power of 41.6 kW. For Cr:LiCAF, further fine tuning of dispersion via intracavity prism did not provide shorter pulses (q-switched mode-locking, multiple-pulsing and cw-breakthrough instabilities has been observed). As discussed in detail above (Fig. 32), we believe that this is due to the lower emission cross section of the Cr:LiCAF gain media, which results in a very narrow SBR working ranges for sub-50-fs pulses (Fig. 32).

SBR mode-locked Cr:LiCAF and Cr:LiSAF lasers also enable tuning of the central laser wavelength within the reflectivity bandwidth of the SBR [222]. For that purpose, a 3-mm thick quartz birefringent filter with an optical axis 45° to the surface of the plate was used for the tuning of the femtosecond pulses (more information on tuning characteristics of this BRF is given above in Section 1.5.1). Using Cr:LiCAF gain medium, and an AlGaAs based SBR with a bandwidth centered around 800 nm, a mode-locked tuning range of 767–817 nm (50 nm), with average pulsewidths of 133-fs and average pulse energies of 1.48 nJ was obtained at an absorbed pump power of 700 mW. Employing the 800-nm SBR, the Cr:LiSAF laser could be tuned from 803 to 831 nm (28 nm), with average pulsewidths of 140-fs and average pulse energies of 1 nJ. Using a SBR centered at 850 nm, a femtosecond tuning range of 828–873 nm (45 nm) was obtained from the Cr:LiSAF laser, with average pulsewidths of ~190 fs and average pulse energies of 1.87 nJ. Furthermore, a 910-nm SBR resulted in a tuning range from 890 to 923 nm with the same laser. Fig. 36 shows sample optical spectra obtained during tuning from SBR mode-locked Cr:LiCAF and Cr:LiSAF lasers. The total tuning range covers wavelengths from 767 nm to 922 nm, and

Table 5
Summary of SBR mode-locking results obtained with Cr:LiCAF gain medium using single-transverse-mode (SMD) laser diodes as pump sources.

Pump source	Pulse width (fs)	Average power (mW)	Pulse energy (nJ)	Peak power (kW)	Rep rate (MHz)	Mode Locking	Year	Ref.
4 × 150 mW	63	144	1.13	18	127	SBR	08	[235]
4 × 150 mW	72	178	1.4	19.5	127	SBR	08	[229]
4 × 150 mW	98	95	9.92	101.2	9.58	SBR	09	[305]
4 × 150 mW	39	125	1.62	41.6	77	SBR	10	[222]
1 × 130 mW	95	33	0.39	3.58	85.5	SBR	12	[52]

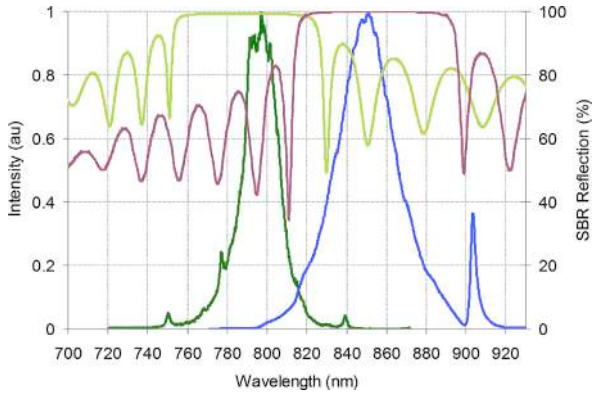

Fig. 35. Optical spectra of shortest pulses generated from SBR mode-locked Cr:LiSAF and Cr:LiCAF lasers, along with the reflectivity of the SBRs used for mode-locking [222]. For Cr:LiSAF spectra is centered around 850 nm and has a FWHM of 33 nm, whereas for Cr:LiCAF spectra is centered around 805 nm and has a FWHM of 19 nm. Reproduced with permission from Ref. [222].

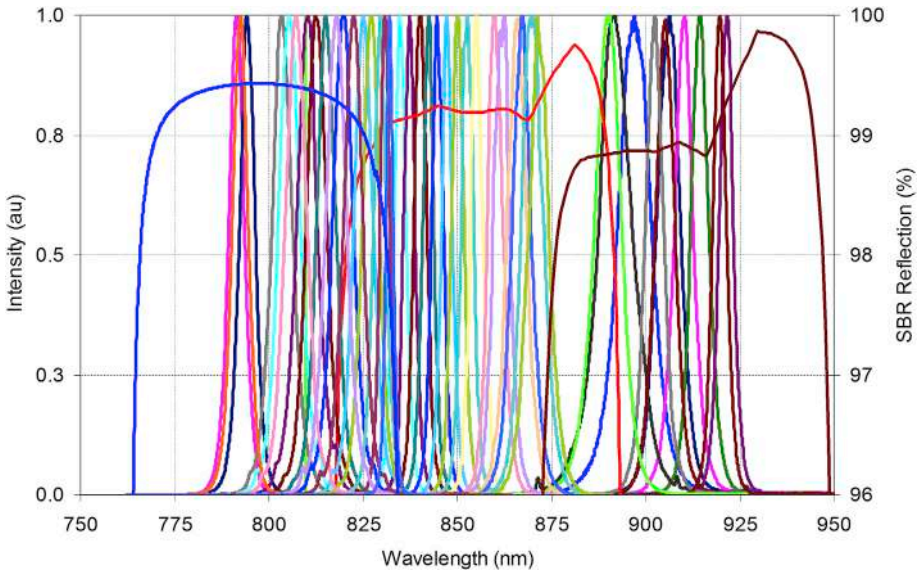

Fig. 36. Sample spectra from the SBR mode-locked Cr:LiSAF and Cr:LiSAF lasers, showing tunability of central wavelength from 767 nm to 922 nm [222]. Calculated small signal reflectivity of the SBRs are also shown. Reproduced with permission from Ref. [222].

requires the usage of 3 different SBRs due to narrow reflectivity bandwidth of the regular AlGaAs based SBR structures.

As an alternative to standard AlGaAs based SBRs, oxidized SBRs could be used to generate saturable absorber structures with bandwidths larger than 250 nm around a central wavelength of 800 nm [306–309]. In oxidized SBRs the index contrast in the Bragg stack is increased by using low-index Al_xO_y (n~1.6) layers instead of AlAs (n~3) [306–309]. With this high index contrast, a Bragg stack consisting of seven pairs of Al_xO_y and $Al_{0.17}Ga_{0.83}As$ layers was enough to generate the desired reflectivity. A 6-nm-thick strained $In_{0.14}Ga_{0.86}As$ quantum well sandwidthched between $Al_{0.17}Ga_{0.83}As$ barriers was used in the SBR to provide broadband saturable absorber in the ~800–920 nm wavelength range. When a Cr:LiSAF laser is mode-locked with this oxidized SBR, femtosecond pulses with 150–200 fs width and 100–150 mW average power could be continuously tuned from 800 nm to 905 nm with the simple rotation of the off surface optical axis BRF plate (Fig. 37).

1.7.1.4. SBR mode-locking performance with multi-mode diode pumping. In the previous section we have seen that, pumping Cr:Colquiriite oscillators with one SMD, results in 30–40 mW average power in SBR mode-locked operation. Usage of more SMD diodes (up to 6) is possible by combining diode outputs using wavelength and polarization coupling and by pumping the system from both sides, and as a result the average powers could be scaled to 150–250 mW level. However, this increases the complexity and cost of system (6 diode drivers, 6 diode holders, 6 collimating lens, etc …), and makes the system more prone to misalignments. Hence, at this point it is interesting to look at what other diode pumping options could provide in SBR mode-locked Cr:Colquiriites. For that purpose, Tables 6 and 7 summarizes mode-locking results obtained from Cr:LiSAF and Cr:LiCAF oscillators pumped by higher power diodes such as broad-

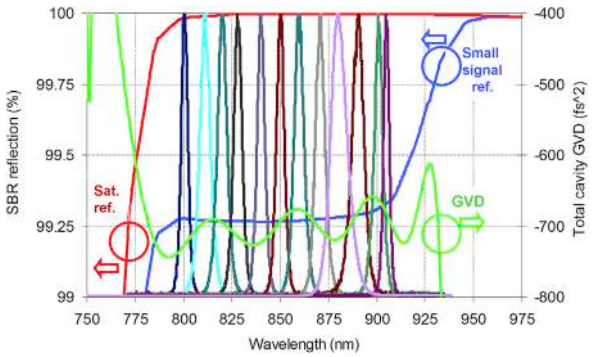

Fig. 37. Sample spectra from the oxidized SBR mode-locked Cr:LiSAF laser, showing tunability of the central wavelength of the laser from 800 nm to 905 nm [81]. Calculated small signal and saturated reflectivity of the oxidized SBR are also shown. Reproduced with permission from Ref. [81].

stripe single-emitter diodes, tapered diodes (TDLs), and laser diode arrays (15 W source in Table 6). Again similar to the SMDs, once can see the progress in brightness of multimode diodes over the years, which enabled power scaling of laser outputs.

The highest average power obtained from SBR mode-locked Cr:LiSAF lasers to date is 580 mW, where four 1.8 W broad-stripe single-emitter multimode diodes were used as the pump source [57]. The results are summarized in Fig. 38. Dispersion compensation has been performed using GTI mirrors centered around 800 nm, and a slit near the OC was used to push the laser to operate in TEM_{00} mode. Due to the losses of additional GTI mirrors and the hard aperture near the output coupler, the laser had a lasing threshold of 1 W, and a slope efficiency of only 14%. The laser first operated in cw regime for pump powers up to 1.5 W, then switched to observed Q-switched mode-locking (QSML), and above 4 W of pump power stable cw mode-locked (CWML) operation could be achieved (Fig. 38 (a)). The laser produced 185-fs long pulses with 580 mW of average power at an absorbed pump power of 5.45 W. The optical-to-optical conversion efficiency of the system was only 8%. As a reminder, SMD pumped SBR mode-locked Cr:Colquiriite lasers could provide 20–30% optical-to-optical conversion efficiencies. The drawback of the multimode diodes are their low brightness, which limits the mode-matching between the asymmetric multimode pump beam and the symmetric TEM_{00} laser beam challenging, reducing efficiencies, and creating extra thermal problems. As another approach, Kopf et al. obtained 110-fs long pulses with 500 mW average power in mode-locked operation [240] from a well-engineered Cr:LiSAF laser system that is pumped by a 15 W diode array (cw results from the same group is discussed above, using Fig. 26). Since the diode arrays has even lower beam quality (M^2 of 1200 in slow axis) [240], the optical-to-optical conversion efficiency of the system was quite low (3.3%).

Using a similar cavity pumped by four 1.8 W broad-stripe single-emitter multimode diodes, 105-fs pulses with 750 mW of average power was obtained from an SBR mode-locked Cr:LiCAF laser (Fig. 39) [276]. The repetition rate of the laser was 96.4 MHz, and corresponding pulse energies and peak powers were 7.7 nJ and 65 kW, respectively. For cw mode-locked operation, the optical-to-optical conversion efficiency of the system was above 10% (750 mW/7.2 W), which is slightly better than the Cr:LiSAF results obtained from a similar system due to the better thermal specification of the LiCAF host. Moreover, the cavity produced 250-fs long pulses with up to 10.3 nJ of pulse energy in quasi-cw mode-locked operation (also named as burst mode operation) [280].

One other approach to scale pulse energies in Cr:Colquiriite lasers is exploring the Q-switched mode-locked operation regime [276]. In this scheme, the laser produces femtosecond pulses under a Q-switched intensity envelope, and peak pulse energies could be much higher than what is achievable from similar average power cw mode-locked lasers. From the 4 × 1.8 W MMD pumped Cr:LiCAF laser, Q-switched mode-locked operation with average powers as high as 1625 mW have been obtained at a pump power of 5.5 W (Fig. 40). Q-switched and Q-switched mode-locked repetition rates were 33 kHz and 143.5 MHz, respectively. Fig. 40 (d) shows the corresponding microwave spectrum, where beating of the 143.5 MHz peak with the 33 kHz Q-switched envelope is seen. The peak pulse energies within the Q-switched envelope were above 150 nJ. The optical spectrum of the pulses was centered around 795 nm with a FWHM of 2.75 nm, ideally supporting 250-fs long pulses, with the corresponding peak power above 500 kW.

Table 6
Summary of SBR mode-locking results obtained with Cr:LiSAF gain medium where multimode laser diodes (broad-stripe single-emitter diodes, tapered diodes, and laser diode arrays) has been used as the pump source.

Pump source	Pulse width (fs)	Average power (mW)	Pulse energy (nJ)	Peak power (kW)	Rep rate (MHz)	Year	Ref.
2 × 400 mW	98	50	0.625	5.6	80	94	[310]
1 × 500 mW	100	11	0.06	0.55	178	95	[311]
2 × 500 mW	45	105	0.6	11.7	176	97	[312]
1 × 15 W	50	340	2.27	40	150	97	[240]
	110	500	3.34	26.7			
1 × 1.2 W (TDL)	105	232	1.84	16.5	126	11	[239]
4 × 1.8 W	185	580	5.8	26.2	100	15	[57]

Table 7
Summary of SBR mode-locking results obtained with Cr:LiCAF gain medium pumped by multimode diodes such as broad-stripe single-emitter diodes (MMDs), and tapered diode lasers (TDLs).

Pump source	Pulse width (fs)	Average power (mW)	Pulse energy (nJ)	Peak power (kW)	Rep rate (MHz)	Year	Ref.
6 × 1 W	67	300	2.5	37.3	120	08	[234]
6 × 1 W	50	150	1.25	25	120	08	[234]
2 × 1.6 W	97	390	2.8	37.3	140	08	[235]
2 × 1.6 W	60	280	1.9	31.1	150	08	[235]
1 × 1.2 W (TDL)	55	217	2.04	3.26	106.6	11	[239]
2 × 1.2 W (TDL)	220	415	5.4	21.6	77	11	[239]
4 × 1.8 W	105	750	7.7	65	96.4	15	[276]
	250	1100	10.3	36.6	106	16	[280]

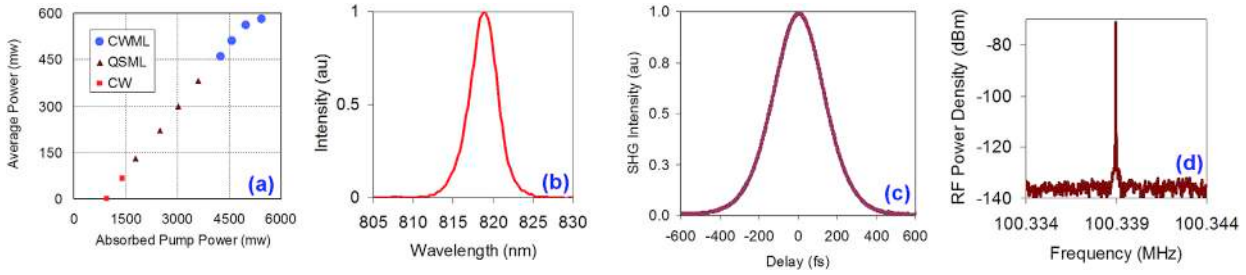

Fig. 38. Cw mode-locked operation results obtained by 4 × 1.8 W MMD pumped Cr:LiSAF laser using a 1% output coupler. The laser produced 185 fs, 5.8 nJ pulses centered around 820 nm at a repetition rate of 100.3 MHz [57]. (a) Laser efficiency, (b) Optical spectrum, (c) background-free intensity autocorrelation trace, and (d) microwave spectrum. CW: Continuous wave, QSML: Q-switched mode-locked, CWML: CW mode-locked. Reproduced with permission from Ref. [57].

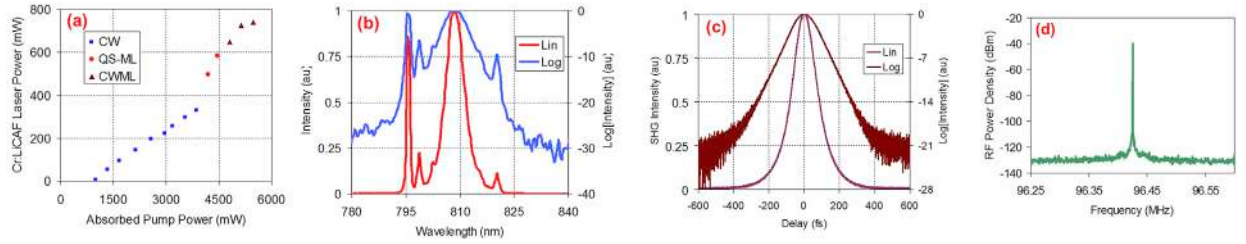

Fig. 39. Cw mode-locked operation results obtained by 4 × 1.8 W MMD pumped Cr:LiCAF laser using a 2% output coupler. The laser produced 105 fs, 7.7 nJ pulses centered around 805 nm at a repetition rate of 96.4 MHz [276]. (a) Laser efficiency, (b) Optical spectrum, (c) background-free intensity autocorrelation trace, and (d) microwave spectrum. CW: Continuous wave, QSML: Q-switched mode-locked, CWML: CW mode-locked. Reproduced with permission from Ref. [276].

1.7.2. Cr:Colquiriite Lasers mode-locked by KLM

If one looks into the literature in detail, it is clear that for mode-locking of Cr:Colquiriite laser systems usually saturable Bragg reflectors were employed. As outlined in detail above, with SBR mode-locking self-starting mode-locked operation with optical-to-optical conversion efficiencies up to 30% and electrical-to-optical conversion efficiencies of 10% could be achieved [225,228,300]. On the other hand, the low refractive index difference between GaAs and AlAs, which are the common materials used in the Bragg reflector design of SBRs, limit the bandwidth of these devices. We have seen that, in systems mode-locked by regular SBRs, this relatively narrow reflectivity bandwidth restricts the obtainable tuning ranges to 30–50 nm, and pulsewidths to 25-fs level. On the other hand, Cr:Colquiriite lasers has much broader gain bandwidths that could enable tuning of fs pulses in a 150–250 nm range, and generation of sub-7-fs long pulses.

Kerr-lens mode-locking (KLM) is the second widely used technique in generation of ultrashort pulses in Cr:Colquiriite lasers (Tables 8 and 9). KLM is first discovered in Ti:Sapphire lasers by Spence et al., in 1990 [313], and it is initially called self mode-locking [313] or magic mode-locking [220]. Later the underlying physics behind KLM is understood as an intensity dependent refractive index change resulting in a time and position dependent Kerr lens, along with a soft and/or hard aperture creating a mechanism that favors intense pulses over cw operation. In general, Kerr-lensing mechanism does not impose any practical intrinsic bandwidth limitation and hence, enables the generation of shortest pulses and demonstration of broadest tuning ranges in mode-locked operation. However, KLM process requires well engineered systems in Cr:Colquiriite lasers to achieve long-term stable and robust operation due to their relatively low

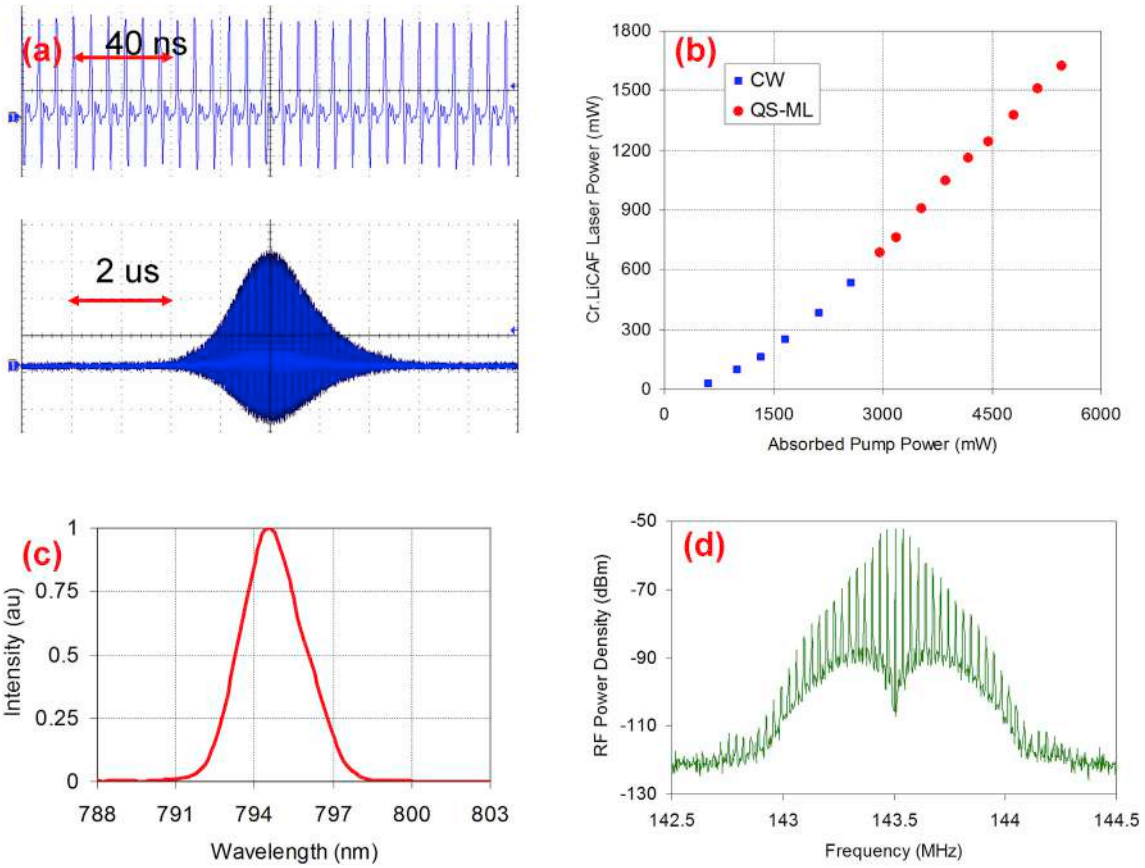

Fig. 40. Q-switched mode-locked operation results obtained by 4×1.8 W MMD pumped Cr:LiCAF laser using a 2% output coupler. The laser produced up to 1.6 W of average power [276]. (a) Q-switched pulse train intensity versus time. (b) Laser efficiency, (c) Optical spectrum, and (d) microwave spectrum. CW: Continuous wave, QSML: Q-switched mode-locked. Reproduced with permission from Ref. [276].

Table 8
Summary of mode-locking results obtained with Cr:LiSAF via Kerr-lens mode-locking using different pump sources.

Pump source	Pulse width (fs)	Average power (mW)	Pulse energy (pJ)	Peak power (W)	Rep rate (MHz)	Year	Ref.
Krypton	150	50	610	3.6×10^3	82	91	[247]
Argon	50	150	1830	31.5×10^3	84	92	[250]
1×250 mW (MMD)	97	2.7	35	300	80	94	[314]
SH of Nd:YLF (659 nm)	90	20	0.2	2.2	100	94	[255]
2×400 mW (MMD)	70	50	–	–	–	95	[315]
4×500 mW (MMD)	40	70	935	20.6×10^3	75	95	[316]
	27	10	135	4×10^3			
2×400 mW (MMD)	34	42	525	13.6×10^3	80	95	[317]
SH of Nd:YAG (532 nm)	90	100	1.06	11.8	85	96	[256]
1×30 mW (SMD)	200	0.23	1.3	6	180	97	[225]
2×50 mW (SMD)	60	1.57	9	137	180		
1×800 mW (MMD)	26	6.2	–	–	–	97	[318]
Krypton	15	70	1	66.7	70	97	[55,248]
Krypton	37	10	–	–	–	97	[155]
2×500 mW (MMD)	80	110	1.25×10^3	13.8×10^3	88	98	[238]
2 x ~400 mW (MMD)	12	6.5	32.5	2.4×10^3	200	99	[295]
	9.9	2.3	11.5	1×10^3	200	00	[58]
	10.4	6.2	31	2.6×10^3	200	03	[156]
	14	23	115	7.2×10^3	200		
1×130 mW (SMD)	13	25	200	15×10^3	126	14	[294]
1×1.2 W (TDL)	14.5	106	940	60×10^3	113	15	[290]

nonlinear refractive index value (as discussed earlier, n_2 of Cr:LiCAF is 0.4×10^{-16} cm^2/W [13], which is 8 times smaller than Ti:Sapphire [13]). Especially for the generation of ultrashort pulses, all the available gain bandwidth of the laser active medium needs to

Table 9
Summary of mode-locking results obtained with Cr:LiCAF via Kerr-lens mode-locking using different pump sources.

Pump source	Pulse width (fs)	Pulse energy (nJ)	Average power (mW)	Peak power (kW)	Rep rate (MHz)	Year	Ref.
Krypton laser	170	~1.1	100	6.5	90	92	[319]
2 × 500 mW (MMD)	52	~0.8	75	15.4	95	98	[320]
	20	~0.14	13	7	95		
Ti:Sapphire	9	~2.2	220	244.4	97	02	[53]
2 × 500 mW	10	~0.37	40	37	110	03	[232]

be used. However, the gain of the laser active media are not flat over the whole gain bandwidth, and hence strong gain filtering effect is present. As a result a large Kerr nonlinearity induced self-amplitude modulation is required to exceed the gain filtering effect, which then usually demands use of low output coupling for boosting the intracavity nonlinearities, and critical cavity alignment near the edge of the laser stability region. On the other hand, these demands might contradict with efficient laser operation, might diminish laser efficiency, reduce output beam quality and create long-term stability problems. We note here that, due to the high FOM of the crystals, Cr:Colquiriite lasers could be operated efficiently even at low output coupling, which somehow balances their drawback in KLM due to low n_2 values. In short, as the results in literature also shows stable KLM action in Cr:Colquiriite lasers are possible (Tables 8 and 9), but in general requires a more carefully engineered system compared to SBR mode-locking.

KLM was first demonstrated in Cr:Colquiriite lasers in 1991 [247], just one year after its discovery in Ti:Sapphire [313]. In this initial work, Miller et al. pumped a 0.8% Cr-doped 15 mm long Cr:LiSAF crystal with 1 W of power from a Krypton pump laser and obtained 150 fs long pulses with 50 mW average power at a repetition rate of 82 MHz [247]. However, an acusto-optic modulator was also involved in initiating and sustaining mode-locking. Just a few months later, an "unambiguous demonstration" of KLM has been shown in a similar Argon ion pumped Cr:LiSAF laser, and 50 fs pulses with 150 mW average power has been achieved [250]. First KLM mode-locking of Cr:LiCAF followed shortly afterwards, where Likam Wa et al. used a Krypton laser as the pump source and obtained 170 fs long pulses with 100 mW average power at a repetition rate of 90 MHz [319]. KLM operation was first demonstrated in a diode pumped Cr:Colquiriite laser in 1994 [314]. In this study, Dymott and Ferguson used two 250 mW multimode diodes to pump a prism dispersion compensated Cr:LiSAF cavity and achieved 97 fs pulses with 2.7 mW of average power at a repetition rate of 80 MHz [314].

The shortest pulses obtained with KLM Cr:LiSAF lasers to date is 10 fs long (Fig. 41) [58]. For that result Uemura and Torizuka used a 1.5% Cr-doped Cr:LiSAF crystal pumped by two multimode diodes at a total pump power of 800 mW. As an initial work, group delay dispersion (GDD) and third-order dispersion (TOD) of Cr:LiSAF crystal were measured carefully [154]. Several prism pairs were investigated both experimentally and numerically to find the optimum dispersion setting for ultrashort pulses. Using a 0.1% transmitting output coupler, and a N-ZK7 prism pair with a 60 cm separation, 9.9 fs long pulses with 2.3 mW of average power was obtained at a repetition rate of 200 MHz [58]. Note that a knife edge was required to sustain KLM mode-locked operation (hard aperture mode-locking). The corresponding pulse energies and peak powers were 11.5 pJ and 1 kW, respectively. Moreover, due to the usage of very low output coupling, the optical-to-optical conversion efficiency of the system is only around 0.3% (2.3/800). Using LaKL21 prism pair with a separation of 36 cm and a 0.3% output coupler, 10.4 fs long pulses with 6.2 mW average power, and using BK7 prism pair with a separation of 47 cm and a 0.7% output coupler, 14 fs long pulses 23 mW average power were also reported [156]. The corresponding optical-to-optical conversion efficiency for these longer pulses were 0.8% and 2.9%, respectively [156]. Note the, the optical spectrum of the mode-locked pulses extends only up to around 950–975 nm (Fig. 41), due to limited reflectivity and dispersion bandwidths of the cavity optics. On the other hand, as cw tuning results has shown Cr:LiSAF has gain extending up to around 1125 nm, hence, we believe that a broadband DCM mirror set covering all the 700–1150 nm range should in principle enable generation of sub-7-fs long pulses from the Cr:LiSAF laser system.

The highest peak powers obtained from KLM Cr:LiSAF lasers to date is 60 kW, where Cihan et al. used 1 W of pump power from a high brightness tapered diode laser [290], and obtained 14.5 fs pulses with 105 mW of average power at a repetition rate of 113 MHz.

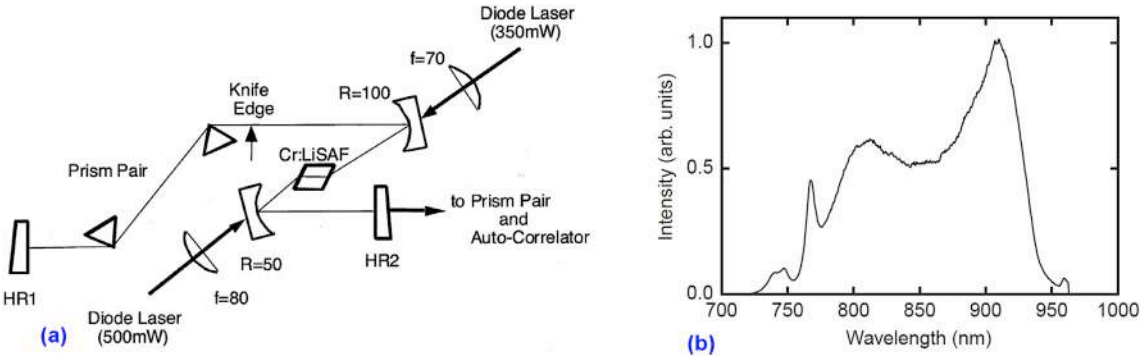

Fig. 41. Cw mode-locked operation results obtained from a Kerr-lens mode-locked Cr:LiSAF laser pumped by one 500 mW and one 350 mW MMD diode [58]. The laser produced 10 fs, 0.37 nJ pulses at a repetition rate of 110 MHz. (a) Schematic of the laser cavity, (b) Mode-locked optical spectrum (reprinted with permission from Ref. [58]).

The corresponding optical-to-optical conversion efficiency was 11%. In that study a gain matched output coupler (GMOC) [321] with a transmission profile that matches the gain spectrum of the laser medium was also used to balance the effect of gain filtering, and as a result a hard aperture was not required in KLM operation.

In the case of Cr:LiCAF, the shortest pulses obtained is 9-fs from a Ti:Sapphire pumped system [53], and 10 fs from a diode pumped system (Fig. 42) [232]. For the diode pumped results, Wagenblast et al. used two 500 mW multimode diodes to pump a 10% Cr-doped 2-mm long Cr:LiCAF crystal [232]. Broadband double chirped mirrors were used to compensate second and third order dispersion and a fused quartz prism pair with a separation of 30 cm was used for fine adjustment of the dispersion. When mode-locked with a soft aperture KLM, the laser produced 10 fs long pulses with an average power of 40 mW at a repetition rate of 110 MHz [232]. For comparison the same group of researchers obtained 9-fs long pulses with 220 mW of average power at 97 MHz, using a very similar cavity, but this time using 2.1 W of diffraction limited output of a Ti:Sapphire laser at 693 nm as the pump source [53]. The optical-to-optical conversion efficiency of the system is around 4% and 10% for the diode and Ti:Sapphire pumped systems, respectively. This shows the potential improvements we can observe in efficiencies of the Cr:Colquiriite lasers as the brightness of the red diode technology gets better over the coming decades.

1.8. Frequency conversion with Cr:Colquiriite lasers

As we discussed above, the fundamental tuning range of Cr:Colquiriite cover the long wavelength side of visible and near-infrared regions from around 720 nm–1100 nm. In this section we will cover nonlinear frequency conversion techniques such as second-harmonic generation, third harmonic generation and optical parametric amplification that is used to shift this fundamental output to near ultraviolet, visible and mid-infrared regions of the spectrum.

1.8.1. CW intracavity second harmonic generation

Light sources in the blue and ultraviolet regions of the optical spectrum are on demand for many applications including spectroscopy, optical imaging, medical diagnosis, undersea communications, information storage and remote atmospheric sensing [322]. On the other hand, there are only a few selected accessible sources in this wavelength range (GaN/GaInN diodes [323,324], Ce-doped lasers [41,46], thulium doped upconversion lasers [325], second/third harmonic of Nd-based lasers [326], Ti:Sapphire [327] and GaAsP based diodes [328]), and these sources have several drawbacks including limited tunability, high-cost, complexity, low efficiency, and disability to produce cw output. For these reasons, frequency doubling of low-cost and broadly tunable Cr:Colquiriite lasers into this spectral region could present an attractive alternative.

As discussed earlier, one advantage of Cr:Colquiriite lasers is the high FOM of the crystals which enables construction of high-Q-cavities that can efficiently store very high laser powers inside the cavity. As an example, a Cr:Colquiriite laser that is pumped by 1-W of pump power, could produce around 400 mW of output power using a 1% output coupler, and then the corresponding intracavity laser powers are around 40 W. On the other hand, due to the low losses of the cavity, one can ideally decrease the output coupling to 0.1%, and boost up the intracavity power levels to 200 W level. For a system that is just pumped by a 1 W pump, this is 200 times enhancement in power levels. Note that this type of power enhancement could not be achieved with Ti:Sapphire lasers due to an order of magnitude higher passive losses of the laser crystal. Hence, Cr:Colquiriite possess an intrinsic efficiency advantage in terms of intracavity nonlinear conversion studies due to their power enhancing cavities.

Fig. 43 shows schematic of a typical Cr:Colquiriite resonator that could be used for efficient cw second harmonic generation. The Cr:Colquiriite cavity is similar to what has been described earlier for cw experiments. On top of that, for intracavity cw blue generation experiments, the cavity was extended and two more curved high reflective mirrors (M4 and M5) have been inserted to generate a second focus within the cavity, which is used to place the nonlinear crystals. As the nonlinear converter, 2-mm long flat-flat cut BBO samples that were optimized for second-harmonic generation at 800 nm, 850 nm and 900 nm have been placed at the newly generated focus between M3 and M4 (corresponding cut angles were 29.2°, 27.5° and 26.1°; respectively). The nonlinear crystals had antireflection coatings both at the fundamental and second-harmonic wavelengths. An output coupler with a transmission of only 0.1% was used to maximize intracavity power levels and improve nonlinear conversion efficiency. Curved mirrors M4 and M5 have relatively large transmission of around 80–90% around the second harmonic wavelengths, acting as output couplers for the frequency doubled beam. A

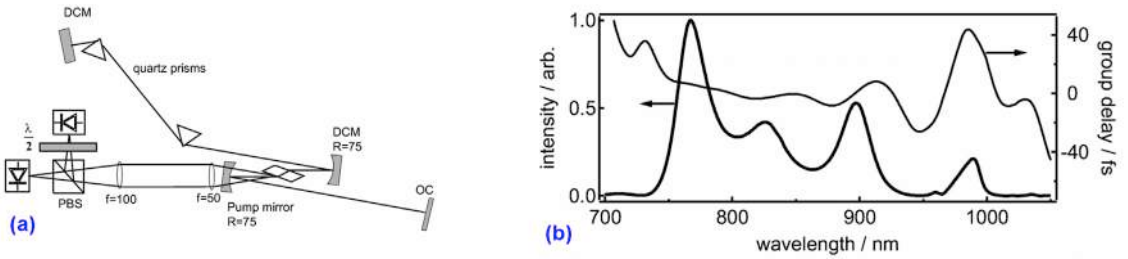

Fig. 42. Cw mode-locked operation results obtained from a Kerr-lens mode-locked Cr:LiCAF laser pumped by 2 × 500 mW MMD diodes under 0.8% output coupling. The laser produced 10 fs, 11.5 pJ pulses at a repetition rate of 200 MHz. (a) Schematic of the laser cavity, (b) Mode-locked optical spectrum and group delay (reprinted with permission from Ref. [232]).

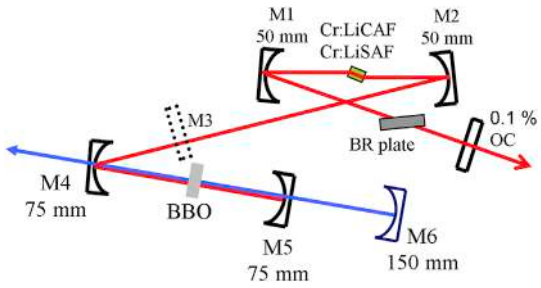

Fig. 43. Schematic of the cw Cr:LiCAF/Cr:LiSAF laser setups that was used in intracavity second harmonic generation experiments. Pump modules are not shown.

metallic high reflector (M6) with a radius of curvature of 150 mm was used to retro-reflect back the blue power transmitted from M4, generating a single blue output. The off-surface optical-axis quartz birefringent tuning plate was used for wavelength tuning of the fundamental and hence the harmonic emissions. For each wavelength, the position and tilt of the BBO samples were adjusted to optimize the second harmonic conversion efficiency.

Fig. 44 shows the tuning range obtained in the intracavity cw frequency-doubling experiments using (a) Cr:LiCAF and (b) Cr:LiSAF gain media. In the case of Cr:LiCAF the second harmonic output could be tuned from 375 to 433 nm (58 nm) with optical powers up to 265 mW around 400 nm (using a system pumped by two 1 W tapered diodes). In the case of Cr:LiSAF, an overall cw tuning range extending from 387 nm to 463 nm could be achieved with output powers approaching 1.2 W around 430 nm. The optical-to-optical-conversion efficiencies of the systems were 13.3% and 16%, respectively. According to the intracavity optical second harmonic generation theory [329], maximum obtainable second harmonic powers could be as high as the maximum available fundamental power from the laser. Hence, with further optimization obtained blue powers from Cr:Colquiriite could potentially be scaled up around 2 fold in future studies. For comparison purposes, Table 10 provides a summary of representative intracavity second harmonic generation results obtained with Cr:Colquiriites as well as Ti:Sapphire and Nd:YAG. Note that the o-to-o conversion efficiencies demonstrated with Cr:Colquiriites are about 3 times better than Ti:Sapphire, and gets close to single-wavelength Nd-based systems, which lack the tuning ability.

1.8.2. CW intracavity optical parametric oscillator operation

The power enhancement advantage of Cr:Colquiriite cavities was also used to demonstrate tunable cw intracavity optical parametric oscillators in the telecom wavelength region, which is potentially important for applications such as all-optical networks based on wavelength division multiplexing [346]. For this Maestre et al. placed a 20 mm long periodically poled stoichiometric lithium tantalate (PPSLT) crystal with a poling period of 22.1 μm inside a Cr:LiCAF resonator pumped by two fiber coupled 750 mW multimode laser diodes (see Fig. 45) [345]. The Cr:LiCAF laser wavelength is narrowed down below 30 p.m. using an external grating in Littrow configuration which also enabled tuning of the laser wavelength [345,347]. The cavity mirrors M1 (coated surface of the Cr:LiCAF crystal) and M2 had high reflectivity both at the lasing and the OPO wavelengths. The system provided up to 10 mW of OPO power, and tunability of wavelength in the 1450–1750 nm range. The performance in this study was limited due to the low brightness of the pump diodes as well as a parasitic free running oscillation that stole energy from the narrowband Cr:LiCAF output [345]. We believe in future

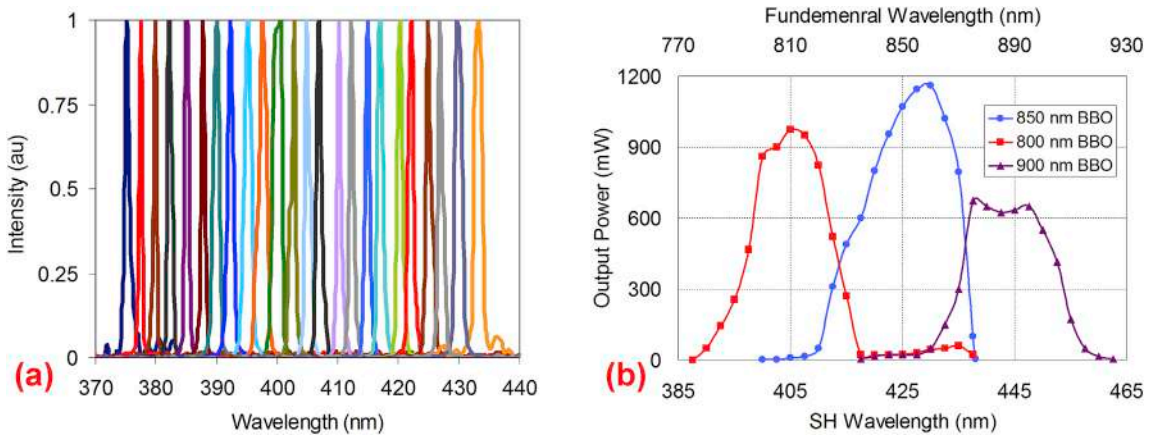

Fig. 44. (a) Optical spectra obtained in from the cw intracavity frequency doubled Cr:LiCAF laser. The cw blue light is tunable from 375 to 433 nm (58 nm) with optical powers up to 265 mW around 400 nm [52,336]. (b) Measured cw frequency-doubled tuning range (387–463 nm) for the multimode diode-pumped Cr:LiSAF laser (reproduced with permission from Ref. [57]).

Table 10
Summary of cw intracavity second harmonic (SH) generation experiments performed with Cr:Colquiriites. Representative cw intracavity frequency doubling results obtained with other gain media have also been shown.

Material	Pump source	Pump power (W)	SH crystal	SH power (mW)	SH wavelength (nm)	o-to-o efficiency (%)	Year	Ref.
Cr:LiSAF	Multimode diode	1 × 0.5 1 × 0.4	$KNbO_3$	13	435 (427–443)	1.4	95	[330]
Cr:LiSAF	Multimode diode (fiber bundle)	4	LBO	20	435 (432–442)	0.5	97	[331]
Cr:LiSAF	Multimode diode	0.35	$KNbO_3$	0.37	430	1.1	98	[332]
Cr:LiSAF	Multimode diode	1	LBO	67.8	430	6.8	00	[333]
Cr:LiSAF	Multimode diode	1.2	LBO	120	430	10	01	[334]
Cr:LiSAF	Multimode diode	1	LBO	32	430	3.2	02	[335]
Cr:LiCAF	Single-mode diode	0.145	BBO	3.5	400 (375–433)	2.4	12	[52]
Cr:LiCAF	Tapered diode	2 × 1	BBO	265	395–405	13.3	13	[336]
Cr:LiCAF	Fiber coupled diode	1.2	BiBO	34	390–415	2.8	15	[337]
Cr:LiSAF	Multimode diode	4 × 1.8 W	BBO	1160	430 (387–463)	16	15	[57]
Nd:YAG	Fiber coupled diode	23	PPKTP	500	473	2.2	03	[326]
Nd:YAG	Fiber coupled diode	23	PPKTP	200	469	0.9	03	[326]
$Nd:GdVO_4$	Fiber coupled diode	30	LBO	5,300	456	17.7	06	[338]
$Nd:YVO_4$	Fiber coupled diode	30	LBO	4,600	457	15.3	06	[339]
$Nd:YVO_4$	Fiber coupled diode	210	LBO	62,000	532	29	07	[340]
$Nd:GdVO_4$	Fiber coupled diode	25	$KNbO_3$	300	440	1.2	08	[341]
Nd:SBN	Fiber coupled diode	1.2	SBN	<1	455–462 525–545	<0.1	05	[342]
Nd:BNN	Fiber coupled diode	0.8	BNN	1	535 (527–547)	0.1	06	[343]
Ti:Sapphire	Argon ion	7.2	LBO	460	398	6.4	95	[344]
Ti:Sapphire	532 nm	10	BiBO	690	423	6.9	07	[327]

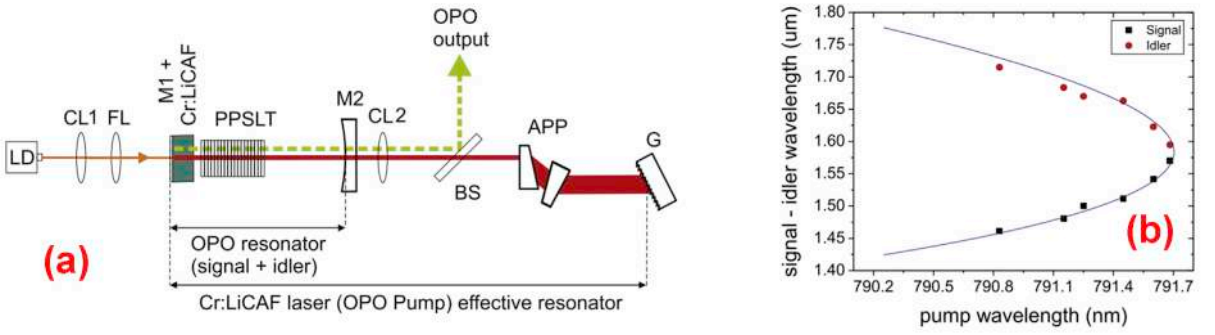

Fig. 45. (a) Intracavity cw OPO resonator based on Cr:LiCAF [345]. (b) Achieved tuning of the signal and idler wavelengths with the variation of pump wavelength (reprinted with permission from Ref. [345]).

studies the output powers from intracavity Cr:Colquiriite OPOs could be potentially scaled to multi 100 mW regime.

1.8.3. Extracavity second and third harmonic generation and OPO pumping

In continuous wave operation, the output powers of Cr:Colquiriite lasers are usually not sufficient to drive extracavity frequency conversion schemas in an efficient way. On the other hand short (ns) and ultrashort (fs) pulsed Cr:Colquiriite systems could provide enough peak powers for efficient extracavity frequency conversion. In one of the earlier studies, Pinto et al. used a tunable flashlamp pumped Q-switched Cr:LiSAF laser producing 20-ns long pulses with around 100 mJ of output energy at 1 Hz for extracavity frequency conversion [267,348]. The output of the laser was first used to generate second-harmonic signal using a 15 mm long LBO crystal utilizing Type I phase matching (cut angle: 22.9°), which is then followed by an 8.5 mm long Type II phase matched BBO crystal (cut angle: 37.5°) for mixing the fundamental with the second harmonic signal generating third harmonic [267]. The system generated tunable second harmonic from 390 to 480 nm with energies up to 20 mJ, and third-harmonic light from 260 to 320 nm with energies up to 6 mJ [267]. The corresponding optical-to-optical conversion efficiency from the fundamental to the third harmonic was above 5%.

A similar Q-switched tunable (830–883 nm) Cr:LiSAF laser with sub-100-ns pulses with a pulse energy of 18 mJ at 10 Hz was used to pump a potassium titanyl arsenate (KTA) based optical parametric oscillator [349,350]. The laser output was focused to a spot size of 400 μm inside the KTA crystal. The OPO cavity was a simple two mirror cavity, which was resonant for the signal wavelengths (around 1200 nm) and was transmittive for the idler wavelengths (around 2940 nm). The system produced up to 1 mJ of signal and 0.5 mJ of idler output [349]. Tuning of the idler wavelength between 2880 nm and 3400 nm could be achieved by tuning the wavelength of the Cr:LiSAF laser. The system was successfully employed in mid-infrared matrix-assisted laser desorption/ionization measurements [349,

350].

Another approach followed for frequency conversion of Cr:Colquiriite lasers is based on usage of high peak powers from femtosecond Cr:Colquiriite lasers [227,301,351,352]. High peak powers generated from fs sources enables efficient (30%) frequency doubling in single pass geometry [301]. Agate et al. used 200 fs pulses with 140 pJ energy at 330 MHz from a low-cost SMD pumped Cr:LiSAF laser as the driving laser source (Fig. 46) [301]. The laser output was focused into a 3 mm long potassium niobate crystal using a 15 mm focal length lens. The system produced 550 fs long blues pulses with an energy of 36 pJ and average power of 12 mW [301]. The optical to optical conversion efficiency of the system from the fundamental to the second harmonic was 26.7%, and the electrical-to-optical efficiency was around 1%, showing the promising performance of the system [301].

1.9. Ultrafast Cr:Colquiriite amplifiers

In this section we would like to review femtosecond pulse amplification results obtained with Cr:Colquiriite gain media. When one looks at the literature (Table 11), one can divide the efforts in three categories: flashlamp pumped amplifier results, argon or krypton laser pumped amplifier results, and diode pumped amplifier results.

In the case of flashlamp pumping, due to thermal issues, the repetition rate of the amplifiers are very low (the best case is 10 Hz [353], the slowest case has a shot in every 10 min: 0.0017 Hz [205,356]). On the other hand, to our knowledge, the highest energy obtained from ultrafast Cr:Colquiriite amplifiers is 1.05 J [359], and it is obtained in a flashlamp pumped system. In that work Ditmire et al. first stretched 110-fs pulses from a Ti:Sapphire amplifier and used the 450-ps long 1-nJ pulses as seeder [359]. In the first stage the pulses were amplified to 12 mJ level in a regenerative amplifier using a 4 mm aperture Cr:LiSAF rod [359]. A serrated aperture is then used to create a super-Gaussian beam profile. Then the pulse first passes through a 4-mm aperture Cr:LiSAF rod, makes two passes in a 9.5 mm aperture Cr:LiSAF rod, and makes another pass through a second 9.5 mm aperture Cr:LiSAF rod, and gets amplified to 400 mJ level [359]. A final pass through a 19-mm aperture Cr:LiSAF rod results in a pulse energy of 1.7 J, which is then compressed to a width of 125 fs. The compressed pulse energy was 1.05 J, corresponding to a peak power of 8.4 TW. On the other hand, the system operates only at a repetition rate of 0.05 Hz, and the average power of the compressed pulses were 52.5 mW [359]. Moreover, the system is relatively complex, inefficient and high-cost.

As an alternative to flashlamp pumping, much higher repetition rates could be achieved from Cr:Colquiriite amplifier systems pumped by Argon/Krypton ion lasers [360,362]. These systems could provide 220 fs pulses with 6.5 μJ pulse energy, 30 MW peak power at up to 10 kHz [362]. The optical-to-optical-conversion efficiency of the system was around 2% [362]. However, these systems do not possess any clear advantage when compared to Ti:Sapphire based technology due to the requirement for complex pump sources.

Directly diode pumped Cr:Colquiriite amplifiers potentially provide attractive alternatives to Ti:Sapphire based technology [206,316,361–363]. On the other hand, there is limited number of earlier work, and the highest pulse energy reported in these studies is only 10.5 μJ (pulse energy before compression, pulses are then compressed down to 170-fs level and the compressed pulse energy was only around 5 μJ) [206,363]. Fig. 47 graphically summarizes the results obtained with Cr:Colquiriite amplifier systems so far along with the state-of-the art Ti:Sapphire and Yb:YAG amplifier results. It is clear that, to compete with already existing technology, the performance of diode pumped Cr:Colquiriite amplifiers should be scaled orders of magnitude both in terms of obtainable energies and peak powers. We believe this then requires a very carefully engineered amplifier systems that could handle the thermal load at high repetition rate operation, probably by employing the newly developed ideas (such as thin disk and/or zig-zag pass geometries, and cryogenic operation) into the Cr:Colquiriites.

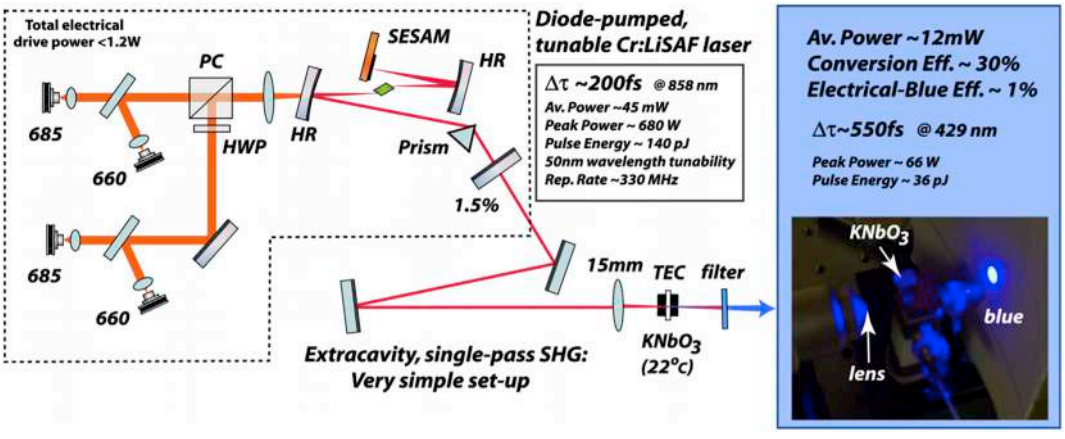

Fig. 46. A single-mode diode pumped Cr:LiSAF laser system efficiently generating femtosecond blue pulses via extracavity conversion in a potassium niobate crystal (reprinted with permission from Ref. [301]).

Table 11
Summary of ultrafast amplification results obtained using Cr:Colquiriites.

Pump	System	Output pulse energy (mJ)	Output pulse width (fs)	Output pulse peak power (GW)	Rep rate (Hz)	Average power (mW)	Year	Ref.
Flashlamp	regen	8	150	53	10	80	92	[353]
Flashlamp	regen + multipass	150	120	1250	1	150	92	[354]
Flashlamp	2 regens	1.2	100	12	6	7.2	93	[355]
Flashlamp	regen + 3 multipass	750	90	8333	0.0017	1.25	93	[205, 356]
Flashlamp	regen + 2 multipass	150	135	1111	0.5	75	93	[357]
Flashlamp	regen + 2 multipass	280	135	2075	1	280	94	[358]
Flashlamp	regen + 4 multipass	1050	125	8400	0.05	52.5	95	[359]
Flashlamp	regen + multipass	30	60	500	5	150	08	[243]
Krypton	regen	0.0036	170	0.021	5000	18	93	[360]
Diode	regen	0.0015	190	0.0079	16000	24	94	[361]
Argon	regen	0.002	220	0.010	20000	40	95	[362]
		0.006		0.029	10000	60		
		0.0065		0.031	5000	32.5		
		0.0065		0.031	1000	6.5		
		0.0065		0.031	1	0.0065		
Diode	regen	0.000625	190	0.0033	15000	9.375		
		0.00075		0.004	10000	7.5		
		0.00075		0.004	1000	0.75		
		0.00075		0.004	100	0.075		
		0.00075		0.004	10	0.0075		
		0.00075		0.004	10	0.0075		
		0.00075		0.004	1	0.00075		
Diode	regen	0.001	197	0.0051	25000	25	95	[289, 316]
Diode	regen	0.004	225	0.0178	2000	8	02	[363]
Diode	regen	0.005	170	0.0295	1000	5	06	[206]
		0.003	170	0.0177	16000	48		

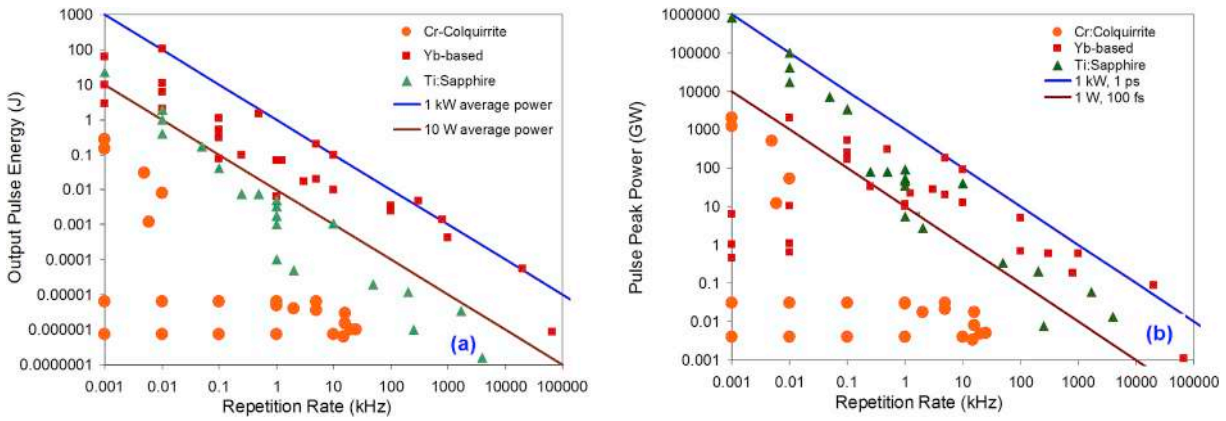

Fig. 47. Output pulse energies (a) and pulse peak powers (b) obtained from Cr:Colquiriite amplifiers to date [206,243,244,316,353–366]. For comparison purposes, representative results from the state of the art Ti:Sapphire and Yb:YAG based amplifier systems are also shown.

1.10. Ultralow timing jitter noise from Cr:Colquiriite oscillators

Timing jitter of an oscillator is the timing error Δt of the power-weighted center of the pulse from the ideally equally-spaced temporal positions defined by the pulse repetition rate f_{rep} [266]. Timing jitter of electronic clocking circuits and the jitter performance of electronic oscillators are currently around 100 fs for state-of-the- art on-chip electronic oscillators [367,368]. On the other hand, optical pulse trains from mode-locked lasers can have timing jitter in the attosecond (as) range, making them very attractive for applications like low phase noise microwave generation [369–373], arbitrary waveform generation [374,375], femtosecond precision long term stable timing distribution and synchronization of large-scale facilities [376–380], and high-speed, high-resolution optical sampling and

analog-to-digital conversion [381].

The achievable timing jitter performance of a mode-locked laser is fundamentally limited by quantum effects: amplified spontaneous emission (ASE) noise from the gain medium (Eq. (18)), coupling of ASE induced center frequency fluctuations into timing jitter (Eq. (19)), and pulse position fluctuations induced by shot noise of the pulse train upon detection with a photodiode (Eq. (20)), and their corresponding spectral power densities could be calculated using [266,382–384]:

$$S_{\Delta t}(f) = \frac{1}{24}(\Theta)\left(f_{\text{rep}}\right)\frac{1}{f^2}(L)\frac{\tau^2}{N_o} \tag{18}$$

$$S_{\Delta t}(f) = \frac{3}{\pi^2}\left(\frac{f_{rep}^3\Omega_g^4}{L^2 f_{rep}^2 + 9\pi^2 f^2\Omega_g^4\tau^4}\right)|D|^2(\Theta)\frac{1}{f^2}(L)\frac{\tau^2}{N_o} \tag{19}$$

$$S_{\Delta t}(f) \approx 0.822\frac{1}{f_{rep}}\frac{\tau^2}{N_o} \tag{20}$$

In the above equations f is the frequency, f_{rep} is the pulse repetition rate, $\tau = \tau_{FWHM}/1.76$ where τ_{FWHM} is the full-width-half-maximum of intracavity pulse duration, N_o is the total photon number in a single intracavity pulse, L is the laser intracavity losses, Ω_g is the half-width-half-maximum gain/cavity bandwidth, D is the intracavity dispersion, and Θ is the excess noise factor, which usually originates from amplitude fluctuations of the input signal [370]. The total quantum limited timing jitter noise is then summation of integral of all the contributions in the desired frequency range:

$$\Delta t_{rms} = \left(2\sqrt{\int_{f_1}^{f_2} S(f)df}\right) \tag{21}$$

Note that in the microwave community the timing jitter is usually represented as a phase error $\Delta\varphi = 2\pi\Delta t \cdot f_{\text{rep}}$ of the fundamental microwave signal acquired upon detection of the pulse train. Looking at Equation (18)–(20), we see that timing jitter noise of lasers are minimized when the laser pulsewidths (τ) are short, when the laser intracavity photon numbers (N_o) are high and when the cavity losses (L) are low. Basically, a mode locked laser generating ultrashort pulses, with high intracavity pulse energies with a high cavity Q can produce pulses with superior timing jitter. We know from our discussions so far that Cr:Colquiriites are very good candidates for this, since their broad gain bandwidth supports sub-10-fs pulses, the low passive losses of the crystals enables working with high-Q-cavities that can store large amount of intracavity photons, and their low nonlinear refractive index minimizes the required cavity dispersion for soliton mode-locking.

As an example Fig. 48 shows calculated quantum noise limited timing jitter noise estimates for reasonable SBR and KLM mode-locked Cr:Colquiriite lasers with 1 nJ output pulse energies at a repletion rates of 100 MHz, and with pulsewidths of 100 fs (SBR) and 10 fs (KLM), respectively. Note that for the SBR mode-locked laser, the estimated quantum noise limited timing jitter noise is 2 as,

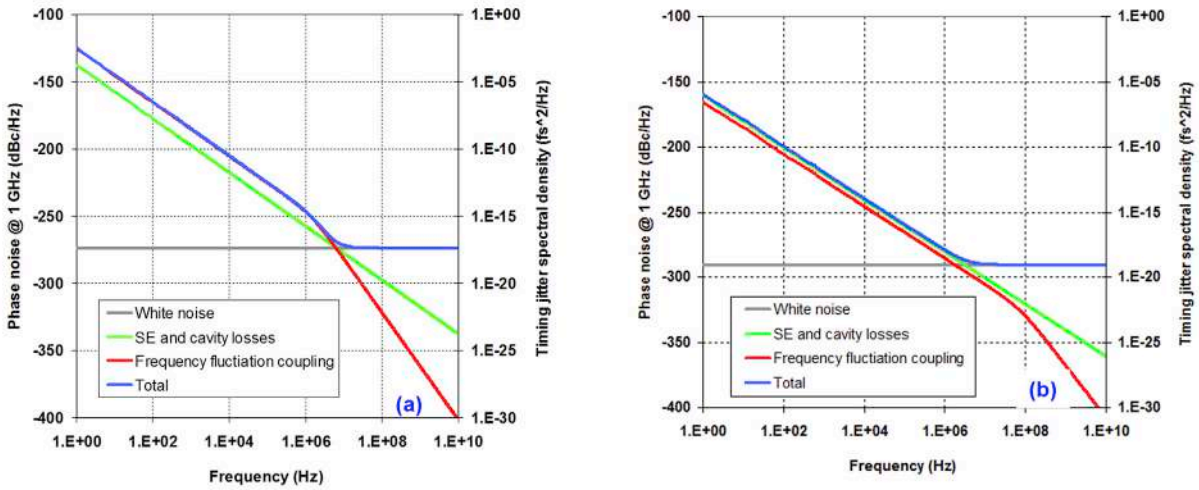

Fig. 48. Calculated quantum-limited single sided phase noise at 1-GHz carrier and timing jitter noise spectral density: (a) for an SBR mode-locked Cr:Colquiriite laser producing 100 fs long 1 nJ pulses at 100 MHz repetition rate (100 nJ intracavity pulse energy, L = 2%, D = −700 fs^2, Θ = 1), (a) for an KLM mode-locked Cr:Colquiriite laser producing 10 fs long 1 nJ pulses at 100 MHz repetition rate (100 nJ intracavity pulse energy, L = 1%, D = −100 fs^2, Θ = 1). Integrated jitter from 10 kHz to 10 MHz is 2 as (a) and 25 zs (b), respectively. White noise term (Eq. (20)), SE (spontaneous emission) and cavity losses term (Eq. (18)), frequency fluctuation coupling term (Eq. (19)).

and for the KLM mode-locked laser it reduces down to 25 zeptosecond (zs). Of course in a real laser technical noise sources such as pump power fluctuations, mechanical vibrations, and temperature fluctuations could produce orders of magnitude higher noise, and hence well engineered lasers systems are required to realize lasers with timing jitter noise close to quantum limited noise baseline. Moreover, due to their inherent ultralow noise characteristics accurate measurement of timing jitter noise of optical pulse trains from mode-locked lasers is a quite challenging task [385–387]. Using balanced nonlinear optical intensity cross correlation, Li et al. succeeded in measuring the upper limit of an SBR mode-locked Cr:LiSAF laser as 30 as (integrated from 10 kHz to 50 MHz) [266,388]. The measurement set only an upper limit, and was limited by the low measurement sensitivity of the system at higher frequencies. This measurement showed that the technical noise of Cr:Colquiriite lasers could be controlled/minimized and the laser sources could actually achieve timing jitter performance close to quantum noise limit. Similar performance was also obtained from other fiber and solid state lasers [389,390], showing the potential of these sources in applications requiring ultra-low timing jitter noise oscillators.

1.11. Application areas of Cr:Colquiriites

In the earlier sections, we have talked about potential usage of Cr:Colquiriite in application requiring low-noise timing jitter sources [266,388], in mid-infrared matrix-assisted laser desorption/ionization measurements [349,350], in optical networks based on wavelength division multiplexing [346], as pump sources for nonlinearities such as second/third harmonic generation and optical parametric oscillators. Cr:Colquiriite sources have further used or proposed to be used in optical coherence tomography (Fig. 49 (a)) [391], multi-photon microscopy (Fig. 49 (b)) [392–395], optical trapping [395], high harmonic generation (Fig. 49 (d)) [396], photo-acoustic imaging, as frequency down-shifters [397], for laser ablation [398], in measurement of bacterial fluorescence [399], in short-coherence photorefractive holography [400], in fluorescence lifetime imaging [401,402], airborne water vapor differential absorption LIDAR and laser induced fluorescence LIDAR (Fig. 49 (c)) [403,404], white light frequency comb generation [405], and holography (Fig. 49 (e)) [406]. In the following, we will present the multiphoton microscopy imaging in a little bit more detail as a representative application area for Cr:Colquiriites.

Multiphoton microscopy (MPM), also known as multiphoton excitation fluorescence microscopy, is a kind of optical sectioning fluorescence microscopy [407], and along with confocal microscopy, it is now one of the most powerful imaging modalities in biomedical microscopy. MPM enables 4-dimensional (x-y-z-t [408]) high-resolution deep imaging of biological samples with minimal damage to the sample [408–412], and hence facilitates imaging of both intact tissue and live animals. Nowadays, MPM is widely used in several diverse areas of biology such as neuroscience, immunology, embryology and cancer research [409]. MPM use nonlinear effects such as two/three photon excitation and second/third harmonic generation [409] to excite the sample, which enables 3-dimensional optical sectioning (3-D localized excitation [409]) by preventing out-of-focus excitation. It is this nonlinear excitations scheme that provides an advantage to MPM compared to traditional (linear) microscopy techniques such as confocal microscopy. The main advantages of MPM compared to linear microscopy are: (i) less amount of photodamage to the sample (polymerization, temperature

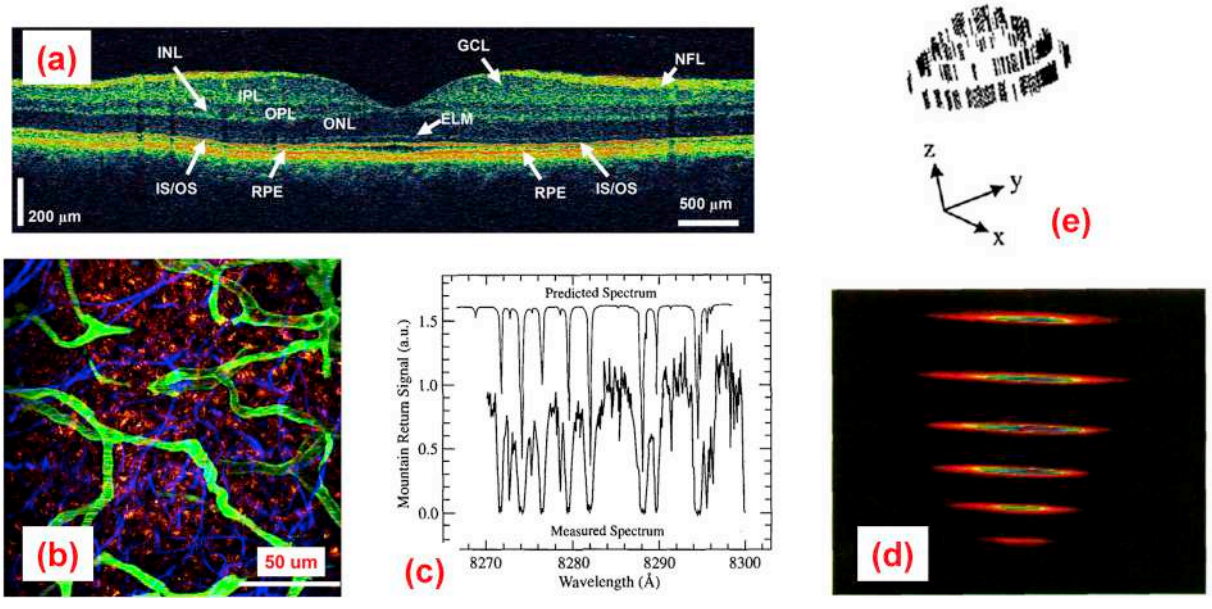

Fig. 49. (a) Optical coherence images of normal retina taken with a femtosecond Cr:LiCAF laser ~3.4 μm axial resolution in tissue (95 dB sensitivity) [391], (b) Multiphoton microscopy images of a mouse popliteal lymph node taken with a femtosecond Cr:LiCAF laser [392], (c)Water vapor absorption profile measured over 32 km path length using a Cr:LiSAF laser with a linewidth of 5 p.m. [404], (d) High harmonics (19th to 29th) generated by a femtosecond Cr:LiSAF amplifier system in argon [396], (e) Computer generated three-dimensional reconstruction of the test object from holographic images taken with a Cr:LiSAF laser [406].

effects) [408,412,413], (ii) possibility of deep tissue imaging [412], and (iii) higher resolution in scattering tissue [409]. Choosing an optimum laser source is very critical for MPM, since parameters of the laser source, such as average power, pulsewidth, repetition rate, i.e., affect the quality of the obtained image directly.

MPM imaging was performed using colliding pulse dye lasers [407,409,414], Ti:Sapphire based laser systems, Yb-based lasers, Nd-based laser systems [415–417], and diode lasers [418–421]. Two photon absorption bands of the common molecular fluorophores used in MPM are centered mostly in the near infrared region between 700 and 1000 nm, with typical bandwidths (FWHM) of ~100 nm [408,418,422]. As a result, Ti:Sapphire which can generate sub-100-fs pulses with hundreds of kW peak power in the 680–1080 nm region has dominance in the field, and are the current workhorse for most of the MPM systems. The main disadvantage of Ti:Sapphire femtosecond laser technology is its high cost, which limits widespread use of MPM. As a result, lower cost Cr:Colquiriite lasers with tunable femtosecond output in the similar spectral region could be a strong alternative for Ti:Sapphire in multiphoton-microscopy. Several groups have demonstrated MPM imaging with Cr:Colquiriites covering a wide range of MPM applications [393,394,423]. We believe the development of lower cost femtosecond laser technology promises to be an important step in enabling wider spread use of multi-photon microscopy, accelerating fundamental research in biology and medicine. In that sense, with further advancement of diode technology, recent MPM imaging efforts with the directly diode pumped Ti:Sapphire systems also could provide a cost-advantage in the coming decades [424].

2. Conclusions and outlook

In this review, we tried to provide a fair presentation of pros and cons of Cr:Colquiriite laser materials. We started with presenting laser related optical, thermal and mechanical properties of Cr:Colquiriites in comparison to well-known materials such as Ti:Sapphire, Alexandrite and Yb:YAG. Then, a summary of research efforts with Cr:Colquiriite gain media over the last decades was summarized, and challenges for future progress has also been discussed. It is shown that main weakness of Cr:Colquiriites lies in its thermal and mechanical properties, which makes power scaling quite challenging. As a result, current Cr:Colquiriite oscillators are limited at best to 2–3 W of average power in cw regime, and to around 0.5 W of average power in femtosecond regime. On the other hand, Cr:Colquiriite materials has broad absorption bands in the visible region that allow direct-diode pumping by well-developed low-cost red diodes, and their broad emission bands in the near infrared support generation of sub-10-fs long pulses. Moreover, Cr: Colquiriites can be grown with very low passive-losses enabling construction of high-Q-cavities. That allows construction of highly efficient and low-cost laser systems pumped only by 100–150 mw of pump power, enables efficient intracavity nonlinear experiments and facilitates realization of record-low laser noise levels. With future improvement of the brightness of red diodes, and with implementation of thin-disk like laser geometries and/or with the practice of cryogenic operation future Cr:Colquiriite oscillators/amplifiers has the potential to reach average powers above 10 W. Recent progress in diode pumped Ti:Sapphire and Alexandrite laser/amplifier systems also provide encouraging results, which will all serve the needs of the photonics community in a much better way in the coming decades.

Acknowledgements

Dr. Demirbas would like to personally acknowledge and thank Prof. Dr. Alphan Sennaroglu, Adnan Kurt and Prof. Dr. Mehmet Somer of Koc University, Prof. Dr. Alfred Leitenstorfer of Konstanz University, Prof. Dr. Franz X. Kärtner and Dr. Huseyin Cankaya of Hamburg University and Prof. Dr. James G. Fujimoto of Massachusetts Institute of Technology for sharing their deep expertise in photonics, laser physics & ultrafast laser technology, and their lifelong professional support.

This research has been partially supported by TÜBİTAK (The Scientific and Technological Research Council of Turkey: 112T220, 112T967, 113F199, 114F191), European Union Marie Curie Career Integration Grant (PCIG11-GA-2012-321787), Bilim Akademisi (BAGEP award), Alexander von Humboldt-Foundation and Center for Applied Photonics of Konstanz University.

References

[1] A. Einstein, Quantum theory of radiation, Phys. Z. 18 (1917) 121–128.
[2] J. Hecht, Short history of laser development, Opt. Eng. 49 (Sep 2010).
[3] W.E. Lamb, R.C. Retherford, Fine structure of the hydrogen atom by a microwave method, Phys. Rev. A 72 (1947) 241.
[4] J.P. Gordon, H.J. Zeiger, C.H. Townes, Molecular microwave oscillator and new hyperfine structure in microwave spectrum of NH3, Phys. Rev. 95 (1954) 282.
[5] J.P. Gordon, H.J. Zeiger, C.H. Townes, The maser–new type of microwave amplifier, frequency standard, and spectrometer,", Phys. Rev. 99 (1955) 1264.
[6] A.L. Schawlow, C.H. Townes, Infared and optical masers, Phys. Rev. 112 (1958) 1940–1949.
[7] W. Koechner, Solid-state laser engineering, in: 6th Rev. And Updated, Springer, New York, 2006.
[8] T.H. Maiman, Stimulated optical radiation in ruby, Nature 187 (1960) 493–494.
[9] M.J. Weber, Handbook of Laser Wavelengths, CRC Press, 1998.
[10] S.R. Wilk, Defunct lasers, OPN Optics Photon. News 21 (2010) 10–11.
[11] A.A. Kaminskii, Laser Crystals: Their Physics and Properties, Springer-Verlag, Heidelberg, 1981.
[12] H. Fattahi, H.G. Barros, M. Gorjan, T. Nubbemeyer, B. Alsaif, C.Y. Teisset, M. Schultze, S. Prinz, M. Haefner, M. Ueffing, A. Alismail, L. Vamos, A. Schwarz, O. Pronin, J. Brons, X.T. Geng, G. Arisholm, M. Ciappina, V.S. Yakovlev, D.E. Kim, A.M. Azzeer, N. Karpowicz, D. Sutter, Z. Major, T. Metzger, F. Krausz, Third-generation femtosecond technology, Optica 1 (2014) 45–63. Jul 22.
[13] E. Sorokin, Solid-state materials for few-cycle pulse generation and amplification, in: F.X. Kärtner (Ed.), In Few-Cycle Laser Pulse Generation and its Applications, vol. 95, Springer-Verlag, Berlin, 2004, pp. 3–71.
[14] P.F. Moulton, Tunable solid-state lasers, Proc. IEEE 80 (1992) 348–364.
[15] A.J. Demaria, Review of cw high-power Co2-lasers, Proc. IEEE 61 (1973) 731–748.
[16] W.R. Bennett, Excitation and inversion mechanisms in gas lasers, Ann. N. Y. Acad. Sci. 122 (1965) 579.
[17] F.P. Schafer, Principles of dye-laser operation, Top. Appl. Phys. 1 (1990) 1–89.
[18] F.P. Schäfer, F.P.W. Schmidth, J. Volze, Organic dye solution laser, Appl. Phys. Lett. 9 (1966) 306–308.

[19] P.P. Sorokin, J.R. Lankard, Stimulated Emission observed from an organic dye, cloro-aluminum phthalocyanine," IBM J, Res. Rev. 10 (1966) 162–163.
[20] J.A. Valdmanis, R.L. Fork, J.P. Gordon, Generation of optical pulses as short as 27 fs directly from a laser balancing self-phase modulation, group-velocity dispersion, saturable absorption, and saturable gain, Opt. Lett. 10 (1985) 131–133.
[21] R.L. Fork, C.H.B. Cruz, P.C. Becker, C.V. Shank, Compression of optical pulses to six femtoseconds by using cubic phase compensation, Opt. Lett. 12 (July 1987) 483–485, 1987.
[22] R. Paschotta, Encyclopedia of Laser Physics and Technology, Wiley-VCH, 2008.
[23] R. Paschotta, U. Keller, Ultrafast solid-state lasers, in: Ultrafast Lasers: Technology and Applications: Marcel Dekker, Inc, 2003.
[24] P.F. Moulton, Spectroscopic and laser characteristics of Ti:Al_2O_3, JOSA B 3 (1986) 125–133.
[25] L.K. Smith, S.A. Payne, W.F. Krupke, L.D. DeLoach, R. Morris, E.W. O'Dell, D.J. Nelson, Laser emission from the transition-metal compound LiSrCrF6, Opt. Lett. 18 (1993) 200–202.
[26] Y. Kalisky, The Physics and Engineering of Solid State Lasers, TT71, SPIE Publications, 2006.
[27] O. Svelto, Principles of Lasers, Plenum Press, New York, 1989.
[28] I.T. Sorokina, Crystalline mid-infrared lasers, in: I.T. Sorokina, K.L. Vodopyanov (Eds.), Solid-State Mid-infrared Laser Sources, vol 89, Springer, Berlin Heidelberg, 2003, pp. 255–349.
[29] E. Snitzer, Glass lasers, Appl. Opt. 5 (October 1966) 1487–1499, 1966.
[30] http://en.wikipedia.org/wiki/Transition_metal.
[31] http://goldbook.iupac.org/T06456.html.
[32] S.A. Payne, L.L. Chase, L.K. Smith, W.L. Kway, H.W. Newkirk, Laser performance of $LiSAlF_6$:Cr^{3+}, J. Appl. Phys. 66 (1989) 1051–1056.
[33] S.A. Payne, L.K. Smith, R.J. Beach, B.H.T. Chai, J.H. Taasano, L.D. DeLoach, W.L. Kway, R.W. Solarz, W.F. Krupke, Properties of Cr:$LiSrAlF_6$ crystals for laser operation, Appl. Opt. 33 (1994) 5526–5536.
[34] S.A. Payne, L.L. Chase, H.W. Newkirk, L.K. Smith, W.F. Krupke, $LiCaAlF_6$:Cr^{3+} a promising new solid-state laser material, IEEE J. Quantum Electron. 24 (Nov 1988) 2243–2252.
[35] R. Scheps, J.F. Myers, S.A. Payne, Cw and Q-switched operation of a low threshold Cr^{+3}-Licaalf$_6$ laser, IEEE Photonics Technol. Lett. 2 (Sep 1990) 626–628.
[36] S.A. Payne, L.L. Chase, L.K. Smith, B.H.T. Chai, Flashlamp-pumped laser performance of $LiCaAlF_6$ Cr^{3+}, Opt. Quant. Electron. 22 (Jul 1990) S259–S268.
[37] L.K. Smith, S.A. Payne, W.L. Kway, L.L. Chase, B.H.T. Chai, Investigation of the laser properties of Cr^{3+}:$LiSrGaF_6$, IEEE J. Quantum Electron. 28 (1992) 2612–2618.
[38] B.H.T. Chai, J.-L. Lefaucheur, M. Stalder, M. Bass, Cr:$LiSr_{0.8}Ca_{0.2}AlF_6$ tunable laser, Opt. Lett. 17 (1992) 1584–1586.
[39] A. Sennaroglu, Broadly tunable Cr^{4+} -doped solid-state lasers in the near infrared and visible, Prog. Quantum Electron. 26 (2002) 287–352, 2002.
[40] I.T. Sorokina, Broadband mid-infrared solid-state lasers," in mid-infrared coherent sources and applications, in: M. Ebrahim-Zadeh, I.T. Sorokina (Eds.), NATO Science for Peace and Security Series B: Physics and Biophysics, Springer, 2008.
[41] A.J.S. McGonigle, D.W. Coutts, C.E. Webb, 530-mW 7-kHz cerium LiCAF laser pumped by the sum-frequency-mixed output of a copper-vapor laser, Opt. Lett. 24 (1999) 232–234.
[42] D.W. Coutts, A.J.S. McGonigle, Cerium-doped fluoride lasers, IEEE J. Quantum Electron. 40 (2004) 1430–1440.
[43] S. Ono, Z. Liu, N. Sarukura, in: Solid-State Lasers, Applications A. Sennaroglu (Eds.), All-Solid-State Ultraviolet Cerium Lasers, 2006, pp. 163–191.
[44] E. Granados, D.W. Coutts, D.J. Spence, Mode-locked deep ultraviolet Ce:LiCAF laser, Opt. Lett. 34 (2009) 1660–1662.
[45] Z. Liu, T. Kozeki, Y. Suzuki, N. Sarukura, K. Shimamura, T. Fukuda, M. Hirano, H. Hosono, Chirped-pulse amplification of ultraviolet femtosecond pulses by use of Ce^{3+}:$LiCaAlF_6$ as a broadband, solid-state gain medium, Opt. Lett. 26 (2001) 301–303.
[46] A.J.S. McGonigle, S. Girard, D.W. Coutts, R. Moncorgé, 10-kHz continuously tunable Ce:LiLuF laser, Electron. Lett. 35 (1999) 1640–1641.
[47] J.F. Pinto, L. Esterowitz, G.J. Quarles, High performance Ce :LiSrAlF/LiCaAlF lasers with extended tunability, Electron. Lett. 31 (1995) 2009–2010.
[48] R. Ell, U. Morgner, F.X. Kärtner, J.G. Fujimoto, E.P. Ippen, V. Scheuer, G. Angelow, T. Tschudi, Generation of 5 fs pulses and octave-spanning spectra directly from a Ti:sapphire laser, Opt. Lett. 26 (2001) 373–375.
[49] J.C. Walling, O.G. Peterson, H.P. Jenssen, R.C. Morris, E.W. O'Dell, Tunable alexandrite lasers, IEEE J. Quantum Electron. 16 (1980) 1302–1315.
[50] C. Cihan, A. Muti, I. Baylam, A. Kocabas, U. Demirbas, A. Sennaroglu, 70 femtosecond Kerr-lens mode-locked multipass-cavity Alexandrite laser, Opt. Lett. 43 (2018) 1315–1318. Mar 15.
[51] U. Demirbas, D. Li, J.R. Birge, A. Sennaroglu, G.S. Petrich, L.A. Kolodziejski, F.X. Kärtner, J.G. Fujimoto, Low-cost, single-mode diode-pumped Cr:Colquiriite lasers, Opt. Express 17 (2009) 14374–14388.
[52] U. Demirbas, R. Uecker, D. Klimm, J. Wang, Low-cost, broadly tunable (375-433 nm & 746-887 nm) Cr:LiCAF laser pumped by one single-spatial-mode diode, Appl. Opt. 51 (2012) 8440–8448.
[53] P. Wagenblast, U. Morgner, F. Grawert, V. Scheuer, G. Angelow, M.J. Lederer, F.X. Kärtner, Generation of sub-10-fs pulses from a Kerr-lens modelocked Cr^{3+}: LiCAF laser oscillator using third order dispersion compensating double chirped mirrors, Opt. Lett. 27 (2002) 1726–1729.
[54] I.T. Sorokina, E. Sorokin, E. Wintner, A. Cassanho, H.P. Jenssen, M.A. Noginov, Efficient cw TEM_{00} and femtosecond Kerr-lens modelocked Cr:LiSrGaF laser, Opt. Lett. 21 (1996) 204–206.
[55] I.T. Sorokina, E. Sorokin, E. Wintner, A. Cassanho, H.P. Jenssen, R. Szipocs, 14-fs pulse generation in Kerr-lens mode-locked prismless Cr:LiSGaF and Cr:LiSAF lasers: observation of pulse self-frequency shift, Opt. Lett. 22 (1997) 1716–1718.
[56] M. Stalder, B.H.T. Chai, M. Bass, Flashlamp pumped Cr:$LiSrAlF_6$ laser, Appl. Phys. Lett. 58 (1991) 216–218.
[57] U. Demirbas, I. Baali, Power and efficiency scaling of diode pumped Cr: LiSAF lasers: 770–1110 nm tuning range and frequency doubling to 387–463 nm, Opt. Lett. 40 (2015) 4615–4618.
[58] S. Uemura, K. Torizuka, Generation of 10 fs pulses from a diode-pumped Kerr-lens mode-locked Cr : LiSAF laser, Japan. J. Appl. Phys. Part 1 Regul. Pap. Short Notes Rev. Pap. 39 (Jun 2000) 3472–3473.
[59] E. Sorokin, M.H. Ober, I. Sorokina, E. Wintner, A.J. Schmidt, A.I. Zagumennyi, G.B. Loutts, E.W. Zhariko, I.A. Shcherbakov, Femtosecond solid-state lasers using Nd3+-doped mixed scandium garnet, JOSA B 10 (1993) 1436–1442.
[60] F. Druon, F. Balembois, P. Georges, New laser crystals for the generation of ultrashort pulses, Compt. Rendus Phys. 8 (Mar 2007) 153–164.
[61] J.A.D. Au, D. Kopf, F. MorierGenoud, M. Moser, U. Keller, 60-fs pulses from a diode-pumped Nd:glass laser, Opt. Lett. 22 (1997) 307–309. Mar 1.
[62] V.G. Baryshevskii, M.V. Korzhik, A.E. Kimaev, M.G. Livshits, V.B. Pavlenko, M.L. Meil'man, B.I. Minkov, Tunable chromium forsterite laser in the near IR region, J. Appl. Spectrosc. 53 (1990) 675–676.
[63] C. Chudoba, J.G. Fujimoto, E.P. Ippen, H.A. Haus, U. Morgner, F.X. Kärtner, V. Scheuer, G. Angelow, T. Tschudi, All-solid-state Cr:forsterite laser generating 14 fs pulses at 1.3 um, Opt. Lett. 26 (2001) 292–294.
[64] S. Kuck, K. Petermann, U. Pohlmann, U. Schonhoff, G. Huber, Tunable room-temperature laser action of a Cr-4+-doped Y3ScxAl5-xO12, Appl. Phys. B 58 (1994) 153–156.
[65] D.J. Ripin, C. Chudoba, J.T. Gopinath, J.G. Fujimoto, E.P. Ippen, U. Morgner, F.X. Kartner, V. Scheuer, G. Angelow, T. Tschudi, Generation of 20-fs pulses by a prismless Cr^{4+}: YAG laser, Opt. Lett. 27 (2002) 61–63. Jan 1.
[66] S. Uemura, K. Torizuka, Sub-40-fs pulses from a diode-pumped kerr-lens mode-locked Yb-doped yttrium aluminum garnet laser, Jpn. J. Appl. Phys. 50 (Jan 2011).
[67] F. Cornacchia, E. Sani, A. Toncelli, M. Tonelli, M. Marano, S. Taccheo, G. Galzerano, P. Laporta, Optical spectroscopy and diode-pumped laser characteristics of codoped Tm-Ho:YLF and Tm-Ho:BaYF: a comparative analysis, Appl. Phys. B 75 (2002) 817–822.
[68] R.C. Stoneman, L. Esterowitz, Efficient, broadly tunable, laser-pumped Tm:YAG and Tm:YSGG cw lasers, Opt. Lett. 15 (May 1, 1990) 486–488, 1990.
[69] A. Gluth, Y.C. Wang, V. Petrov, J. Paajaste, S. Suomalainen, A. Harkonen, M. Guina, G. Steinmeyer, X. Mateos, S. Veronesi, M. Tonelli, J. Li, Y.B. Pan, J.K. Guo, U. Griebner, GaSb-based SESAM mode-locked Tm:YAG ceramic laser at 2 mu m, Opt. Express 23 (2015) 1361–1369. Jan 26.
[70] A. Dergachev, K. Wall, P.F. Moulton, A CW side-pumped Tm:YLF laser, in: OSA TOPS Advanced Solid State Lasers, 2002, pp. 343–346.

[71] J.F. Pinto, L. Esterowitz, Tm^{3+}:YLF laser continuously tunable between 2.20 and 2.46 μm, Opt. Lett. 19 (1994) 883–885.
[72] F. Canbaz, I. Yorulmaz, A. Sennaroglu, Kerr-lens mode-locked 2.3-μm Tm^{3+}:YLF laser as a source of femtosecond pulses in the mid-infrared, Opt. Lett. 42 (2017) 3964–3967. Oct 1.
[73] D. Welford, P.F. Moulton, Romm-temperature operation of a Co:MgF_2 laser, Opt. Lett. 13 (November 1988) 975–977, 1988.
[74] I.T. Sorokina, E. Sorokin, S. Mirov, V. Fedorov, V. Badikov, V. Panyutin, K. I.Schaffers, "Broadly tunable compact continuous-wave Cr^{2+}:ZnS laser, Opt. Lett. 27 (June 15, 2002) 1040–1042, 2002.
[75] E. Sorokin, I.T. Sorokina, M.S. Mirov, V.V. Fedorov, I.S. Moskalev, S.B. Mirov, Ultrabroad continuous-wave tuning of ceramic Cr:ZnSe and Cr:ZnS lasers, in: OSA/ASSP/LACSEA/LS&C: OSA, 2010. AMC2.
[76] S. Vasilyev, I. Moskalev, M. Mirov, S. Mirov, V. Gapontsev, Three optical cycle mid-IR Kerr-lens mode-locked polycrystalline Cr^{2+}:ZnS laser, Opt. Lett. 40 (2015) 5054–5057. Nov 1.
[77] J. McKay, K.L. Schepler, G. C.Catella, "Efficient grating-tuned mid-infrared Cr^{2+}:CdSe laser, November 15, Opt. Lett. 24 (1999) 1575–1577, 1999.
[78] V.A. Akimov, M.P. Frolov, Y.V. Korostelin, V.I. Kozlovsky, A.I. Landman, Y.P. Podmar'kov, Y.K. Skasyrsky, A.A. Voronov, Pulsed broadly tunable room-temperature Cr2+:CdS laser, Dec, Appl. Phys. B Laser Opt. 97 (2009) 793–797.
[79] V.A. Akimov, V.I. Kozovskii, Y.V. Korostelin, A.I. Landman, Y.P. Podmar'kov, Y.K. Skasyrskii, M.P. Frolov, Efficient pulsed Cr^{2+}: CdSe laser continuously tunable in the spectral range from 2.26 to 3.61, Mar, Quantum Electron. 38 (2008) 205–208.
[80] U. Demirbas, A. Sennaroglu, Intracavity-pumped Cr^{2+}: ZnSe laser with ultrabroad tuning range between 1880 and 3100 nm, AUG 1, Opt. Lett. 31 (2006) 2293–2295.
[81] U. Demirbas, J. Wang, G.S. Petrich, S. Nabanja, J.R. Birge, L.A. Kolodziejski, F.X. Kartner, J.G. Fujimoto, 100-nm tunable femtosecond Cr:LiSAF laser mode locked with a broadband saturable Bragg reflector, Appl. Opt. 56 (2017) 3812–3816. May 1.
[82] J. Kernal, V.V. Fedorov, A. Gallian, S.B. Mirov, V.V. Badikov, 3.9-4.8 μm gain-switched lasing of Fe:ZnSe at room temperature, Opt. Express 13 (2005) 10608–10615.
[83] P.F. Moulton, Ti-doped sapphire: tunable solid-state laser, Nov./Dec., in: Optics News, 1982, p. 9.
[84] L.G. DeShazer, K.W. Kangas, Extended infared operation of titanium sapphire laser, in: Conference on Lasers and Electro Optics, vol 14, 1987, pp. 296–298.
[85] P.W. Roth, A.J. Maclean, D. Burns, A.J. Kemp, Directly diode-laser-pumped Ti:sapphire laser, Opt. Lett. 34 (2009) 3334–3336.
[86] P.W. Roth, D. Burns, A.J. Kemp, Power scaling of a directly diode-laser-pumped Ti:sapphire laser, Opt. Express 20 (2012) 20629–20634. Aug 27.
[87] S. Sawai, A. Hosaka, H. Kawauchi, K. Hirosawa, F. Kannari, Demonstration of a Ti:sapphire mode-locked laser pumped directly with a green diode laser, APEX 7 (2014) 022702.
[88] K. Gürel, M. Hoffmann, C.J. Saraceno, V.J. Wittwer, S. Hakobyan, B. Resan, A. Rohrbacher, K. Weingarten, S. Schilt, T. Südmeyer, Ultrafast diode-pumped Ti: sapphire laser generating 200-mW average power in 68-fs pulses, in: CLEO San Jose, USA: OSA, 2015. STu1O.3.
[89] M.D. Young, S. Backus, C. Durfee, J. Squier, Multiphoton imaging with a direct-diode pumped femtosecond Ti:sapphire laser, J. Microsc. 249 (Feb 2013) 83–86.
[90] C.G. Durfee, T. Storz, J. Garlick, S. Hill, J.A. Squier, M. Kirchner, G. Taft, K. Shea, H. Kapteyn, M. Murnane, S. Backus, Direct diode-pumped Kerr-lens mode-locked Ti:sapphire laser, Opt. Express 20 (2012) 13677–13683. Jun 18.
[91] P.W. Roth, A.J. Maclean, D. Burns, A.J. Kemp, Direct diode-laser pumping of a mode-locked Ti:sapphire laser, Opt. Lett. 36 (2011) 304–306. Jan 15.
[92] P.W. Roth, A.J. Maclean, D. Burns, A.J. Kemp, Modelocking of a diode-laser-pumped Ti:sapphire laser, in: 2010 Conference On Lasers And Electro-Optics (Cleo) And Quantum Electronics And Laser Science Conference (Qels), 2010.
[93] S. Backus, M. Kirchner, C. Durfee, M. Murnane, H. Kapteyn, Direct diode-pumped Kerr Lens 13 fs Ti:sapphire ultrafast oscillator using a single blue laser diode, Opt. Express 25 (2017) 12469–12477. May 29.
[94] S. Backus, M. Kirchner, R. Lemons, D. Schmidt, C. Durfee, M. Murnane, H. Kapteyn, Direct diode pumped Ti:sapphire ultrafast regenerative amplifier system, Opt. Express 25 (2017) 3666–3674. Feb 20.
[95] D.A. Kopylov, M.N. Esaulkov, I.I. Kuritsyn, A.O. Mavritskiy, B.E. Perminov, A.V. Konyashchenko, T.V. Murzina, A.I. Maydykovskiy, Kerr-lens mode-locked Ti: Sapphire laser pumped by a single laser diode, Laser Phys. Lett. 15 (Apr 2018).
[96] A. Rohrbacher, O.E. Olarte, V. Villamaina, P. Loza-Alvarez, B. Resan, Multiphoton imaging with blue-diode-pumped SESAM-modelocked Ti: sapphire oscillator generating 5 nJ 82 fs pulses, Opt. Express 25 (2017) 10677–10684. May 1.
[97] N. Sugiyama, H. Tanaka, F. Kannari, Mode-locked Ti: sapphire laser oscillators pumped by wavelength-multiplexed laser diodes, Jpn. J. Appl. Phys. 57 (May 2018).
[98] A. Muti, A. Kocabas, A. Sennaroglu, 5-nJ Femtosecond Ti3+:sapphire laser pumped with a single 1 W green diode, Laser Phys. Lett. 15 (2018) 055302.
[99] A. Agnesi, A. Greborio, F. Pirzio, G. Reali, 80-fs Nd: silicate glass laser pumped by a single-mode 200-mW diode, Opt. Express 18 (May 2010) 10098–10103.
[100] A. Agnesi, F. Pirzio, G. Reali, Low-threshold femtosecond Nd:glass laser, Opt. Express 17 (2009) 9171–9176.
[101] P. Purnawirman, P.B. Phua, Femtosecond laser pumped by high-brightness coherent polarization locked diodes, Opt. Lett. 36 (2011) 2797–2799.
[102] C. Honninger, R. Paschotta, M. Graf, F. Morier-Genoud, G. Zhang, M. Moser, S. Biswal, J. Nees, A. Braun, G.A. Mourou, I. Johannsen, A. Giesen, W. Seeber, U. Keller, Ultrafast ytterbium-doped bulk lasers and laser amplifiers, Appl. Phys. B Laser Opt. 69 (Jul 1999) 3–17.
[103] W.F. Krupke, Ytterbium solid-state lasers-the first decade, IEEE J. Sel. Top. Quantum Electron. 6 (2000) 1287–1296.
[104] A. Yoshida, A. Schmidt, V. Petrov, C. Fiebig, G. Erbert, J.H. Liu, H.J. Zhang, J.Y. Wang, U. Griebner, Diode-pumped mode-locked Yb:YCOB laser generating 35 fs pulses, Opt. Lett. 36 (2011) 4425–4427.
[105] A.A. Lagatsky, C.T.A. Brown, W. Sibbett, Highly efficient and low threshold diode-pumped Kerr-lens mode-locked Yb:KYW laser, Opt. Express 12 (2004) 3928–3933.
[106] C.R.E. Baer, C. Kränkel, C.J. Saraceno, O.H. Heckl, M. Golling, R. Peters, K. Petermann, T. Südmeyer, G. Huber, U. Keller, Femtosecond thin-disk laser with 141 W of average power, Opt. Lett. 35 (2010) 2302–2304.
[107] W. Sibbett, A.A. Lagatsky, C.T.A. Brown, The development and application of femtosecond laser systems,", Opt. Express 20 (2012) 6989–7001.
[108] F.G. Patterson, R. Gonzales, M.D. Perry, COMPACT 10-TW, 800-FS ND-GLASS LASER, Opt. Lett. 16 (Jul 1991) 1107–1109.
[109] M. Larionov, F. Butze, D. Nickel, A. Giesen, High-repetition-rate regenerative thin-disk amplifier with 116 mu J pulse energy and 250 fs pulse duration, Opt. Lett. 32 (2007) 494–496. Mar 1.
[110] M. Hildebrandt, M. Frede, D. Kracht, Narrow-linewidth ytterbium-doped fiber amplifier system with 45 nm tuning range and 133 W of output power, Opt. Lett. 32 (2007) 2345–2347. Aug 15.
[111] A.L. Calendron, J. Meier, M. Hemmer, L.E. Zapata, F. Reichert, H. Cankaya, D.N. Schimpf, Y. Hua, G.Q. Chang, A. Kalaydzhyan, A. Fallahi, N.H. Matlis, F.X. Kartner, Laser system design for table-top X-ray light source, High Power Laser Sci. Eng. 6 (2018). Mar 21.
[112] H. Cankaya, A.L. Calendron, C. Zhou, S.H. Chia, O.D. Mucke, G. Cirmi, F.X. Kartner, 40-mu J passively CEP-stable seed source for ytterbium-based high-energy optical waveform synthesizers, Opt. Express 24 (2016) 25169–25180. Oct 31.
[113] A. Sennaroglu, Broadly tunable Cr4+ doped solid-state lasers in the near infrared and visible, Prog. Quantum Electron. 26 (2002) 287–352.
[114] A. Godard, Infrared (2-12 um) solid-state laser sources: a review, Compt. Rendus Phys. 8 (Dec 2007) 1100–1128.
[115] S. Mirov, V. Fedorov, K. Graham, I. Moskalev, D. Martyshkin, C. Kim, Progress in Cr^{2+} and Fe^{2+} doped mid-IR laser materials, Laser Photonics Rev. 4 (2010) 21–41.
[116] S.B. Mirov, V.V. Fedorov, D. Martyshkin, I.S. Moskalev, M. Mirov, S. Vasilyev, Progress in mid-IR lasers based on Cr and Fe-doped II-VI chalcogenides, IEEE J. Sel. Top. Quantum Electron. 21 (Jan-Feb 2015).
[117] I.T. Sorokina, Cr^{2+}-doped II-VI materials for lasers and nonlinear optics, Opt. Mater. 26 (2004) 395–412.
[118] E. Sorokin, I.T. Sorokina, E. Wintner, Diode-pumped ultra-short-pulse solid-state lasers, Appl. Phys. B 72 (2001) 3–14, 2001.
[119] S.L. Baldochi, I.M. Ranieri, A short review on fluoride laser crystals grown by Czochralski method at IPEN,", Acta Phys. Pol., A 124 (Aug 2013) 286–294.
[120] T. Sudmeyer, C. Krankel, C.R.E. Baer, O.H. Heckl, C.J. Saraceno, M. Golling, R. Peters, K. Petermann, G. Huber, U. Keller, High-power ultrafast thin disk laser oscillators and their potential for sub-100-femtosecond pulse generation, Appl. Phys. B Laser Opt. 97 (Oct 2009) 281–295.

[121] A. Steimacher, O.A. Sakai, A.C. Bento, M.L. Baesso, A.N. Medina, S.M. Lima, T. Catunda, Angular dependence of the thermal-lens effect on LiSrAlF(6) and LiSrGaF(6) single crystals, Opt. Lett. 33 (2008) 1720–1722. Aug 1.
[122] B.W. Woods, S.A. Payne, J.E. Marion, R.S. Hughes, L.E. Davis, Thermomechanical and thermooptic properties of the $LiCaAlF_6$-Cr^{3+} laser material, J. Opt. Soc. Am. B Opt. Phys. 8 (May 1991) 970–977.
[123] J. Yao, Y. Wang, Solid tunable laser technology, in: Nonlinear Optics and Solid-State Lasers. Vol. 164, Springer Series in Optical Sciences, Berlin, Heidelberg, 2012.
[124] V. Pilla, T. Catunda, S.M. Lima, A.N. Medina, M.L. Baesso, H.P. Jenssen, A. Cassanho, Thermal quenching of the fluorescence quantum efficiency in colquiriite crystals measured by thermal lens spectrometry, J. Opt. Soc. Am. B Opt. Phys. 21 (Oct 2004) 1784–1791.
[125] D. Tabor, Mohs hardness scale - a physical interpretation, in: Proceedings of the Physical Society of London Section B, 67, 1954, pp. 249–257.
[126] C.F. Cline, R.C. Morris, M. Dutoit, P.J. Harget, Physical-properties of Beal2o4 single-crystals, J. Mater. Sci. 14 (1979) 941–944.
[127] E.R. Dobrovinskaya, L.A. Lytvynov, V. Pishchik, Sapphire: Material, Manufacturing, Applications, Springer Science, 2009.
[128] M.C. Richardson, M.J. Soileau, P. Beaud, R.J. DeSalvo, S.V. Garnov, D.J. Hagan, S.M. Klimentov, K.A. Cerqua-Richardson, M. Sheik-Bahae, A.A. Said, E.W.V. Stryland, Bruce H.T. Chai, Self-focusing and optical damage in Cr:LiSAF and Cr:LiCAF, in: 24th Annual Boulder Damage Symposium Proceedings, 1992.
[129] L.J. Atherton, S.A. Payne, C.D. Brandle, Oxide and fluoride laser crystals, Annu. Rev. Mater. Sci. 23 (1993) 453–502.
[130] J.C. Walling, D.F. Heller, H. Samelson, D.J. Harter, J.A. Pete, R.C. Morris, Tunable alexandrite lasers - development and performance, IEEE J. Quantum Electron. 21 (1985) 1568–1581.
[131] J.M. Eichenholz, M. Richardson, Measurement of thermal lensing in Cr^{3+}-doped colquiriites, IEEE J. Quantum Electron. 34 (May 1998) 910–919.
[132] R.D. Peterson, A.T. Pham, H.P. Jenssen, A. Cassanho, V. Castillo, Thermo-optical comparison of LiSAF, LiCAF, and LiSGaF, in: Advanced Solid State Lasers: OSA, 1999. TuB6.
[133] R.L. Aggarwal, D.J. Ripin, J.R. Ochoa, T.Y. Fan, Measurement of thermo-optic properties of Y3Al5O12, Lu3Al5O12, YAIO(3), LiYF4, LiLuF4, BaY2F8, KGd(WO4)(2), and KY(WO4)(2) laser crystals in the 80–300 K temperature range, J. Appl. Phys. 98 (2005). Nov 15.
[134] R. Iffländer, Solid-state laser systems, in: W. Schulz, H. Weber, R. Poprawe (Eds.), Laser Systems, Part 2, vol 12, Springer, Berlin, 2008.
[135] D. Klimm, G. Lacayo, P. Reiche, Growth of Cr : LiCaAlF6 and Cr : LiSrAlF6 by the Czochralski method, J. Cryst. Growth 210 (Mar 2000) 683–693.
[136] J.K. Jabczynski, W. Zendzian, Z. Mierczyk, Z. Frukacz, Chromium-doped LiCAF laser passively Q switched with a V^{3+}:YAG crystal," Applied Optics, vol. 40, pp. 6638-6645 20 (December 2001) 2001.
[137] B. Bussiere, O. Uteza, N. Sanner, M. Sentis, G. Riboulet, L. Vigroux, M. Commandre, F. Wagner, J.Y. Natoli, J.P. Chambaret, Bulk laser-induced damage threshold of titanium-doped sapphire crystals, Appl. Opt. 51 (2012) 7826–7833. Nov 10.
[138] O. Uteza, B. Bussiere, F. Canova, J.P. Chambaret, P. Delaporte, T. Itina, M. Sentis, Laser-induced damage threshold of sapphire in nanosecond, picosecand and femtosecond regimes, Appl. Surf. Sci. 254 (2007) 799–803. Dec 15.
[139] R.E. Samad, S.L. Baldochi, N.D. Vieira, Diagonal scan measurement of Cr : LiSAF 20 ps ablation threshold, Appl. Opt. 47 (2008) 920–924. Mar 1.
[140] J.F. Bisson, Y. Feng, A. Shirakawa, H. Yoneda, J.R. Lu, H. Yagi, T. Yanagitani, K.I. Ueda, Laser damage threshold of ceramic YAG, Japan. J. Appl. Phys. Part 2 Lett. 42 (2003) L1025–L1027. Aug 15.
[141] T. Shimizu, M.V. Luong, M. Cadatal-Raduban, M.J.F. Empizo, K. Yamanoi, R. Arita, Y. Minami, N. Sarukura, N. Mitsuo, H. Azechi, M.H. Pham, H.D. Nguyen, K. Ichiyanagi, S. Nozawa, R. Fukaya, S. Adachi, K.G. Nakamura, K. Fukuda, Y. Kawazoe, K.G. Steenbergen, P. Schwerdtfeger, High pressure band gap modification of LiCaAlF6, Appl. Phys. Lett. 110 (2017). Apr 3.
[142] D.C. Brown, S. Tornegard, J. Kolis, C. McMillen, C. Moore, L. Sanjeewa, C. Hancock, The application of cryogenic laser physics to the development of high average power ultra-short pulse lasers,", Appl. Sci. Basel 6 (Jan 2016).
[143] L.E. Zapata, H. Lin, A.L. Calendron, H. Cankaya, M. Hemmer, F. Reichert, W.R. Huang, E. Granados, K.H. Hong, F.X. Kartner, Cryogenic Yb:YAG composite-thin-disk for high energy and average power amplifiers, Opt. Lett. 40 (2015) 2610–2613. Jun 1.
[144] L.E. Zapata, F. Reichert, M. Hemmer, F.X. Kartner, 250 W average power, 100 kHz repetition rate cryogenic Yb:YAG amplifier for OPCPA pumping, Opt. Lett. 41 (2016) 492–495. Feb 1.
[145] J.E. Graebner, J.A. Mucha, L. Seibles, G.W. Kammlott, The thermal-conductivity of chemical-vapor-deposited diamond films on silicon,", J. Appl. Phys. 71 (1992) 3143–3146. Apr 1.
[146] R.R. Reeber, K. Wang, Thermal expansion, molar volume and specific heat of diamond from 0 to 3000K, J. Electron. Mater. 25 (Jan 1996) 63–67.
[147] J.E. Marion, Appropriate use of the strength parameter in solid-state slab laser design, J. Appl. Phys. 62 (1987) 1595–1604. Sep. 1.
[148] M.F. Ashby, D. Cebon, Materials selection in mechanical design, J. Phys. IV 3 (Nov 1993) 1–9.
[149] J. Marion, Strengthened solid-state laser materials, Appl. Phys. Lett. 47 (1985) 694–696.
[150] P. Russbueldt, T. Mans, J. Weitenberg, H.D. Hoffmann, R. Poprawe, Compact diode-pumped 1.1 kW Yb:YAG Innoslab femtosecond amplifier, Opt. Lett. 35 (2010) 4169–4171. Dec 15.
[151] O.L. Antipov, E.A. Anashkina, K.A. Fedorova, Electronic and thermal lensing in diode end-pumped Yb:YAG laser rods and discs, Quantum Electron. 39 (Dec 2009) 1131–1136.
[152] U. Demirbas, Power scaling potential of continuous-wave Cr:LiSAF and Cr:LiCAF lasers in thin-disk geometry, Appl. Opt. 57 (2018) 10207–10217. Dec 10.
[153] B.C. Stuart, M.D. Feit, A.M. Rubenchik, B.W. Shore, M.D. Perry, Laser-induced damage in dielectrics with nanosecond to subpicosecond pulses, Phys. Rev. Lett. 74 (1995) 2248–2251. Mar 20.
[154] S. Uemura, Dispersion compensation for a femtosecond Cr : LiSAF laser, Japan. J. Appl. Phys. Part 1 Regul. Pap. Short Notes Rev. Pap. 37 (Jan 1998) 133–134.
[155] S. Uemura, K. Miyazaki, Operation of a femtosecond Cr:LiSAF solitary laser near zero group-delay dispersion, Opt. Commun. 133 (1997) 201–204. Jan 1.
[156] S. Uemura, K. Torizuka, Development of a diode-pumped kerr-lens mode-locked Cr.LiSAF Laser, IEEE J. Quantum Electron. 39 (2003) 68–73.
[157] I.T. Sorokina, E. Sorokin, E. Wintner, M.A. Noginov, R. Szipocs, A. Cassanho, H.P. Jenssen, Femtosecond pulses from the novel solid-state laser source Cr:LiSGaF, Laser Phys. 7 (Jan-Feb 1997) 187–195.
[158] J.C. Diels, W. Rudolph, Ultrashort Laser Pulse Phenomena, Academic Press, San Diego, 1996.
[159] A.C. Defranzo, B.G. Pazol, Index of refraction measurement on sapphire at low-temperatures and visible wavelengths, Appl. Opt. 32 (1993) 2224–2234. May 1.
[160] R. Adair, L.L. Chase, S.A. Payne, Nonlinear refractive-index of optical-crystals, Phys. Rev. B 39 (1989) 3337–3350. Feb 15.
[161] P. Loiko, S. Ghanbari, V. Matrosov, K. Yumashev, A. Major, Thermo-optical properties of Alexandrite laser crystal, in: Solid State Lasers XXVII: Technology and Devices, 2018, 105111U.
[162] X.N. Zhu, J.F. Cormier, M. Piche, Study of dispersion compensation in femtosecond lasers, J. Mod. Opt. 43 (Aug 1996) 1701–1721.
[163] P. Loiko, A. Major, Dispersive properties of alexandrite and beryllium hexaaluminate crystals, Opt. Mater. Express 6 (2016) 2177–2183. Jul 1.
[164] J.C. Walling, H.P. Jenssen, R.C. Morris, E.W. O'Dell, O.G. Peterson, Tunable laser performance in $BeAl_2O_4Cr^{3+}$, Opt. Lett. 4 (1979) 182–183.
[165] D. Pugh-Thomas, B.M. Walsh, M.C. Gupta, Spectroscopy of BeAl2O4:Cr3+ with application to high-temperature sensing, Appl. Opt. 49 (2010) 2891–2897. May 20.
[166] J.C. Walling, O.G. Peterson, H.P. Jenssen, R.C. Morris, E.W. Odell, Tunable alexandrite lasers, IEEE J. Quantum Electron. 16 (1980) 1302–1315.
[167] J.W. Kuper, T. Chin, H.E. Aschoff, Extended tuning of alexandrite laser at elevated temperetures," in advanced solid state lasers salt lake city, Utah: OSA (1990). CL3.
[168] W.R. Kerridge-Johns, M.J. Damzen, Temperature effects on tunable cw Alexandrite lasers under diode end-pumping, Opt. Express 26 (2018) 7771–7785.
[169] I. Yorulmaz, E. Beyatli, A. Kurt, A. Sennaroglu, U. Demirbas, Efficient and low-threshold Alexandrite laser pumped by a single-mode diode, Opt. Mater. Express 4 (2014) 776–789. Apr 1.
[170] M. Stalder, M. Bass, B.H.T. Chai, Thermal quenching of fluoresence in chromium-doped fluoride laser crystals, J. Opt. Soc. Am. B 9 (1992) 2271–2273.
[171] Z.Y. Zhang, K.T.V. Grattan, A.W. Palmer, Thermal-characteristics of alexandrite fluorescence decay at high-temperatures, induced by a visible laser diode emission, J. Appl. Phys. 73 (1993) 3493–3498. Apr 1.

[172] F. Balembois, F. Druon, F. Falcoz, P. Georges, A. Brun, Performances of Cr:LiSrAlF6 and Cr:LiSrGaF6 for continuous-wave diode-pumped Q-switched operation, Opt. Lett. 22 (1997) 387–389. Mar 15.
[173] W.R. Rapoport, M.L. Shand, Excited state absorption and upconversion in Cr:LiSrAlF$_6$, Solid State Commun. 84 (1992) 29–31.
[174] M.A. Noginov, V.G. Ostroumov, I.A. Shcherbakov, V.A. Smirnov, D.A. Zubenko, Interaction of excited ions in laser crystals, in: Advanced Solid-State Lasers, 1991, pp. 21–24.
[175] A. Sanchez, R.E. Fahey, A.J. Strauss, R.L. Aggarwal, Room-temperature continuous-wave operation of a Ti:Al_2O_3 laser, Opt. Lett. 11 (Jun 1986) 363–364.
[176] R. Scheps, J.F. Myers, T.R. Glesne, H.B. Serreze, Monochromatic end-pumped operation of an alexandrite laser, Opt. Commun. 97 (1993) 363–366. Apr 1.
[177] S. Matsubara, T. Ueda, S. Kawato, T. Kobayashi, Highly efficient continuous-wave laser oscillation in microchip Yb : YAG laser at room temperature, Japan. J. Appl. Phys. Part 2 Lett. Expr. Lett. 46 (Feb 2007) L132–L134.
[178] H.W.H. Lee, S.A. Payne, L.L. Chase, Excited-state absorption of Cr^{+3} in LiCaAlF$_6$: effects of asymmetric distortions and intensity selection rules, Phys. Rev. B 39 (1989) 8907–8914.
[179] M.L. Shand, J.C. Walling, Excited-state absorption in the lasing wavelength region of alexandrite, IEEE J. Quantum Electron. 18 (1982) 1152–1155.
[180] D.C. Brown, R.L. Cone, Y.C. Sun, R.W. Equall, Yb : YAG absorption at ambient and cryogenic temperatures, IEEE J. Sel. Top. Quantum Electron. 11 (May-Jun 2005) 604–612.
[181] U. Demirbas, S. Eggert, A. Leitenstorfer, Compact and efficient Cr:LiSAF lasers pumped by one single-spatial-mode diode: a minimal cost approach, J. Opt. Soc. Am. B 29 (2012) 1894–1903.
[182] E. Beyatli, I. Baali, B. Sumpf, G. Erbert, A. Leitenstorfer, A. Sennaroglu, U. Demirbas, Tapered diode-pumped continuous-wave alexandrite laser, J. Opt. Soc. Am. B Opt. Phys. 30 (Dec 2013) 3184–3192.
[183] Z. Zhang, K.T.V. Grattan, A.W. Palmer, Fiber-optic thermometry based on fluorescence lifetimes of Cr3+ doped materials," in Measurement Technology and Intelligent Instruments, Wuhan (1993) 476–482.
[184] R. Moncorge, Laser materials based on transition metal ions, Opt. Mater. 63 (Jan 2017) 105–117.
[185] R. Cubeddu, R. Polloni, C.A. Sacchi, O. Svelto, Picosecond pulses, Tem00 mode, mode-locked ruby laser, IEEE J. Quantum Electron. Qe 5 (1969) 470.
[186] J.C. Walling, D.F. Heller, H. Samelson, D.J. Harter, J.A. Pete, R.C. Morris, Tunable alexandrite lasers:development and performance, IEEE J. Quantum Electron. QE-21 (1985) 1568–1581.
[187] J.C. Walling, Tunable cw alexandrite lasers, J. Opt. Soc. Am. 69 (1979), 1436–1436.
[188] S. Guch, C.E. Jones, Alexandrite-laser performance at high-temperature, Opt. Lett. 7 (1982) 608–610.
[189] M.J. Damzen, G.M. Thomas, A. Minassian, Diode-side-pumped Alexandrite slab lasers, Opt. Express 25 (2017) 11622–11636. May 15.
[190] U. Parali, X. Sheng, A. Minassian, G. Tawy, J. Sathian, G.M. Thomas, M.J. Damzen, Diode-pumped Alexandrite laser with passive SESAM Q-switching and wavelength tunability, Opt. Commun. 410 (2018) 970–976. Mar 1.
[191] A. Teppitaksak, A. Minassian, G.M. Thomas, M.J. Damzen, High efficiency > 26 W diode end-pumped Alexandrite laser, Opt. Express 22 (2014) 16386–16392. Jun 30.
[192] S. Ghanbari, K.A. Fedorova, A.B. Krysa, E.U. Rafailov, A. Major, Femtosecond Alexandrite laser passively mode-locked by an InP/InGaP quantum-dot saturable absorber, Opt. Lett. 43 (2018) 232–234. Jan 15.
[193] S. Ghanbari, R. Akbari, A. Major, Femtosecond kerr-lens mode-locked alexandrite laser, Opt. Express 24 (2016) 14836–14840. Jun 27.
[194] M. Fibrich, J. Sulc, D. Vyhlidal, H. Jelinkova, M. Cech, Alexandrite spectroscopic and laser characteristic investigation within a 78-400 K temperature range, Laser Phys. 27 (Nov 2017).
[195] D. Findlay, R.A. Clay, The measurement of internal losses in 4-level lasers,", Phys. Lett. 20 (1966) 277–278.
[196] L.J. Andrews, A. Lempicki, B.C. Mccollum, C.J. Giunta, R.H. Bartram, J.F. Dolan, Thermal quenching of chromium photoluminescence in ordered perovskites .1. Temperature-dependence of spectra and lifetimes, Phys. Rev. B 34 (1986) 2735–2740. Aug 15.
[197] R.H. Bartram, J.C. Charpie, L.J. Andrews, A. Lempicki, Thermal quenching of chromium photoluminescence in ordered perovskites .2. Theoretical-models, Phys. Rev. B 34 (1986) 2741–2750. Aug 15.
[198] V.V. Fedorov, S.B. Mirov, A. Gallian, D.V. Badikov, M.P. Frolov, Y.V. Korostelin, V.I. Kozlovsky, A.I. Landman, Y.P. Podmar'kov, V.A. Akimov, A.A. Voronov, 3-77-5.05-μm tunable solid-state lasers based on Fe^{2+}-doped znse crystals operating at low and room temperatures, IEEE J. Quantum Electron. 42 (2006) 907–917.
[199] M. Stalder, M. Bass, B.H.T. Chai, Thermal quencing of fluoresence in chromium-doped fluoride laser crystals, J. Opt. Soc. Am. B 9 (1992) 2271–2273.
[200] Z. Zhang, K.T.V. Grattan, A.W. Palmer, R. Summers, R. Summan, S. Hughes, Cr:LiSAF fluorescence-lifetime-based fiber optic thermometer and its applications in clinical RF heat treatment, in: Advances in Fluorescence Sensing Technology, Los Angeles, 1993, pp. 300–305.
[201] M.L. Shand, Quantum efficiency of alexandrite, J. Appl. Phys. 54 (1983) 2602–2604.
[202] S.A. Payne, L.L. Chase, L.J. Atherton, J.A. Caird, W.L. Kway, M.D. Shinn, R.S. Hughes, L.K. Smith, Properties and performance of the LiCaAlF$_6$:Cr^{3+} laser material, in: SPIE Solid State Lasers, 1990, pp. 84–93.
[203] P. Beaud, M.C. Richardson, Y.F. Chen, B.H.T. Chai, Optical amplification characteristics of Cr-lisaf and Cr-licaf under flashlamp-pumping, IEEE J. Quantum Electron. 30 (May 1994) 1259–1266.
[204] P. Beaud, Y.-F. Chen, B.H.T. Chai, M.C. Richardson, Gain properties of LiSrAlF$_6$:Cr^{3+}, Opt. Lett. 17 (1992) 1064–1066.
[205] P.A. Beaud, M. Richardson, E.J. Miesak, Multi-terawatt femtosecond Cr-lisaf laser, IEEE J. Quantum Electron. 31 (Feb 1995) 317–325.
[206] A. Isemann, P. Wessels, C. Fallnich, Directly diode-pumped Colquiriite regenerative amplifiers, Opt. Commun. 260 (2006) 211–222. Apr 1.
[207] L.M. Frantz, J.S. Nodvik, Theory of pulse propagation in a laser amplifier, J. Appl. Phys. 34 (August 1963) 2346–2349, 1963.
[208] M.L. Shand, J.C. Walling, R.C. Morris, Excited-state absorption in the pump region of alexandrite, J. Appl. Phys. 52 (1981) 953–955.
[209] M.L. Shand, H.P. Jenssen, Temperature-dependence of the excited-state absorption of alexandrite, IEEE J. Quantum Electron. 19 (1983) 480–484.
[210] V. Pilla, H.P. Jenssen, A. Cassanho, T. Catunda, Discrimination between thermal quenching of the fluorescence and Auger upconversion processes using thermal lens technique, Opt. Commun. 271 (2007) 184–189. Mar 1.
[211] M.A. Noginov, H.P. Jenssen, A. Cassanho, Upconversion in Cr:LiSGaF and Cr:LiSAF', in: Advanced Solid State Lasers, 1993, pp. 376–380.
[212] K. Naganuma, G. Lenz, E.P. Ippen, Variable bandwidth birefringent filter for tunable femtosecond lasers, IEEE J. Quantum Electron. 28 (Oct 1992) 2142–2150.
[213] S.M. Kobtsev, N.A. Sventsitskay, Application of birefringent filters in continuous-wave tunable lasers: a review, Opt Spectrosc. 73 (1992) 114–123.
[214] U. Demirbas, R. Uecker, J.G. Fujimoto, A. Leitenstorfer, Multicolor lasers using birefringent filters: experimental demonstration with Cr:Nd:GSGG and Cr:LiSAF, Opt. Express 25 (2017) 2594–2607.
[215] U. Demirbas, Off-surface optic axis birefringent filters for smooth tuning of broadband lasers, Appl. Opt. 56 (2017) 7815–7825.
[216] U. Demirbas, Optimized birefringent filter design for broadly tunable multicolor laser operation of Nd-based lasers: Nd:YAG example, J. Opt. Soc. Am. B Opt. Phys. 35 (2018) 2994–3003. Dec 1.
[217] E. Beyatli, U. Demirbas, Widely tunable dual-wavelength operation of Tm:YLF, Tm:LuAG, and Tm:YAG lasers using off-surface optic axis birefringent filters, Appl. Opt. 57 (2018) 6679–6686. Aug 10.
[218] S. Tsuda, W.H. Knox, S.T. Cundiff, W.Y. Jan, J.E. Cunningham, Mode-locking ultrafast solid-state lasers with saturable Bragg reflectors, IEEE J. Sel. Top. Quantum Electron. 2 (1996) 454–464. SEP.
[219] U. Keller, K.J. Weingarten, F.X. Kärtner, D. Kopf, B. Braun, I.D. Jung, R. Fluck, C. Hönninger, N. Matuschek, J.A. der Au, Semiconductor saturable absorber mirrors (SESAM's) for femtosecond to nanosecond pulse generation in solid-state lasers, IEEE J. Sel. Top. Quantum Electron. 2 (1996) 435–453.
[220] U. Keller, Recent developments in compact ultrafast lasers, Nature 424 (2003) 831–838.
[221] U. Keller, Ultrafast all-solid-state laser technology, Appl. Phys. B 58 (1994) 347–363.
[222] U. Demirbas, G.S. Petrich, D. Li, A. Sennaroglu, L.A. Kolodziejski, F.X. Kärtner, J.G. Fujimoto, Femtosecond tuning of Cr:Colquiriite lasers with AlGaAs-based saturable Bragg reflectors, JOSA B 28 (2011) 986–993.
[223] R. Scheps, J.F. Myers, H.B. Serreze, A. Rosenberg, R.C. Morris, M. Long, Diode-pumped Cr:LiSrAlF$_6$ laser, Opt. Lett. 16 (1991) 820–822.

[224] S. Tsuda, W.H. Knox, S.T. Cundiff, High efficiency diode pumping of a saturable Bragg reflector-mode-locked Cr:LiSAF femtosecond laser, Appl. Phys. Lett. 69 (1996) 1538–1540.
[225] G.J. Valentine, J.M. Hopkins, P. Loza-Alvarez, G.T. Kennedy, W. Sibbett, D. Burns, A. Valster, Ultralow-pump-threshold, femtosecond Cr^{3+}:$LiSrAlF_6$ laser pumped by a single narrow-stripe AlGaInP laser diode, Opt. Lett. 22 (1997) 1639–1641. Nov 1.
[226] J.M. Hopkins, G.J. Valentine, W. Sibbett, J.A. der Au, F. Morier-Genoud, U. Keller, A. Valster, Efficient, low-noise, SESAM-based femtosecond Cr^{3+}: $LiSrAlF_6$ laser, Opt. Commun. 154 (1998) 54–58. Aug 15.
[227] B. Agate, B. Stormont, A.J. Kemp, C.T.A. Brown, U. Keller, W. Sibbett, Simplified cavity designs for efficient and compact femtosecond Cr:LiSAF lasers, Opt. Commun. 205 (2002) 207–213.
[228] J.M. Hopkins, G.J. Valentine, B. Agate, A.J. Kemp, U. Keller, W. Sibbett, Highly compact and efficient femtosecond Cr : LiSAF lasers, IEEE J. Quantum Electron. 38 (Apr 2002) 360–368.
[229] U. Demirbas, A. Sennaroglu, F.X. Kärtner, J.G. Fujimoto, Highly efficient, low-cost femtosecond Cr^{3+}:LiCAF laser pumped by single-mode diodes, Opt. Lett. 33 (2008) 590–592.
[230] U. Demirbas, D. Li, J.R. Birge, A. Sennaroglu, G.S. Petrich, L.A. Kolodziejski, F.X. Kartner, J.G. Fujimoto, Low-cost, single-mode diode-pumped Cr:Colquiriite lasers, Opt. Express 17 (2009) 14374–14388. Aug 3.
[231] P.M.W. French, R. Mellish, J.R. Taylor, P.J. Delfyett, L.T. Florez, Mode-locked all-solid-state diode-pumped Cr:LiSAF laser, Opt. Lett. 18 (Nov 1993) 1934–1936.
[232] P. Wagenblast, R. Ell, U. Morgner, F. Grawert, F.X. Kärtner, Diode-pumped 10-fs Cr^{3+}: LiCAF laser, Opt. Lett. 28 (Sep 2003) 1713–1715.
[233] A. Isemann, C. Fallnich, High-power colquiriite laser with high slope efficiencies pumped by broad-area laser diodes. Opt. Express 11 (2003) 259–264.
[234] U. Demirbas, A. Sennaroglu, A. Benedick, A. Siddiqui, F.X. Kärtner, J.G. Fujimoto, Diode-pumped, high-average power femtosecond Cr^{+3}:LiCAF laser, Opt. Lett. 32 (2007) 3309–3311.
[235] U. Demirbas, A. Sennaroglu, F.X. Kärtner, J.G. Fujimoto, Comparative investigation of diode pumping for continuous-wave and mode-locked Cr^{3+}:LiCAF lasers, J. Opt. Soc. Am. B 26 (2009) 64–79.
[236] B. Sumpf, K.H. Hasler, P. Adamiec, F. Bugge, F. Dittmar, J. Fricke, H. Wenzel, M. Zorn, G. Erbert, G. Trankle, High-brightness quantum well tapered lasers, IEEE J. Sel. Top. Quantum Electron. 15 (2009) 1009–1020.
[237] B. Sumpf, P. Adamiec, M. Zorn, H. Wenzel, G. Erbert, Nearly diffraction limited tapered lasers at 675 nm with 1 W output power and conversion efficiencies above 30%, IEEE Photonics Technol. Lett. 22 (2011) 266–268.
[238] A. Robertson, R. Knappe, R. Wallenstein, Diode-pumped broadly tunable (809-910 nm) femtosecond Cr : LiSAF laser, Opt. Commun. 147 (1998) 294–298. Feb 15.
[239] U. Demirbas, M. Schmalz, B. Sumpf, G. Erbert, G.S. Petrich, L.A. Kolodziejski, J.G. Fujimoto, F.X. Kärtner, A. Leitenstorfer, Femtosecond Cr:LiSAF and Cr:LiCAF lasers pumped by tapered diode lasers, Opt. Express 19 (2011) 20444–20461.
[240] D. Kopf, K.J. Weingarten, G. Zhang, M. Moser, M.A. Emanuel, R.J. Beach, J.A. Skidmore, U. Keller, High-average-power diode-pumped femtosecond Cr:LiSAF lasers, Appl. Phys. B Laser Opt. 65 (Aug 1997) 235–243.
[241] A. Dergachev, J.H. Flint, Y. Isyanova, B. Pati, E.V. Slobodtchikov, K.F. Wall, P.F. Moulton, Review of multipass slab laser systems, IEEE J. Sel. Top. Quantum Electron. 13 (May-Jun 2007) 647–660.
[242] P. Shukla, J. Lawrence, Y. Zhang, Understanding laser beam brightness: a review and new prospective in material processing,", Opt. Laser. Technol. 75 (Dec 2015) 40–51.
[243] R.E. Samad, G.E.C. Nogueira, S.L. Baldochi, N.D. Vieira, A 5 Hz flashlamp pumped Cr : LiSAF multipass amplifier for ultrashort pulses,", J. Opt. A Pure Appl. Opt. 10 (Oct 2008).
[244] R.E. Samad, G.E.C. Nogueira, S.L. Baldochi, N.D. Vieira, Amplification of ultrashort pulses to 0.5 TW at 5 Hz with a flashlamp pumped Cr : LiSAF gain medium - art. no. 645112, in: Solid State Lasers Xvi: Technol. Dev., vol 6451, 2007, 45112–45112.
[245] R.E. Samad, S.L. Baldochi, G.E.C. Nogueira, N.D. Vieira, 30 W Cr : LiSrAlF6 flashlamp-pumped pulsed laser, Opt. Lett. 32 (2007) 50–52. Jan 1.
[246] D.E. Klimek, A. Mandl, Power scaling of a flashlamp-pumped Cr : LiSAF thin-slab zig-zag laser, IEEE J. Quantum Electron. 38 (Dec 2002) 1607–1613.
[247] A. Miller, P. LiKamWa, B.H.T. Chai, E.W.V. Stryland, Generation of 150-fs tunable pulses in Cr:LiSAF, Opt. Lett. 17 (1992) 195–197.
[248] I.T. Sorokina, E. Sorokin, E. Wintner, A. Cassanho, H.P. Jenssen, R. Szipöcs, Sub-20 fs pulse generation from the mirror dispersion controlled Cr:LiSGaF and Cr: LiSAF lasers, Appl. Phys. B 65 (1997) 245–253.
[249] N.H. Rizvi, P.M.W. French, J.R. Taylor, 50-fs pulse generation from a self-starting cw passively mode-locked Cr:LiSrAlF6 laser, Opt. Lett. 17 (1992) 877–879.
[250] J.M. Evans, D.E. Spence, W. Sibbett, B.H.T. Chai, A. Miller, 50-fs pulse generation from a self-mode-locked Cr:LiSrAlF6 laser, Opt. Lett. 17 (1992) 1447–1449.
[251] N.H. Rizvi, P.M.W. French, J.R. Taylor, Generation of 33-fs pulses from a passively mode-locked Cr^{3+}:$LiSrAlF_6$ laser, Opt. Lett. 17 (1992) 1605–1607.
[252] N.H. Rizvi, P.M.W. French, J.R. Taylor, P.J. Delfyett, L.T. Florez, Generation of pulses as short as 93 fs from a self-starting femtosecond Cr:LiSrAlF6 lasers by exploiting multiple-quantum-well absorbers, Opt. Lett. 18 (1993) 983–985.
[253] D.J. Harter, J. Squier, G. Mourou, Alexandrite-laser-pumped Cr3+Lisralf6, Opt. Lett. 17 (1992) 1512–1514. Nov 1.
[254] M.J.P. Dymott, I.M. Botheroyd, G.J. Hall, J.R. Lincoln, A.I. Ferguson, All-solid-state actively mode-locked Cr:LiSAF laser, Opt. Lett. 19 (1994) 634–636.
[255] J.R. Lincoln, M.J.P. Dymott, A.I. Ferguson, Femtosecond pulses from an all-solid-state Kerr-lens mode-locked Cr:LiSAF laser, Opt. Lett. 19 (1994) 1210–1212.
[256] M.P. Critten, D. Burns, J.M. Evans, K. Lamb, C. Yelland, W. Sibbet, All-solid-state femtosecond Cr3+:LiSAF lasers pumped at 532nm and 670nm, J. Mod. Opt. 43 (May 1996) 919–927.
[257] K. Torizuka, M. Yamashita, T. Yabiku, Continuous-wave alexandrite laser-pumped by a direct-current mercury are lamp, Appl. Opt. 32 (1993) 7394–7398. Dec 20.
[258] R. Scheps, B.M. Gately, J.F. Myers, J.S. Krasinski, D.F. Heller, Alexandrite laser pumped by semiconductor-lasers, Appl. Phys. Lett. 56 (1990) 2288–2290. Jun 4.
[259] B.K. Zhou, T.J. Kane, G.J. Dixon, R.L. Byer, Efficient, frequency-stable laser-diode-pumped Nd-yag laser, Opt. Lett. 10 (1985) 62–64.
[260] A. Agnesi, A. Greborio, F. Pirzio, E. Ugolotti, G. Reali, S.Y. Choi, F. Rotermund, U. Griebner, V. Petrov, Femtosecond Nd:glass lasers pumped by single-mode laser diodes and mode locked with carbon nanotube or semiconductor saturable absorber mirrors, IEEE J. Sel. Top. Quantum Electron. 18 (Jan-Feb 2012) 74–80.
[261] R. Scheps, Cr-$LiCaAlF_6$ laser pumped by visible laser-diodes, IEEE J. Quantum Electron. 27 (Aug 1991) 1968–1970.
[262] A. Agnesi, A. Greborio, F. Pirzio, G. Reali, Efficient femtosecond Yb:YAG laser pumped by a single-mode laser diode, Opt. Commun. 284 (2011) 4049–4051. Aug 1.
[263] E. Beyatli, S. Naghizadeh, A. Kurt, A. Sennaroglu, Low-cost low-threshold diode end-pumped Tm:YAG laser at 2.016 mu m, Appl. Phys. B Laser Opt. 109 (Nov 2012) 221–225.
[264] V. Kubecek, R. Quintero-Torres, J.C. Diels, Ultralow-pump-threshold laser diode pumped Cr : LiSAF laser, Adv. Lasers Sys. 5137 (2002) 43–47.
[265] W.J. Ling, Y.L. Jia, J.H. Sun, Z.H. Wang, Z.Y. Wei, Low-threshold self-starting femtosecond Ti : sapphire laser, Appl. Opt. 45 (2006) 2495–2498. Apr 10.
[266] D. Li, U. Demirbas, A. Benedick, A. Sennaroglu, J.G. Fujimoto, F.X. Kärtner, Attosecond timing jitter pulse trains from semiconductor saturable absorber mode-locked Cr:LiSAF lasers, Opt. Express 20 (2012) 23422–23435.
[267] J.F. Pinto, L. Esterowitz, G.H. Rosenblatt, Frequency tripling of a Q-switched Cr:LiSAF laser to the UV region, IEEE J. Sel. Top. Quantum Electron. 1 (1995) 58–61.
[268] R. Knappe, G. Bitz, K.-J. Boller, R. Wallenstein, Compact single-frequency diode-pumped Cr:LiSAF lasers, Opt. Commun. 143 (1997) 42–46.
[269] K. Kawase, M. Mizuno, S. Sohma, H. Takahashi, T. Taniuchi, Y. Urata, S. Wada, H. Tashiro, H. Ito, Difference-frequency terahertz-wave generation from 4-dimethylamino-N-methyl-4-stilbazolium-tosylate by use of an electronically tuned Ti:sapphire laser, Opt. Lett. 24 (1999) 1065–1067.
[270] P. Gu, F. Chang, M. Tani, K. Sakai, C.-L. Pan, Generation of coherent cw-terahertz radiation using a tunable dual-wavelength external cavity laser diode, Jpn. J. Appl. Phys. 38 (1999) L1246–L1248.
[271] M. Scheller, J.M. Yarborough, J.V. Moloney, M. Fallahi, M. Koch, S.W. Koch, Room temperature continuous wave milliwatt terahertz source, Opt. Express 18 (2010) 27112–27117.

[272] S. Pan, X. Zhao, C. Lou, Switchable single-longitudinal-mode dual-wavelength erbium-doped fiber ring laser incorporating a semiconductor optical amplifier, Opt. Lett. 33 (2008) 764–766.
[273] C.W. Chow, C.S. Wong, H.K. Tsang, All-optical NRZ to RZ format and wavelength converter by dual-wavelength injection locking, Opt. Commun. 209 (2002) 329–334.
[274] R. Gaultona, F.M. Dansonb, F.A. Ramirezb, O. Gunawanb, The potential of dual-wavelength laser scanning for estimating vegetation moisture content,", Remote Sens. Environ. 132 (2013) 32–39.
[275] J. Kühn, T. Colomb, F. Montfort, F. Charrière, Y. Emery, E. Cuche, P. Marquet, C. Depeursinge, Real-time dual-wavelength digital holographic microscopy with a single hologram acquisition, Opt. Express 15 (2007) 7231–7242.
[276] U. Demirbas, I. Baali, D.A.E. Acar, A. Leitenstorfer, Diode-pumped continuous-wave and femtosecond Cr:LiCAF lasers with high average power in the near infrared, visible and near ultraviolet, Opt. Express 23 (2015) 8901–8909.
[277] S. Uemura, K. Miyazaki, Thermal chracteristics of a continuous-wave Cr:LiSAF laser, Jpn. J. Appl. Phys. 36 (1997) 4312–4315.
[278] F. Balembois, F. Falcoz, F. Kerboull, F. Druon, P. Georges, A. Brun, Theoretical and experimental investigations of small-signal gain for a diode-pumped Q-Switched Cr:LiSAF laser, IEEE J. Quantum Electron. 33 (Feb 1997) 269–278.
[279] U. Demirbas, M. Schmalz, B. Sumpf, G. Erbert, G.S. Petrich, L.A. Kolodziejski, J.G. Fujimoto, F.X. Kartner, A. Leitenstorfer, Femtosecond Cr:LiSAF and Cr:LiCAF lasers pumped by tapered diode lasers, Opt. Express 19 (2011) 20444–20461. Oct 10.
[280] U. Demirbas, D.A.E. Acar, Continuous-wave, quasi-continuous-wave, gain-switched, and femtosecond burst-mode operation of multi-mode diode-pumped Cr: LiSAF lasers, J. Opt. Soc. Am. B Opt. Phys. 33 (2016) 2105–2113. Oct 1.
[281] D. Kopf, U. Keller, M.A. Emanuel, R.J. Beach, J.A. Skidmore, 1.1-W cw Cr:LiSAF laser pumped by a 1-cm diode array, Opt. Lett. 22 (1997) 99–101. Jan 15.
[282] D. Kopf, J.A. Derau, U. Keller, G.L. Bona, P. Roentgen, 400-mw continuous-wave diode-pumped Cr-lisaf laser-based on a power-scalable concept, Opt. Lett. 20 (1995) 1782–1784. Sep. 1.
[283] Y. Isyanova, E. Slobodtchikov, J. Flint, P.F. Moulton, C.R. Swim, J. Fox, Compact tunable all-solid-state LWIR source for standoff chemical detection, in: Chemical and Biological Standoff Detection, 2004, pp. 155–162.
[284] http://www.qpeak.com/products/laser-component-solutions/corona.
[285] R.E. Samad, G.E.C. Nogueira, S.L. Baldlochi, N.D. Vieira, Development of a flashlamp-pumped Cr : LiSAF laser operating at 30 Hz, Appl. Opt. 45 (2006) 3356–3360. May 10.
[286] F. Hanson, Cr-lisaf slab laser performance, IEEE J. Quantum Electron. 31 (Apr 1995) 653–656.
[287] R.C. Sam, J.J. Yeh, K.R. Leslie, W.R. Rapoport, Design and performance of a 250 Hz alexandrite laser, IEEE J. Quantum Electron. 24 (Jun 1988) 1151–1166.
[288] A.E. Mandl, D.E. Klimek, A. Zavriyev, Scaling Cr:LiSAF to high average power, in: XI International Symposium on Gas Flow and Chemical Lasers and High Power Laser Conference, Edinburgh, 1997, pp. 56–59.
[289] R. Mellish, S.C.W. Hyde, N.P. Barry, R. Jones, P.M.W. French, J.R. Taylor, C.J. vanderPoel, A. Valster, All-solid-state diode-pumped Cr:LiSAF femtosecond oscillator and regenerative amplifier, Appl. Phys. B Laser Opt. 65 (Aug 1997) 221–226.
[290] C. Cihan, E. Beyatli, F. Canbaz, L.-J. Chen, B. Sumpf, G. Erbert, A. Leitenstorfer, F.X. Kärtner, A. Sennaroğlu, U. Demirbas, Gain-matched output couplers for efficient kerr-lens mode-locking of low-cost and high peak-power Cr: LiSAF lasers, IEEE J. Sel. Top. Quantum Electron. 21 (2015).
[291] A. Agnesi, F. Pirzio, E. Ugolotti, S.Y. Choi, D.-I. Yeom, F. Rotermund, Femtosecond single-mode diode-pumped Cr:LiSAF laser mode-locked with single-walled carbon nanotubes, Opt. Commun. 285 (2012) 742–745.
[292] F. Canbaz, N. Kakenov, C. Kocabas, U. Demirbas, A. Sennaroglu, Graphene mode-locked Cr:LiSAF laser at 850 nm, Opt. Lett. 40 (2015) 4110–4113.
[293] F. Canbaz, N. Kakenov, C. Kocabas, U. Demirbas, A. Sennaroglu, Generation of sub-20-fs pulses from a graphene mode-locked laser, Opt. Express 25 (2017) 2834–2839.
[294] F. Canbaz, E. Beyatli, L.-J. Chen, A. Sennaroglu, F.X. Kärtner, U. Demirbas, Highly efficient and robust operation of Kerr-lens mode-locked Cr:LiSAF lasers using gain-matched output couplers, Opt. Lett. 39 (2014) 327–330.
[295] S. Uemeura, K. Torizuka, Generation of 12-fs pulses from a diode-pumped Kerr-lens mode-locked Cr:LiSAF laser, Opt. Lett. 24 (1999) 780–782.
[296] C. Hönninger, R. Paschotta, F. Morier-Genoud, M. Moser, U. Keller, Q-switching stability limits of continuous-wave passive mode locking, J. Opt. Soc. Am. 16 (January 1999) 46–56, 1999.
[297] F.X. Kärtner, L.R. Brovelli, D. Kopf, M. Kamp, I. Calasso, U. Keller, Control of solid-state laser dynamics by semiconductor devices, Opt. Eng. 34 (1995) 2024–2036.
[298] C. Cihan, C. Kocabas, U. Demirbas, A. Sennaroglu, Graphene mode-locked femtosecond Alexandrite laser, Opt. Lett. 43 (2018) 3969–3972. Aug 15.
[299] A.A. Lagatsky, E.U. Rafailov, C.G. Leburn, C.T.A. Brown, N. Xiang, O.G. Okhotnikov, W. Sibbett, Highly efficient femtosecond Yb:KYW laser pumped by single narrow-stripe laser diode, Electron. Lett. 39 (2003) 1108–1110.
[300] A.J. Kemp, B. Stormont, B. Agate, C.T.A. Brown, U. Keller, W. Sibbett, Gigahertz repetition-rate from directly diode-pumped femtosecond Cr : LiSAF laser, Electron. Lett. 37 (2001) 1457–1458. Nov 22.
[301] B. Agate, A.J. Kemp, C.T.A. Brown, W. Sibbett, Efficient, high repetition-rate femtosecond blue source using a compact Cr : LiSAF laser, Opt. Express 10 (2002) 824–831. Aug 12.
[302] R.P. Prasankumar, Y. Hirakawa, A.M.J. Kowalevicz, F.X. Kärtner, J.G. Fujitimo, W.H. Knox, An extended cavity femtosecond Cr:LiSAF laser pumped by low cost diode lasers, Opt. Express 11 (2003) 1265–1269.
[303] D. Li, U. Demirbas, J.R. Birge, G.S. Petrich, L.A. Kolodziejski, A. Sennaroglu, F.X. Kartner, J.G. Fujimoto, Diode-pumped passively mode-locked GHz femtosecond Cr:LiSAF laser with kW peak power, Opt. Lett. 35 (2010) 1446–1448. May 1.
[304] U. Demirbas, Low-cost, highly efficient and tunable ultrafast laser technology based on directly diode pumped Cr:Colquiriites, PhD, in: EECS. Vol, MIT, Cambridge, 2010, p. 352.
[305] U. Demirbas, A. Sennaroglu, F.X. Kärtner, J.G. Fujimoto, Generation of 15 nJ pulses from a highly efficient, low-cost multipass-cavity Cr^{3+}:LiCAF laser, Opt. Lett. 34 (2009) 497–499.
[306] S.N. Tandon, J.T. Gopinath, A.A. Erchak, G.S. Petrich, L.A. Kolodziejski, E.P. Ippen, Large-area oxidation of AlAs layers for dielectric stacks and thick buried oxides, J. Electron. Mater. 33 (Jul 2004) 774–779.
[307] S.N. Tandon, J.T. Gopinath, H.M. Shen, G.S. Petrich, L.A. Kolodziejski, F.X. Kärtner, E.P. Ippen, Large-area broadband saturable Bragg reflectors by use of oxidized AlAs, Opt. Lett. 29 (2004) 2551–2553. Nov 1.
[308] S.P. Nabanja, L.A. Kolodziejski, G.S. Petrich, M.Y. Sander, J.L. Morse, K. Shtyrkova, E.P. Ippen, F.X. Kärtner, Large-area broad band saturable Bragg reflectors using oxidized AlAs in the circular and inverted mesa geometries, J. Appl. Phys. 113 (2013) 163102.
[309] S.P. Nabanja, L.A. Kolodziejski, G.S. Petrich, Lateral oxidation of AlAs for circular and inverted mesa saturable Bragg reflectors, IEEE J. Quantum Electron. 49 (Sep 2013) 731–738.
[310] D. Kopf, K.J. Weingarten, L.R. Brovelli, M. Kamp, U. Keller, Diode-pumped 100-fs passively mode-locked Cr-lisaf laser with an antiresonant fabry-perot saturable absorber, Opt. Lett. 19 (1994) 2143–2145. Dec 15.
[311] S. Tsuda, W.H. Knox, E.A.d. Souza, W.Y. Jan, J.E. Cunningham, Low-loss intracavity AlAs/AlGaAs saturable Bragg reflector for femtosecond mode locking in solid-state lasers, Opt. Lett. 20 (1995) 1406–1408.
[312] D. Kopf, A. Prasad, G. Zhang, M. Moser, U. Keller, Broadly tunable femtosecond Cr:LiSAF laser, Opt. Lett. 22 (1997) 621–623. May 1.
[313] D.E. Spence, P.N. Kean, W. Sibbett, 60-fsec pulse generation from a self-mode-locked Ti:sapphire laser, Opt. Lett. 16 (1991).
[314] M.J.P. Dymott, A.I. Ferguson, Self-mode-locked diode-pumped Cr:LiSAF laser, Opt. Lett. 19 (1994) 1988–1990.
[315] F. Falcoz, F. Balembois, P. Georges, A. Brun, Self-starting self-mode-locked femtosecond diode-pumped Cr:LiSAF laser, Opt. Lett. 20 (1995) 1874–1876.
[316] R. Mellish, N.P. Barry, S.C.W. Hyde, R. Jones, P.M.W. French, J.R. Taylor, C.J.v. d. Poel, A. Valster, Diode-pumped Cr:LiSAF all-solid-state femtosecond oscillator and regenerative amplifier, Opt. Lett. 20 (1995) 2312–2314.
[317] M.J.P. Dymott, A.I. Ferguson, Self-mode-locked diode-pumped Cr:LiSAF laser producing 34-fs pulses at 42-mW average power, Opt. Lett. 20 (1995) 1157–1159.

[318] S. Uemura, K. Miyazaki, Femtosecond Cr:LiSAF laser pumped by a single diode laser, Opt. Commun. 138 (1997) 330–332.
[319] P. LiKamWa, B.H.T. Chai, A. Miller, Self-mode-locked Cr^{3+}:$LiCaAlF_6$ laser, Opt. Lett. 17 (1992) 1438–1440.
[320] K.M. Gabel, P. Russbuldt, R. Lebert, A. Valster, Diode pumped Cr3+: LiCAF fs-laser, Opt. Commun. 157 (1998) 327–334. Dec 1.
[321] L.J. Chen, M.Y. Sander, F.X. Kartner, Kerr-lens mode locking with minimum nonlinearity using gain-matched output couplers, Opt. Lett. 35 (2010) 2916–2918. Sep. 1.
[322] R. Paschotta, Encyclopedia of Laser Physics and Technology Vol, Wiley-VCH, 2008.
[323] S. Nakamura, M. Senoh, S.-i. Nagahama, N. Iwasa, T. Yamada, T. Matsushita, H. Kiyoku, Y. Sugimoto, InGaN-based multi-quantum-well-structure laser diodes, Jpn. J. Appl. Phys. 35 (1996) L74–L76.
[324] A. Khan, K. Balakrishnan, T. Katona, Ultraviolet light-emitting diodes based on group three nitrides, Nat. Photonics 2 (2008) 77–84.
[325] R. Paschotta, N. Moore, W.A. Clarkson, A.C. Tropper, D.C. Hanna, G. Maze, 230 mW of blue light from a thulium-doped upconversion fiber laser, IEEE J. Sel. Top. Quantum Electron. 3 (1997) 1100–1102.
[326] S. Bjurshagen, D. Evekull, R. Koch, Efficient generation of blue light by frequency doubling of a Nd:YAG laser operating on 4 F 3/2–>4 I 9/2 transitions, Appl. Phys. B 76 (2003) 135–141.
[327] L.S. Cruz, F.C. Cruz, External power-enhancement cavity versus intracavity frequency doubling of Ti:sapphire lasers using BIBO, Opt. Express 15 (2007) 11913–11921.
[328] J.H. Lundeman, O.B. Jensen, P.E. Andersen, S. Andersson-Engels, B. Sumpf, G. Erbert, P.M. Petersen, High power 404 nm source based on second harmonic generation in PPKTP of a tapered external feedback diode laser, Opt. Express 16 (2008) 2486–2493.
[329] R.G. Smith, Theory of intracavity optical second-harmonic generation, IEEE J. Quantum Electron. 6 (1969) 215–223.
[330] F. Falcoz, F. Balembois, P. Georges, A. Brun, D. Rytz, All-solid-state continuous-wave tunable blue-light source by intracavity doubling of a diode-pumped Cr: LiSAF laser, Opt. Lett. 20 (1995) 1274–1276.
[331] P. Laperle, K.J. Snell, A. Chandonnet, P. Galarneau, R. Vallée, Tunable diode-pumped and frequency-doubled Cr:LiSAF lasers, Appl. Opt. 36 (1997) 5053–5057.
[332] J.M. Eichenholz, M. Richardson, G. Mizell, Diode pumped, frequency doubled LiSAF microlaser, Opt. Commun. 153 (1998) 263–266.
[333] S. Makio, T. Miyai, M. Sato, T. Sasaki, 67-mW continuous-wave blue light generation by intracavity frequency doubling of a diode pumped Cr:LiSrAlF6 laser, Jpn. J. Appl. Phys. 39 (2000) 6539–6541.
[334] S. Makio, M. Sato, T. Sasaki, High-power, continuous-wave and blue light generation by intracavity frequency doubling of a Cr:LiSrAlF6 laser, Jpn. J. Appl. Phys. 40 (2001) 2278–2281.
[335] S. Makio, H. Matsumoto, A. Miyamoto, M. Sato, T. Sasaki, Low-noise blue light generation of intracavity frequency-doubled LD-pumped Cr:LiSAF laser by single-mode method, Electr. Eng. Jpn. 120 (2002) 910–915.
[336] U. Demirbas, R. Uecker, D. Klimm, B. Sumpf, G. Erbert, Intra-cavity frequency-doubled Cr:LiCAF laser with 265 mW continuous-wave blue (395-405 nm) output, Opt. Commun. 320 (2014) 38–42.
[337] H. Maestre, A.J. Torregrosa, J. Capmany, Tunable blue-violet Cr3+:LiCAF + BiBO compact laser, Laser Phys. 25 (Mar 2015).
[338] F. Jia, Q. Xue, Q. Zheng, Y. Bu, L. Qian, 5.3 W deep-blue light generation by intra-cavity frequency doubling of Nd:GdVO4, Appl. Phys. B 87 (2007) 245–247.
[339] Q.H. Xue, Q. Zheng, Y.K. Bu, F.Q. Jia, L.S. Qian, High-power efficient diode-pumped Nd:YVO4/LiB3O5 457 nm blue laser with 4.6 W of output power, Opt. Lett. 31 (2006) 1070–1072.
[340] L. McDonagh, R. Wallenstein, Low-noise 62W CW intracavity-doubled TEM00 Nd:YVO4 green laser pumped at 888nm, Opt. Lett. 32 (2007) 802–804.
[341] M. Castaing, F. Balembois, P. Georges, Continuous-wave laser at 440 nm based on frequency-doubled diode-pumped Nd:GdVO4 crystal, Opt. Lett. 33 (2008) 1957–1959.
[342] M.O. Ramirez, J.J. Romero, P. Molina, L.E. Bausa, Near infrared and visible tunability from a diode pumped Nd3+ activated strontium barium niobate laser crystal, Appl. Phys. B Laser Opt. 81 (Oct 2005) 827–830.
[343] A. Rodenas, M.O. Ramirez, D. Jaque, J.G. Sole, A.A. Kaminskii, Wide infrared and visible tunability from a Nd3+: Ba2NaNbO15 self-frequency-converter disordered laser crystal, J. Appl. Phys. 99 (2006). Jan 15.
[344] W.-L. Zhou, Y. Mori, T. Sasaki, S. Nakai, K. Nakano, S. Niikura, B. Craig, Intracavity frequency doubling of a continuous wave Ti:sapphire laser with over 70% conversion efficiency, Appl. Phys. Lett. 66 (1995) 2463–2466.
[345] H. Maestre, A.J. Torregrosa, J. Capmany, Intracavity Cr3+:LiCAF + PPSLT optical parametric oscillator with self-injection-locked pump wave, Laser Phys. Lett. 10 (2013) 035806.
[346] A.J. Torregrosa, H. Maestre, J. Capmany, Towards a versatile active wavelength converter for all-optical networks based on quasi-phase matched intra-cavity difference-frequency generation, Opt. Express 21 (2013) 27933–27945. Nov 18.
[347] H. Maestre, A.J. Torregrosa, J.A. Pereda, C.R. Fernandez-Pousa, J. Capmany, Dual-wavelength Cr3+:LiCaAlF6 solid-state laser with tunable THz frequency difference, IEEE J. Quantum Electron. 46 (Nov 2010) 1681–1685.
[348] J.F. Pinto, L. Esterowitz, Unstable Cr : LiSAF laser resonator with a variable reflectivity output coupler, Appl. Opt. 37 (1998) 3272–3275. May 20.
[349] M. Sadeghi, Z. Olumee, X.D. Tang, A. Vertes, Z.X. Jiang, A.J. Henderson, H.S. Lee, C.R. Prasad, Compact tunable Cr:LiSAF laser for infrared matrix-assisted laser desorption/ionization, Rapid Commun. Mass Spectrom. 11 (1997) 393–397.
[350] K.L. Caldwell, D.R. McGarity, K.K. Murray, Matrix-assisted laser desorption/ionization with a tunable mid-infrared optical parametric oscillator, J. Mass Spectrom. 32 (Dec 1997) 1374–1377.
[351] B. Agate, E.U. Rafailov, W. Sibbett, S.M. Saltiel, P. Battle, T. Fry, E. Noonan, Highly efficient blue-light generation from a compact, diode-pumped femtosecond laser by use of a periodically poled KTP waveguide crystal, Opt. Lett. 28 (2003) 1963–1965. Oct 15.
[352] B. Agate, E.U. Rafailov, W. Sibbett, S.M. Saltiel, K. Koynov, M. Tiihonen, S.H. Wang, F. Laurell, P. Battle, T. Fry, T. Roberts, E. Noonan, Portable ultrafast blue light sources designed with frequency doubling in KTP and KNbO3, IEEE J. Sel. Top. Quantum Electron. 10 (2004) 1268–1276. Nov-Dec.
[353] M.D. Perry, D. Strickland, T. Ditmire, F.G. Patterson, Crlisralf6 regenerative amplifier, Opt. Lett. 17 (1992) 604–606. Apr 15.
[354] W.E. White, J.R. Hunter, L. Vanwoerkom, T. Ditmire, M.D. Perry, 120-Fs terawatt Ti-Al2o3/Cr-Lisralf6 laser system, Opt. Lett. 17 (1992) 1067–1069. Aug 1.
[355] P. Beaud, E. Miesak, Y.F. Chen, B.H.T. Chai, M.C. Richardson, 110-Fs fourier-transform limited Gaussian pulses from a crlisaf regenerative amplifier, Opt. Commun. 95 (1993) 46–50. Jan 1.
[356] P. Beaud, M. Richardson, E.J. Miesak, B.H.T. Chai, 8-Tw 90-fs crlisaf laser, Opt. Lett. 18 (1993) 1550–1552. Sep. 15.
[357] T. Ditmire, M.D. Perry, Terawatt Cr-Lisralf6 laser system, Opt. Lett. 18 (1993) 426–428. Mar 15.
[358] T. Ditmire, H. Nguyen, M.D. Perry, Design and performance of a multiterawatt Cr-Lisralf6 laser system, J. Opt. Soc. Am. B Opt. Phys. 11 (1994) 580–590. Apr.
[359] T. Ditmire, H. Nguyen, M.D. Perry, Amplification of femtosecond pulses to 1-J in Cr-Lisralf6, Opt. Lett. 20 (1995) 1142–1144. May 15.
[360] F. Balembois, P. Georges, F. Salin, A. Brun, High-repetition-rate cw-pumped Cr3+Lisralf6 femtosecond regenerative amplifier, Opt. Lett. 18 (1993) 1250–1252. Aug 1.
[361] N.P. Barry, S.C.W. Hyde, R. Mellish, P.M.W. French, J.R. Taylor, C.J. Vanderpoel, A. Valster, All-solid-state femtosecond diode-pumped Cr-lisaf regenerative amplifier, Electron. Lett. 30 (1994) 1761–1762. Oct 13.
[362] S.C.W. Hyde, N.P. Barry, R. Mellish, P.M.W. French, J.R. Taylor, C.J.v. d. Poel, A. Valster, Argon-ion-pumped and diode-pumped all-solid-state femtosecond Cr: LiSAF regenerative amplifiers, Opt. Lett. 20 (1995) 160–162.
[363] A. Isemann, H. Hundertmark, C. Fallnich, Diode-pumped Cr : LiCAF fs regenerative amplifier system seeded by an Er-doped mode-locked fiber laser, Appl. Phys. B Laser Opt. 74 (2002) 299–306. Apr.
[364] T. Ditmire, M.D. Perry, Amplification of femtosecond pulses to above 1 J with large aperture Cr-Lisralf6 amplifiers, in: Generation, Amplification, and Measurement of Ultrashort Laser Pulses Ii, vol 2377, 1995, pp. 301–310.
[365] R.E. Samad, G.E.C. Nogueira, S.L. Baldochi, N.D. Vieira, Development of a TW level Cr : LiSAF multipass amplifier, Riao/Optilas 2007 (vol. 992) (2008) 398–402.

[366] F. Balembois, P. Georges, A. Brun, Lisaf regenerative amplifier for femtosecond pulses operating at 5-khz repetition rate," mode-locked and solid state lasers, Amplifiers, and Applications 2041 (1994) 88–92.
[367] R.H. Walden, Analog-to-digital conversion in the early 21st century," in international microwave symposium honolulu. Wiley Encyclopedia of Computer Science and Engineering, 2007, pp. 1–14.
[368] G.C. Valley, Photonic analog-to-digital converters, Opt. Express 15 (Mar 2007) 1955–1982.
[369] J. Kim, F. Ludwig, M. Felber, F.X. Kartner, Long-term stable microwave signal extraction from mode-locked lasers, Opt. Express 15 (2007) 8951–8959. Jul 9.
[370] E.N. Ivanov, J.J. McFerran, S.A. Diddams, L. Hollberg, Noise properties of microwave signals synthesized with femtosecond lasers, IEEE Trans. Ultrason. Ferroelectr. Freq. Control 54 (Apr 2007) 736–745.
[371] J.J. McFerran, E.N. Ivanov, A. Bartels, G. Wilpers, C.W. Oates, S.A. Diddams, L. Hollberg, Low-noise synthesis of microwave signals from an optical source, Electron. Lett. 41 (2005) 650–651. May 26.
[372] A. Bartels, S.A. Diddams, C.W. Oates, G. Wilpers, J.C. Bergquist, W.H. Oskay, L. Hollberg, Femtosecond-laser-based synthesis of ultrastable microwave signals from optical frequency references, Opt. Lett. 30 (2005) 667–669. Mar 15.
[373] S.A. Diddams, A. Bartels, T.M. Ramond, C.W. Oates, S. Bize, E.A. Curtis, J.C. Bergquist, L. Hollberg, Design and control of femtosecond lasers for optical clocks and the synthesis of low-noise optical and microwave signals, IEEE J. Sel. Top. Quantum Electron. 9 (Jul-Aug 2003) 1072–1080.
[374] B. Jalali, P. Kelkar, V. Saxena, Photonic arbitrary waveform generator, in: IEEE LEOS, 2001, pp. 253–254.
[375] N.K. Fontaine, R.P. Scott, J. Cao, A. Karalar, W. Jiang, K. Okamoto, J.P. Heritage, B.H. Kolner, S.J.B. Yoo, 32 phase X 32 amplitude optical arbitrary waveform generation, Opt. Lett. 32 (Apr 2007) 865–867.
[376] J. Kim, J. Chen, Z. Zhang, F.N.C. Wong, F.X. Kartner, F. Loehl, H. Schlarb, Long-term femtosecond timing link stabilization using a single-crystal balanced cross correlator, Opt. Lett. 32 (2007) 1044–1046. May 1.
[377] J.-F. Cliche, B. Shillue, Precision timing control for radioastronomy, in: IEEE control sys. Mag., vol 26, 2006, pp. 19–26.
[378] S.M. Foreman, K.W. Holman, D.D. Hudson, D.J. Jones, J. Ye, Remote transfer of ultrastable frequency references via fiber networks, Rev. Sci. Instrum. 78 (2007) 021101.
[379] D.D. Hudson, S.M. Foreman, S.T. Cundiff, J. Ye, Synchronization of mode-locked femtosecond lasers through a fiber link, Opt. Lett. 31 (Jul 2006) 1951–1953.
[380] P.J. Delfyett, D.H. Hartman, S.Z. Ahmad, Optical clock distribution using a mode-locked semiconductor-laser diode system, J. Light. Technol. 9 (Dec 1991) 1646–1649.
[381] P.W. Juodawlkis, J.C. Twichell, G.E. Betts, J.J. Hargreaves, R.D. Younger, J.L. Wasserman, F.J. O'Donnell, K.G. Ray, R.C. Williamson, Optically sampled analog-to-digital converters, in: Microwave Theory And Techniques, IEEE Transactions on, vol 49, 2001, pp. 1840–1853.
[382] R. Paschotta, Noise of mode-locked lasers (Part I): numerical model, Appl. Phys. B Laser Opt. 79 (Jul 2004) 153–162.
[383] R. Paschotta, Noise of mode-locked lasers (Part II): timing jitter and other fluctuations, Appl. Phys. B Laser Opt. 79 (Jul 2004) 163–173.
[384] H.A. Haus, Mecozzi, "Noise in modelocked lasers,", IEEE J. Quantum Electron. 18 (1993) 51.
[385] R.P. Scott, C. Langrock, B.H. Kolner, High-dynamic-range laser amplitude and phase noise measurement techniques, IEEE J. Sel. Top. Quantum Electron. 7 (Jul-Aug 2001) 641–655.
[386] J. Kim, J. Chen, J. Cox, F.X. Kärtner, Attosecond-resolution timing jitter characterization of free-running mode-locked lasers, Opt. Lett. 32 (2007) 3519–3521. Dec 15.
[387] Y.F. Chen, J. Jiang, D.J. Jones, Remote distribution of a mode-locked pulse train with sub 40-as jitter, Opt. Express 14 (2006) 12134–12144. Dec 11.
[388] U. Demirbas, A. Benedick, A. Sennaroglu, D. Li, J. Kim, J.G. Fujimoto, F.X. Kärtner, Attosecond resolution timing jitter characterization of diode pumped femtosecond Cr:LiSAF lasers, in: CLEO San Jose, California, 2010. CTuDD6.
[389] H. Kim, P. Qin, Y.J. Song, H. Yang, J. Shin, C. Kim, K. Jung, C.Y. Wang, J. Kim, Sub-20-Attosecond timing jitter mode-locked fiber lasers, IEEE J. Sel. Top. Quantum Electron. 20 (Sep-Oct 2014).
[390] A.J. Benedick, J.G. Fujimoto, F.X. Kärtner, Optical flywheels with attosecond jitter, Nat. Photonics 6 (2012) 97–100.
[391] P.C. Wagenblast, T.H. Ko, J.G. Fujimoto, F.X. Kaertner, U. Morgner, Ultrahigh-resolution optical coherence tomography with a diode-pumped broadband Cr3+: LiCAF laser, Opt. Express 12 (2004) 3257–3263. Jul 12.
[392] S. Sakadzic, U. Demirbas, T.R. Mempel, A. Moore, S. Ruvinskaya, D.A. Boas, A. Sennaroglu, F.X. Kartner, J.G. Fujimoto, Multi-photon microscopy with a low-cost and highly efficient Cr:LiCAF laser, Opt. Express 16 (2008) 20848–20863. Dec 8.
[393] K. Svoboda, W. Denk, W.H. Knox, S. Tsuda, Two-photon-excitation scanning microscopy of living neurons with a saturable Bragg reflector mode-locked diode-pumped Cr:LiSrAlFl laser, Opt. Lett. 21 (1996) 1411–1413. Sep. 1.
[394] G. Robertson, D. Armstrong, M.J.P. Dymott, A.I. Ferguson, G.L. Hogg, Two-photon fluorescence microscopy with a diode-pumped Cr:LiSAF laser, Appl. Opt. 36 (1997) 2481–2483. Apr 20.
[395] V.G. Savitski, N.K. Metzger, S. Calvez, D. Burns, W. Sibbett, C.T.A. Brown, Optical trapping with "on-demand" two-photon luminescence using Cr:LiSAF laser with optically addressed saturable Bragg reflector, Opt. Express 20 (2012) 7066–7070.
[396] P. Salieres, T. Ditmire, K.S. Budil, M.D. Perry, A. Lhuillier, Spatial profiles of high-order harmonics generated by a femtosecond crlisaf laser, J. Phys. B At. Mol. Opt. Phys. 27 (1994) L217–L222. May 14.
[397] S. Payziyev, K. Makhmudov, Solar pumped Nd:YAG laser efficiency enhancement using Cr:LiCAF frequency down-shifter, Opt. Commun. 380 (2016) 57–60. Dec 1.
[398] D. Parsons-Karavassilis, R. Jones, M.J. Cole, P.M.W. French, J.R. Taylor, Diode-pumped all-solid-state ultrafast Cr : LiSGAF laser oscillator-amplifier system applied to laser ablation, Opt. Commun. 175 (2000) 389–396. Mar 1.
[399] M. Seaver, D.C. Roselle, J.F. Pinto, J.D. Eversole, Absolute emission spectra from Bacillus subtilis and Escherichia coli vegetative cells in solution, Appl. Opt. 37 (1998) 5344–5347. Aug 1.
[400] D. Parsons-Karavassilis, Y. Gu, Z. Ansari, P.M.W. French, J.R. Taylor, Diode-pumped spatially dispersed broadband Cr : LiSGAF and Cr : LiSAF c.w. laser sources applied to short-coherence photorefractive holography, Opt. Commun. 181 (2000) 361–367. Jul 15.
[401] R. Jones, K. Dowling, M.J. Cole, D. Parsons-Karavassilis, M.J. Lever, P.M.W. French, J.D. Hares, A.K.L. Dymoke-Bradshaw, Fluorescence lifetime imaging using a diode-pumped all-solid-state laser system, Electron. Lett. 35 (1999) 256–258. Feb 18.
[402] E. Mendez, D.S. Elson, M. Koeberg, C. Dunsby, D.D.C. Bradley, P.M.W. French, Fluorescence lifetime imaging using a compact, low-cost, diode-based all-solid-state regenerative amplifier, Rev. Sci. Instrum. 75 (May 2004) 1264–1267.
[403] V.A. Fromzel, V.V. Ter-Mikirtychev, J.S. Smucz, C.R. Prasad, C.C. Johnson, N.P. Barnes, J.C. Barnes, R.J. DeYoung, Diode-pumped tunable narrow-linewidth Cr: LiSAF lasers for water vapor differential absorption lidars, in: Chemical and Biological Sensing II, 2001, pp. 82–89.
[404] J.W. Early, C.S. Lester, C.R. Quick, J.J. Tiee, T. Shimada, N.J. Cockroft, Continuously-tunable, narrow-linewidth, Q-switched Cr:LiSAF laser for lidar applications, in: Advanced Solid State Lasers, 1995, p. AP3.
[405] R. Holzwarth, M. Zimmermann, T. Udem, T.W. Hansch, P. Russbuldt, K. Gabel, R. Poprawe, J.C. Knight, W.J. Wadsworth, P.S.J. Russell, White-light frequency comb generation with a diode-pumped Cr : LiSAF laser, Opt. Lett. 26 (2001) 1376–1378. Sep. 1.
[406] D. Parsons-Karavassilis, Y. Gu, Z. Ansari, P.M.W. French, J.R. Taylor, Diode-pumped spatially dispersed broadband Cr:LiSGAF and Cr:LiSAF c.w. laser sources applied to short-coherence photorefractive holography, Opt. Commun. 181 (2000) 361–367.
[407] D.L. Wokosin, V. Centonze, J.G. White, D. Armstrong, G. Robertson, A.I. Ferguson, All-solid-state ultrafast lasers facilitate multiphoton excitation fluorescence imaging, IEEE J. Sel. Top. Quantum Electron. 2 (Dec 1996) 1051–1065.
[408] A. Diaspro, P. Bianchini, G. Vicidomini, M. Faretta, P. Ramoino, C. Usai, Multi-photon excitation microscopy, Biomed. Eng. Online 5 (2006). Jun 6.
[409] W.R. Zipfel, R.M. Williams, W.W. Webb, Nonlinear magic: multiphoton microscopy in the biosciences, Nat. Biotechnol. 21 (Nov 2003) 1368–1376.
[410] J.M. Girkin, Optical physics enables advances in multiphoton imaging, J. Phys. D Appl. Phys. 36 (2003) R250–R258. Jul 21.
[411] J.M. Girkin, G. McConnell, Advances in laser sources for confocal and multiphoton microscopy, Microsc. Res. Tech. 67 (May 2005) 8–14.
[412] F. Helmchen, W. Denk, Deep tissue two-photon microscopy, Nat. Methods 2 (Dec 2005) 932–940.

[413] J.M. Squirrell, D.L. Wokosin, J.G. White, B.D. Bavister, Long-term two-photon fluorescence imaging of mammalian embryos without compromising viability, Nat. Biotechnol. 17 (Aug 1999) 763–767.
[414] W. Denk, J.H. Strickler, W.W. Webb, 2-Photon laser scanning fluorescence microscopy, Science 248 (1990) 73–76. Apr 6.
[415] G. McConnell, G.L. Smith, J.M. Girkin, A.M. Gurney, A.I. Ferguson, Two-photon microscopy of fura-2-loaded cardiac myocytes with an all-solid-state tunable and visible femtosecond laser source, Opt. Lett. 28 (2003) 1742–1744. Oct 1.
[416] G. McConnell, E. Riis, Photonic crystal fibre enables short-wavelength two-photon laser scanning fluorescence microscopy with fura-2, Phys. Med. Biol. 49 (2004) 4757–4763. Oct 21.
[417] G. McConnell, Nonlinear optical microscopy at wavelengths exceeding 1.4 mu m using a synchronously pumped femtosecond-pulsed optical parametric oscillator, Phys. Med. Biol. 52 (2007) 717–724. Feb 7.
[418] K. Taira, T. Hashimoto, H. Yokoyama, Two-photon fluorescence imaging with a pulse source based on a 980-nm gain-switched laser diode, Opt. Express 15 (2007) 2454–2458. Mar 5.
[419] M. Kuramoto, N. Kitajima, H.C. Guo, Y. Furushima, M. Ikeda, H. Yokoyama, Two-photon fluorescence bioimaging with an all-semiconductor laser picosecond pulse source, Opt. Lett. 32 (2007) 2726–2728. Sep. 15.
[420] H. Yokoyama, H.C. Guo, T. Yoda, K. Takashima, K. Sato, H. Taniguchi, H. Ito, Two-photon bioimaging with picosecond optical pulses from a semiconductor laser, Opt. Express 14 (2006) 3467–3471. Apr 17.
[421] H. Yokoyama, H. Tsubokawa, H.C. Guo, J. Shikata, K. Sato, K. Takashima, K. Kashiwagi, N. Saito, H. Taniguchi, H. Ito, Two-photon bioimaging utilizing supercontinuum light generated by a high-peak-power picosecond semiconductor laser source, J. Biomed. Opt. 12 (2007). Sep-Oct.
[422] C. Xu, W.W. Webb, Measurement of two-photon excitation cross sections of molecular fluorophores with data from 690 to 1050 nm, J. Opt. Soc. Am. B Opt. Phys. 13 (1996) 481–491. Mar.
[423] V.G. Savitski, N.K. Metzger, S. Calvez, D. Burns, W. Sibbett, C.T.A. Brown, Optical trapping with "on-demand" two-photon luminescence using Cr:LiSAF laser with optically addressed saturable Bragg reflector, Opt. Express 20 (2012) 7066–7070. Mar 26.
[424] A. Rohrbacher, O.E. Olarte, V. Villamaina, P. Loza-Alvarez, B. Resan, Multiphoton imaging with blue-diode-pumped SESAM-modelocked Ti:sapphire oscillator generating 5 nJ 82 fs pulses, Opt. Express 25 (2017) 10677–10684.